2008

Computation with spin foam models of quantum gravity

Igor Khavkine
Western University

Computation with spin foam models of quantum gravity

(Spine title: Computation with spin foam models of quantum gravity)

(Thesis format: Integrated-Article)

by

Igor Khavkine

Graduate Program
in
Theoretical Physics
Department of Applied Mathematics

A thesis submitted in partial fulfillment
of the requirements for the degree of
Doctor of Philosophy

The School of Graduate and Postdoctoral Studies
The University of Western Ontario
London, Ontario, Canada

Abstract

The focus of this thesis is the study of spin foam models of quantum gravity on a computer. These models include the standard Barrett-Crane (BC) spin foam model, as well as the new Engle-Pereira-Rovelli (EPR) and Freidel-Krasnov (FK) models. New numerical algorithms are developed and implemented, based on the existing Christensen-Egan (CE) algorithm, to allow computations with the BC model in the presence of a cosmological constant (implemented through q-deformation) and to allow computations with the recently proposed EPR and FK models.

For the first time, we show that the inclusion of a positive cosmological constant, a long standing open problem for spin foams, curiously changes the behavior of the BC model, rendering the expectation values of its observables discontinuous in the limit of zero cosmological constant. Also, unlike previous work, this investigation was carried out on large triangulations, which are closer to large semiclassical space-times.

Efficient numerical algorithms are described and implemented, for the first time, allowing the evaluation of the EPR and FK spin foam vertex amplitudes. An initial application of these algorithms is the study of the effective single vertex large spin asymptotics of the new models. Their asymptotic behavior is found to be qualitatively similar to that of the BC model. The leading asymptotic behavior does not exhibit the oscillatory character expected by analogy with the Ponzano-Regge model.

Two important tests of the spin foam semiclassical limit are wave packet propagation and evaluation of the graviton propagator matrix elements. These tests are generalized to encompass the three major spin foam models. The wave packet propagation test is carried out in greater generality than previously. The results indicate that conjectures about good semiclassical behavior of the new spin foam models may have been premature.

Table of Contents

List of Figures

Chapter 1
Introduction

1.1 Quantum gravity

The problem of quantum gravity, in broad strokes, consists of constructing a quantum mechanical model of the gravitational field. The success of this program should be measured by the agreement of the constructed model with experiments. Unfortunately, to date, the most sensitive experiments have yet to yield any measurable effect that can be unambiguously attributed to quantum gravity [4]. In the absence of experimental data, the constructed model should also agree with existing physical theories, at least within the realm where their validity has been established. This requirement includes reproducing Einstein's theory of general relativity (GR) [55] in the classical limit. An excellent and comprehensive overview of the historical development of quantum gravity can be found in Appendix B of [48]. A briefer and more focused review is presented below.

Following the successful quantization of electrodynamics and other wave and matter fields, the methods of quantum field theory (QFT) were applied to perturbative gravity. That is, the linearized deviation of the gravitational field from a fixed classical background was treated as a quantum field, with higher order terms in the GR Lagrangian treated as interactions [34, 35]. The standard Fock space quantization method ensured agreement with perturbative GR in the classical limit [29]. Unfortunately, the inclusion of interactions revealed the theory to be non-renormalizable [54], unlike for other fundamental fields. This feature makes the perturbative quantization of GR an unsuitable basis for the definition of quantum gravity, as the theory would require an infinite number of empirical parameters to be fully specified. However, recent work, treating perturbatively quantized GR as an effective field theory, has shown that despite non-renormalizability it can yield unambiguous physical predictions at finite precision [15].

An approach that does not require a perturbative treatment is canonical quantization. In its most basic form, it requires an explicit parametrization of the GR phase space by generalized conjugate "position" and "momentum" coordinates, which are

then promoted to operators satisfying canonical commutation relations. Unfortunately, such an explicit parametrization has proved extremely difficult. The alternative is an implicit parametrization of the GR phase space as a constrained system, embedded in a larger phase space, which includes unphysical degrees of freedom. Similarly, applying canonical quantization to a constrained system aims to describe it implicitly as a subsystem of a larger quantum mechanical system. The treatment of GR as a constrained canonical system goes back to the seminal works of Dirac and Bergmann [16, 17, 27]. Unfortunately, the expressions of the constraints in terms of metric variables have proved difficult to work with. Much later, Ashtekar formulated GR in terms of the connection and tetrad variables, which resulted in a simplification of the constraints to polynomial expressions [5].

Ashtekar's formulation of GR is closely analogous to that of Yang-Mills gauge theories. This analogy prompted the introduction of holonomy and later spin network observables [33], similar to Wilson loop observables in Yang-Mills theory. The quantization of this algebra of observables allowed the construction of the Hilbert space of spin network states, which describe quantum states of 3-geometries. These states satisfy the constraints generating spatial diffeomorphisms (in a $3+1$ formulation of GR). The result of this program is known as loop quantum gravity (LQG) [48, 53]. However, this space needs to be further reduced by the Hamiltonian constraint, which generates temporal diffeomorphisms, to recover physical states. Unfortunately, the construction of the quantum Hamiltonian constraint met with difficulties. It is still an active research topic [52].

The absence of a well-defined Hamiltonian constraint is akin to the absence of well-defined dynamics for the gravitational field. As the difficulties of constructing the Hamiltonian constraint in a $3+1$ formulation became apparent, spin foams emerged as an alternative space-time way of specifying dynamics.

Spin foam models were first defined a decade ago [7, 11, 12]. They resemble discrete path integral or statistical models. A spin foam is a discretization of space-time where the fundamental degrees of freedom are the areas labelling its 2-dimensional faces. A given spin foam model may also be interpreted as a transition amplitude for a particular process evolving one spin network state into another.

The spin foam formalism is quite general. It naturally appears in the study of discretized BF theory (a topological quantum field theory) [6] and in the study of group field theory (field theory defined on group manifolds) [30, 43]. In fact, both BF theory and group field theories have been used to derive new spin foam models [28, 31, 43, 45]. The relation with BF theory will be explored further in section 4.2. The same

formalism has also been applied to the dual formulation of lattice Yang-Mills gauge theories [19, 22, 26, 41, 42, 46]. Historically, the first spin-foam model (retrospectively so classified) was the Ponzano-Regge model for 3-d Riemannian gravity [47].

While the previously discussed non-perturbative approaches to quantum gravity avoid the non-renormalizability problem, discussed at the beginning of the previous section, they suffer from difficulties in recovering the expected classical or semiclassical limit. In large part this difficulty is computational. In these models, when defined, physical observables tend to be complicated functions of many parameters. These functions are difficult to evaluate analytically and often expensive to compute numerically. Fortunately, much progress has been made recently from the computational angle [8–10, 20, 21, 23–25]. Analytical calculations have also been fruitful in some cases [14, 32, 38, 49]. In particular, the semiclassical limit of the standard Barrett-Crane spin foam model [11] does not correctly reduce to GR [2, 3]. This discovery prompted the proposals of so-called *new models* [28, 31]. Their investigation is a current research topic and our results in this direction will be discussed in chapters 4 and 5.

1.2 Abstract spin networks

Abstract spin networks, or just *spin networks*, are mathematical objects that naturally arise in the LQG [48, Chapter 6] and spin foam [7] approaches to quantum gravity, but also in other contexts [44], including the dual formulations of gauge theory [19, 22, 26]. Their evaluation is the most computationally expensive part of studying spin foams on a computer. The bulk of the work presented in this thesis is based on designing and implementing efficient algorithms for spin network evaluation.

In general, spin networks are closely related to tensor contractions. Given an $\binom{n}{m}$-tensor (with m covariant and n contravariant indices), it can be represented graphically as a vertex with n outgoing and m incoming edges incident on it. For example, a $\binom{3}{2}$-tensor T_{ij}^{klm} would be represented as

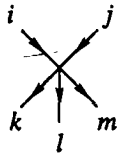

(1.1)

The outer (a.k.a. Kronecker or tensor) product of two tensors is represented by jux-

taposition. For $T_{ij}^{klm}\delta_a^b$, this is

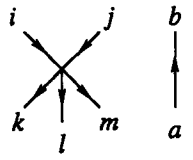

(1.2)

Note that the relative orientation of the tensor vertices is irrelevant. Also, edge labels are necessary only indicate the tensor index a given edge corresponds to. The same problem can also be solved by some fixed ordering convention for edges around the vertex. In that case, two tensors that are index permutations of each other are represented by the same vertex, but with the incident edges braided to distinguish one from the other. Both conventions are convenient and used in the literature. Contraction of tensor indices is indicated by joining the edges representing the contracted index pairs. The examples for T_{ij}^{klj} and $T_{ij}^{nlm}S_m^{jn}$ are

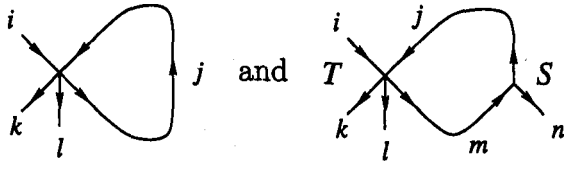

(1.3)

The case relevant for us is when each index of a tensor carries a representation of a group G. Even more so is the case when each representation is irreducible and the vertices correspond to *intertwiners* (tensors that are invariant under the simultaneous action of G on all their indices). Thus, a *spin network* is a graph[1] whose edges are labelled by irreducible representations (*irreps*) of G, while its vertices are labelled by intertwiners between them. The particular group G used in this thesis, as well as in most of the spin network literature, is $SU(2)$. Consequently, the group irreps are classified by an integer or half-integer called a *spin*[2],whence the name spin network.

1. LQG actually defines an additional notion of *embedded spin networks*, where the graph is supplemented with an embedding into a 3-manifold with a G-connection. Embedded spin networks define functions on the space of G-connections on the given manifold. These functions are evaluated in the same way as spin networks described above, with the exception of inserting between each pair of contracted indices a representation of the group element effecting parallel transport over the corresponding embedded graph edge.

2. Traditionally, *spins* are half-integral (0,1/2, 1, 3/2, 2, ...). Multiplying these labels by a factor of 2, we get only integral quantities called *twice-spins*. Chapters 2 and 3 use spins, while chapters 4 and 5 use twice-spins. Footnotes indicate which convention is used if confusion is possible.

$SU(2)$ representation theory has a number of helpful features, which simplify the notation. Particularly, all $SU(2)$ spin networks can be written as undirected trivalent (cyclically ordered) ribbon graphs. The ribbon structure becomes necessary when the graph directedness is dropped. The details are explicitly discussed in chapter 2, with all the mathematical details supplied in the monographs [18] and [36]. These simplifications also apply to Spin(4) networks. This group is the double cover of $SO(4)$ and decomposes as Spin(4) $= SU(2) \times SU(2)$. Expressing Spin(4) irreps as tensor products of $SU(2)$ irreps, each Spin(4) spin network can be written in terms of $SU(2)$ networks.

1.3 Evaluating spin networks

Now that we have defined spin networks, we will show how to evaluate some of them. As a relevant example, consider the so-called $SU(2)$ $15j$-symbol:

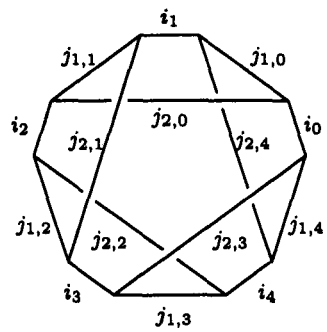

(1.4)

The 3-valent vertex here corresponds to the Clebsch-Gordan 3-index intertwiner, C_{abc}, whose normalization is fixed according to the conventions of [18] and [36] (cf. section 3.A):

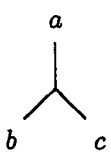

(1.5)

If the value of the $15j$-symbol network is written out explicitly as a tensor contraction, there will be 10 3-index tensors with 15 pairs of contracted indices. Each index ranges over a basis for an irrep of $SU(2)$, specified by the twice-spin, say j', labelling the corresponding edge. The dimension of this space is $(j'+1)$. Suppose that each spin labelling the $15j$-symbol is taken to be $O(j)$, that is, to be of the same order of magnitude as some average spin j. Then, each tensor index contraction requires a summation over a range of size $O(j)$. With 15 summations, a naive implementation of

the tensor contraction evaluation will require $O(j^{15})$ operations[3]. This is a very high exponent polynomial complexity, which makes its use prohibitively expensive already for small values of j. This example only underscores the importance of developing more efficient ways of evaluating spin networks.

The structure of the tensor contractions in the $15j$-symbol can be exploited to reorder some summations and tensor products to reduce the number of operations necessary to compute its value. However, any variation of this method still suffers from a deficiency; it requires explicit computation of the tensor components of the Clebsch-Gordan intertwiner, which invariably leads to making choices regarding the phases in its normalization factors: not impossible, but tedious. However, the knowledge of some identities from $SU(2)$ representation theory can help avoid evaluating the Clebsch-Gordan tensors directly and reduce the evaluation's run time complexity even more dramatically.

The basic identity is the so-called *recoupling identity* [cf. equation (3.43)]:

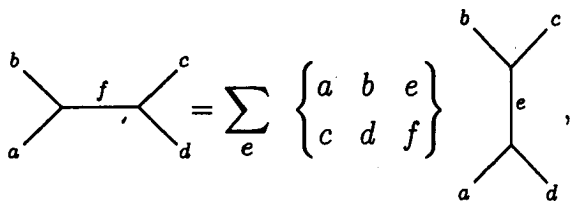

(1.6)

where the curly brackets denote the so-called $6j$-*symbol*. It is closely related to the Wigner-Racah $6j$-symbol familiar from the quantum theory of angular momentum [40] and its definition in the current normalization can be read off from equation (3.43) (see also [36, Chapter 9]), where the relevant notation is is also defined in context.

The $15j$-symbol can be redrawn as the ladder network illustrated in figure 3.1(c). Its rungs are the spins $j_{1,e}$ $(e = 0, \cdots, 4)$, and the rest of the spin labels can be deduced from the graph's topology. The recoupling identity is applied to each rung, yielding the network depicted in figure 3.1(d), prefixed by a $6j$-symbol and a summation over an extra recoupling spin m_e for each recoupled rung $j_{1,e}$. Fortunately, Schur's lemma guarantees that the only non-vanishing terms in this sum are those where all recoupling spins are equal, $m_e = m$, and also that each bubble network is proportional to the Kronecker δ, with an easily deducible proportionality factor. The

3. We shall generally assume that the tensor components of the Clebsch-Gordan tensor may be computed in $O(1)$ time. That is, our estimates may underestimate the actual run time complexity, which is sufficient for the purposes of this discussion.

result is that the $15j$-symbol evaluates to the following expression:

$$\sum_m (-)^m (m+1) \prod_{e=0}^{4} \frac{\theta(i_e, j_{2,e-1}, m)}{(-)^m (m+1)} \begin{Bmatrix} i_e & j_{2,e} & m \\ i_{e+1} & j_{2,e-1} & j_{1,e} \end{Bmatrix}. \tag{1.7}$$

Note that the index e is always taken mod 5. An explanation of the notation and full details of this computation are presented in the original paper deriving the Christensen-Egan algorithm [24]. The notation is also explained in section 3.A, where the θ symbol is explicitly defined. Note that each $6j$-symbol in the above expression can be computed in $O(j)$ time, as evidenced by the explicit formulas of section 3.A. Further, the range of the recoupling spin m is bounded by linear inequalities involving the fixed spins (known as the *triangle inequalities*; cf. *admissible spins* in section 3.A), making it $O(j)$ in size as well. Therefore, we have managed to reduce the run time complexity for evaluating the $15j$-symbol to $O(j^2)$, a dramatic improvement over the previous $O(j^{15})$ estimate.

Unfortunately, the search for efficiency never stops. The Barrett-Crane spin foam model defines the so-called $10j$*-symbol*, one of its basic building blocks and a highly non-trivial spin network to evaluate. It is defined by combining equations 3.5 and 3.4. Ultimately, the $10j$-symbol is defined by a sum of a product of two identical $15j$-symbols with some coefficients, which do not significantly impact the complexity of the computation. The sum is five-fold and ranges over all allowed values of the i_e spins of equation (1.4):

$$\{10j\} = \sum_{\{i_e\}} (\cdots) \{15j\}^2. \tag{1.8}$$

Using the formula of equation (1.7) and naively implementing the outer sums, we estimate the run time complexity of the $10j$-symbol evaluation as $O(j^7)$, given that the i_e sums have ranges of size $O(j)$ (again, due to bounds by triangle inequalities). The insight of the Christensen-Egan algorithm is to notice that the summand in the $15j$-symbol evaluation formula (1.7) factors into terms that depend on no more than two consecutive i_e spins, i_e and i_{e+1}. So, concentrating at the moment only on the spins that are summed over, the $10j$-symbol evaluation (1.8) can be rewritten as

$$\{10j\} = \sum_{m_1, m_2} \phi \sum_{\{i_e\}} T^{i_4}_{i_0} T^{i_3}_{i_4} T^{i_2}_{i_3} T^{i_1}_{i_2} T^{i_0}_{i_1}, \tag{1.9}$$

where ϕ depends only on m_1 and m_2, the recoupling spins coming from each $15j$-symbol factor, and each $T^{ie}_{i_{e+1}}$ also depends on m_1, m_2, as well as on the $j_{1,e}$ and $j_{2,e}$

spins. It should be straightforward to recognize the i_e summations over the Ts as the trace of a product of five matrices:

$$\{10j\} = \sum_{m_1,m_2} \phi \operatorname{tr}[T_4 T_3 T_2 T_1 T_0], \tag{1.10}$$

where each T_e is an $O(j) \times O(j)$ matrix. To compute the above expression, for each value of m_1 and m_2, we must fill the five T_e matrices (each matrix element contains a product of $6j$-symbols and hence takes $O(j)$ time to compute), compute their five-fold product and the product's trace. Clearly, it takes $O(j^3)$ time to fill the T_e matrices, and it is well known that the successive product of a fixed number of $O(j) \times O(j)$ matrices also takes $O(j^3)$ operations. Including the m_1 and m_2 sums, the overall run time complexity estimate for the Christensen-Egan $10j$-symbol evaluation algorithm is $O(j^5)$ operations. It is a factor of $O(j^2)$ faster than our previous naive version. The efficiency of the Christensen-Egan algorithm has made tractable the numerical investigation of the asymptotic large-j behavior of the Barrett-Crane $10j$-symbol, which was one of its first applications [9].

The product-trace structure (1.10) of the Christensen-Egan algorithm has proven to be very robust. It is the basis of the q-deformed generalization presented in chapter 3 and of the new algorithms of chapters 4 and 5. With the basic computational problem that is attacked in this thesis outlined, the next section describes the subsequent contents.

1.4 Summary of thesis

Numerical calculations provide a strong check for theoretical hypotheses and analytical calculations. They are especially useful for detecting errors (essentially, as an independent means of verifying a calculation) and for indicating new avenues of investigation.

One of the first tests of the Barrett-Crane (BC) spin foam vertex amplitude as a building block of a theory of gravity was an analytical calculation of its asymptotic expansion in the limit of large spins [13]. The hope was to find a term of the form $e^{iS[j]}$, where $S[j]$ is the Regge action for simplicial gravity, and j collectively describes the input spins. The stationary phase arguments of [13] yielded a leading asymptotic of the form $O(j^{-9/4} \cos S[j])$. This result was tested numerically [9], as one of the first applications of the Christensen-Egan (CE) algorithm. The numerical calculation revealed a non-oscillatory leading asymptotic of the form $O(j^{-2})$. This inconsistency

quickly revealed an error in the original asymptotic analysis and subsequent analytical calculations yielded the correct leading asymptotic term [14, 32].

Shortly after the graviton propagator problem was proposed for the BC model by Rovelli [49] (cf. section 5.2.2), its numerical investigation was begun. An implementation of these calculations on a computer requires explicit and detailed descriptions of each step. The necessity for such precision of formulation prompted refinements and clarifications to the problem's theoretical framework [38]. The synthesis of these theoretical and numerical investigations culminated in [25].

This thesis presents some further numerical investigation of the BC model and its variations, as well as of the new models. The algorithms presented in chapters 4 and 5 allow efficient numerical evaluation of the new vertex amplitudes, as the CE algorithm did for the BC vertex. The discovery and implementation of these algorithms is a crucial step for studying the new spin foam models on a computer. The first paper to use numerics to study one of the new models was [39]. Already, by adopting our algorithms, they were able to push their calculations much further [1]. Related calculations are also presented in chapter 5. As anticipated, investigation of the new models on a computer is already bearing fruit.

This thesis is structured as follows. Each chapter is essentially self contained, with its own introductory, concluding and bibliography sections. The overarching theme connecting them is the goal of developing efficient computational tools needed to investigate spin foam models. As mentioned previously, one of the biggest obstacles to the development of spin foam models is the difficulty in evaluating physical observables and extracting their semiclassical limit. Numerical methods have proven to be an invaluable aid in working toward this goal. The relevance of the algorithms and software libraries described below to the problem of extracting the classical limit is emphasized in each chapter. Although spin foam models can be defined for both Lorentzian and Riemannian metric signatures, this thesis will consider only the latter, as does much of the existing literature.

Chapter 2 is an excerpt from [22]. It is included for reference. It explains the relation between tensor contractions and spin networks described in section 1.2 and illustrates how spin networks and spin foams arise in the dual treatment of lattice gauge theory. Its original purpose in [22] was to summarize the basics of spin foam models and of the recoupling approach to evaluating spin networks to an audience only familiar with the lattice gauge theory literature.

Chapter 3 describes a generalization of the classic CE algorithm [24] to the case of so-called q-deformed spin foam amplitudes. It is based on [37]. Section 3.2.2

describes q-deformation and how it incorporates a positive cosmological constant into the standard Barrett-Crane (BC) spin foam model [11], following Smolin's identification of the Kodama state as the LQG analog of de Sitter space [50, 51]. Section 3.3 describes how q-deformation modifies the BC model, answering this long standing question. Then, section 3.4 describes statistical simulation techniques used to compute spin foam partition functions (already introduced in previous work [10]), extending these techniques to arbitrarily large space-time triangulations. Section 3.5 then summarizes the application of these tools to the computation of some physical observables and points out the surprising result that they are not continuous as a function of the cosmological constant, taken to zero through positive values, providing some information about another long standing problem (posed in the original paper of Barrett and Crane [11]): how q-deformation affects the physics of spin foam models.

Chapter 4 examines the previously discussed new models. Besides [39], this is the first study of these models on a computer. The significant contributions of chapters 4 and 5 include the description of new, efficient algorithms for the evaluation of new spin foam vertex amplitudes, both more general and more efficient than those used in [39]. Section 4.2 discusses the relation between the new models and BF theory, and puts them, as well as the BC model, into a unified framework, following [31]. Section 4.3 describes and extends the CE algorithm to encompass the new models as well. Finally, section 4.4 uses the new algorithm to give the first data on their effective asymptotic behavior and compares it to that of the Barrett-Crane model.

Chapter 5 builds on the developments of chapter 4 to describe an efficient algorithm for computing a spin foam partition function including a boundary state. Such a computation would have been intractable otherwise. The large class of problems this algorithm is applicable to includes two important ones, described in section 5.2 (semiclassical wave packet propagation and graviton propagator calculation), known to be relevant for extracting the semiclassical limit. The algorithm is presented in section 5.3 and applied in section 5.4. The applications involve a generalized version of the wave packet propagation problem posed in [39] and call for more careful scrutiny of hypotheses put forward in that paper.

Chapter 6 summarizes important results from the preceding chapters and points out promising avenues for future work.

Bibliography

[1] Alesci E, Bianchi E, Magliaro E, and Perini C 2008 Intertwiner dynamics in the flipped vertex arXiv:0808.1971

[2] Alesci E and Rovelli C 2007 Complete LQG propagator: Difficulties with the Barrett-Crane vertex *Physical Review D* **76** 104012–104033 (*Preprint* arXiv:0708.0883)

[3] Alesci E and Rovelli C 2008 Complete LQG propagator. II. Asymptotic behavior of the vertex *Physical Review D* **77** 044024–044034 (*Preprint* arXiv:0711.1284)

[4] Amelino-Camelia G 2008 Quantum gravity phenomenology (*Preprint* arXiv:0806.0339)

[5] Ashtekar A 1991 Lectures on non-perturbative canonical gravity (*Advanced Series in Astrophysics and Cosmology* vol 6) (Singapore: World Scientific)

[6] Baez J C 1996 4-dimensional BF theory as a topological quantum field theory *Letters in Mathematical Physics* **38** 129–43 (*Preprint* arXiv:q-alg/9507006)

[7] Baez J C 1998 Spin foam models *Classical and Quantum Gravity* **15** 1827–58 (*Preprint* arXiv:gr-qc/9709052)

[8] Baez J C and Christensen J D 2002 Positivity of spin foam amplitudes *Classical and Quantum Gravity* **19** 2291–306 (*Preprint* arXiv:gr-qc/0110044)

[9] Baez J C, Christensen J D, and Egan G 2002 Asymptotics of $10j$ symbols *Classical and Quantum Gravity* **19** 6489–513 (*Preprint* arXiv:gr-qc/0208010)

[10] Baez J C, Christensen J D, Halford T R, and Tsang D C 2002 Spin foam models of Riemannian quantum gravity *Classical and Quantum Gravity* **19** 4627–48 (*Preprint* arXiv:gr-qc/0202017)

[11] Barrett J W and Crane L 1998 Relativistic spin networks and quantum gravity *Journal of Mathematical Physics* **39** 3296–302 (*Preprint* arXiv:gr-qc/9709028)

[12] Barrett J W and Crane L 2000 A Lorentzian signature model for quantum general relativity *Classical and Quantum Gravity* **17** 3101–18 (*Preprint* arXiv:gr-qc/9904025)

[13] Barrett J W and Williams R M 1999 The asymptotics of an amplitude for the 4-simplex *Advances in Theoretical and Mathematical Physics* **3** 209–215 (*Preprint* arXiv:gr-qc/9809032)

[14] Barrett J W and Steele C M 2003 Asymptotics of relativistic spin networks *Classical and Quantum Gravity* **20** 1341–1362 (*Preprint* arXiv:gr-qc/0209023)

[15] Burgess C P 2004 Quantum gravity in everyday life: general relativity as an effective field theory *Living Reviews in Relativity* **7** 5

[16] Bergmann P G 1949 Non-linear field theories *Physical Review* **75** 680–685

[17] Bergmann P G and Brunings J H M 1949 Non-linear field theories II. Canonical equations and quantization *Reviews of Modern Physics* **21** 480–487

[18] Carter J S, Flath D E, and Saito M. 1995 The classical and quantum $6j$-symbols (*Mathematical Notes* vol 43) (Princeton, New Jersey: Princeton University Press)

[19] Cherrington J W 2008 A dual algorithm for non-abelian Yang-Mills coupled to dynamical fermions *Nuclear Physics B* **794** 195–215 (*Preprint* arXiv:0710.0323)

[20] Cherrington J W 2006 Finiteness and dual variables for Lorentzian spin foam models *Classical and Quantum Gravity* **23** 701–720 (*Preprint* arXiv:gr-qc/0508088)

[21] Cherrington J W and Christensen J D 2006 Positivity in Lorentzian Barrett-Crane models of quantum gravity *Classical and Quantum Gravity* **23** 721–736 (*Preprint* arXiv:gr-qc/0509080)

[22] Cherrington J W, Christensen J D, and Khavkine I 2007 Dual computations of non-abelian Yang-Mills on the lattice *Physics Review D* **76** 094503–094519 (*Preprint* arXiv:0705.2629)

[23] Christensen J D 2006 Finiteness of Lorentzian 10j symbols and partition functions *Classical and Quantum Gravity* **23** 1679–1688 (*Preprint* arXiv:gr-qc/0512004)

[24] Christensen J D and Egan G 2002 An efficient algorithm for the Riemannian $10j$ symbols *Classical and Quantum Gravity* **19** 1184–93 (*Preprint* arXiv:gr-qc/0110045)

[25] Christensen J D, Livine E R, and Speziale S 2007 Numerical evidence of regularized correlations in spin foam gravity (*Preprint* arXiv:0710.0617)

[26] Conrady F 2005 Geometric spin foams, Yang-Mills theory, and background-independent models (*Preprint* arXiv:gr-qc/0504059)

[27] Dirac P A M 2001 Lectures on Quantum Mechanics (Mineola, NY: Dover) *Reprint of 1966 original.*

[28] Engle J, Pereira R, and Rovelli C 2007 The loop-quantum-gravity vertex-amplitude *Physical Review Letters* **99** 161301–161304 (*Preprint* arXiv:0705.2388)

[29] Feynman R P, Morinigo F B, and Wagner W G 2002 Feynman Lectures on Gravitation (Boulder, CO: Westview Press)

[30] Freidel L 2005 Group field theory: an overview *International Journal of Theoretical Physics* **44** 1769–83 (*Preprint* arXiv:hep-th/0505016)

[31] Freidel L and Krasnov K 2008 A new spin foam model for 4d gravity *Classical and Quantum Gravity* **25** 125018–125053 (*Preprint* arXiv:0708.1595)

[32] Freidel L and Louapre D 2003 Asymptotics of $6j$ and $10j$ symbols *Classical and Quantum Gravity* **20** 1267–1294 (*Preprint* arXiv:hep-th/0209134)

[33] Gambini R and Pullin J 1996 Loops, Knots, Gauge Theory and Quantum Gravity (Cambridge, UK: Cambridge University Press)

[34] Gupta S N 1952 Quantization of Einstein's gravitational field: linear approximation *Proceedings of the Physical Society A* **65** 161–169

[35] Gupta S N 1952 Quantization of Einstein's gravitational field: general treatment *Proceedings of the Physical Society A* **65** 608–619

[36] Kauffman L H and Lins S L 1994 Temperley-Lieb recoupling theory and invariants of 3-manifolds (*Annals of Mathematics Studies* vol 134) (Princeton, New Jersey: Princeton University Press)

[37] Khavkine I and Christensen J D 2007 q-deformed spin foam models of quantum gravity *Classical and Quantum Gravity* **24** 3271–3290 (*Preprint* arXiv:0704.0278)

[38] Livine E R and Speziale S 2006 Group integral techniques for the spinfoam graviton propagator *Journal of High Energy Physics* **11** 092–114 (*Preprint* arXiv:gr-qc/0608131)

[39] Magliaro E, Perini C, and Rovelli C 2007 Numerical indications on the semiclassical limit of the flipped vertex (*Preprint* arXiv:0710.5034)

[40] Messiah A. 1962 Quantum Mechanics, Vol. 2 (Amsterdam, Netherlands: North-Holland) pp 1061–1066

[41] Oeckl R 2005 Discrete Gauge Theory: From Lattices to TQFT (London, UK: Imperial College Press)

[42] Oeckl R and Pfeiffer H 2002 Spin foam model for pure gauge theory coupled to quantum gravity *Physical Review D* **66** 124010–124019

[43] Oriti D 2006 Generalized group field theories and quantum gravity transition amplitudes *Physical Review D* **73** 061502–061506 (*Preprint* arXiv:gr-qc/0512069)

[44] Penrose R 1971 Angular momentum: an approach to combinatorial spacetime *Quantum Theory and Beyond* ed Bastin T (Cambridge, UK: Cambridge University Press) pp 151–180

[45] Perez A 2003 Spin foam models for quantum gravity *Classical and Quantum Gravity* **20** R043–104 (*Preprint* arXiv:gr-qc/0301113)

[46] Pfeiffer H 2003 Exact duality transformations for sigma models and gauge theories *Journal of Mathematical Physics* **44** 2891–2938

[47] Ponzano G and Regge T 1968 Semiclassical limit of Racah coefficients *Spectroscopic and group theoretical methods in physics* ed Bloch F, Cohen S G, De-Shalit A, Sambursky S, and Talmi I (Amsterdam: North-Holland) pp 1–98

[48] Rovelli C 2004 Quantum Gravity (Cambridge, UK: Cambridge University Press)

[49] Rovelli C 2006 Graviton propagator from background-independent quantum gravity *Physical Review Letters* **97** 151301–151304 (*Preprint* arXiv:gr-qc/0508124)

[50] Smolin L 1995 Linking topological quantum field theory and nonperturbative quantum gravity *Journal of Mathematical Physics* **36** 6417–55 (*Preprint* arXiv:gr-qc/9505028)

[51] Smolin L 2002 Quantum gravity with a positive cosmological constant *Preprint* arXiv:hep-th/0209079

[52] Thiemann T 2006 The Phoenix Project: master constraint programme for loop quantum gravity *Classical and Quantum Gravity* **23** 2211–2247

[53] Thiemann T 2007 Modern Canonical Quantum General Relativity (Cambridge, UK: Cambridge University Press)

[54] 't Hooft G and Veltman M 1974 One-loop divergencies in the theory of gravitation *Annales de L'Institut Henri Poincare A* **20** 69–94

[55] Will C M 1993 Theory and Experiment in Gravitational Physics rev ed (New York, NY: Cambridge University Press)

Chapter 2
Spin foams and gauge theory

The following is an excerpt (edited for consistency) of section 2.1 and appendix A of [4]. It is provided here for reference. Section 2.A.1 introduces spin foams as the dual formulation of lattice gauge theory. Sections 2.A.1 and 2.A.2 also elaborate the relation between tensor contractions and spin network diagrams.

2.1 Review of pure Yang-Mills theory on the lattice

First we recall the Euclidean partition function of pure Yang-Mills theory in D dimensions, with gauge group $G = SU(N)$, where $N \geq 2$ (we shall later specialize to the $SU(2)$ case). It takes the form

$$\mathcal{Z} = \int \mathcal{D}A \, \exp(-S), \tag{2.1}$$

with A^a_μ the gauge field, S the action functional, and $\mathcal{D}A$ the functional integration measure. In the continuum version of the theory the standard action functional is

$$S \equiv S[A] = \frac{1}{4g^2} \int d^D x \, F^a_{\mu\nu} F_a^{\mu\nu}, \tag{2.2}$$

where $F^a_{\mu\nu}$ is the field strength tensor and g the continuum coupling. Unfortunately, the continuum functional measure $\mathcal{D}A$ is not well-defined.

One way to give the above path integral rigorous meaning and, at the same time, make it amenable to computational treatment, is to put the theory on a discrete finite lattice. The simplest variant uses a hyper-cubic lattice. Let E and P denote respectively the sets of edges and plaquettes of a hyper-cubic lattice in D dimensions. The gauge field A is replaced by gauge group elements g_e assigned to each oriented lattice edge $e \in E$. The same edge with opposite orientation gets g_e^{-1} instead of g_e.

The functional integral measure can now be replaced by an integral over the product of $|E|$ copies of G using Haar measure:

$$\mathcal{D}A \equiv \prod_{e \in E} dg_e. \tag{2.3}$$

At the same time, the action functional is replaced by a discretized version, $S \equiv S[g]$, that must reproduce the continuum action $S[A]$ as the lattice spacing is taken to zero. The discretized action is usually split into a sum over plaquettes, $S[g] = \sum_{p \in P} S(g_p)$, where the group element g_p is the holonomy around an oriented plaquette p. That is, $g_p = g_1 g_2 g_3 g_4$, where g_i is either the group element assigned to the ith edge of p or its inverse if the orientations of p and the ith edge are opposing. This yields the conventional lattice partition function

$$Z = \int \prod_{e \in E} dg_e \, e^{-\sum_{p \in P} S(g_p)}. \tag{2.4}$$

There are many candidate discretized plaquette actions $S(g_p)$. While the Wilson action [19] is perhaps the most well-known in conventional LGT (it was also used in the dual computations of [8–10]), a variety of actions $S(g_p)$ leading to the correct continuum limit are known and have been used in the literature [11, 13, 14]. In the present work, we use the *heat kernel action* [15]; in the dual model this action leads to plaquette factors that are particularly easy to compute. The heat kernel action (at lattice coupling γ) for a fundamental plaquette p and plaquette holonomy g_p is

$$e^{-S(g_p)} = \frac{K(g_p, \frac{\gamma^2}{2})}{K(I, \frac{\gamma^2}{2})}, \tag{2.5}$$

where the heat kernel K, which is a function of a group element g and of a "time" parameter t, satisfies a diffusion type differential equation

$$\frac{\partial}{\partial t} K(g,t) = \Delta K(g,t), \quad K(g,0) = \delta_I(g). \tag{2.6}$$

Here Δ is the Laplace-Beltrami operator on G and δ_I is the delta function at the group identity I. The denominator in (2.5) represents a normalization of the partition function in which flat holonomies ($g_p = I$) are assigned an amplitude of unity. We shall follow the common practice of discussing the phase structure of a lattice theory using the β parameter $\beta = \frac{4}{\gamma^2}$.

We now turn to the definition of the dual model for the specific case of $G = SU(2)$ pure Yang-Mills in three dimensions. Starting from the conventional formulation of the lattice partition function $\mathcal{Z}$ given in (2.4) above, the duality transformation can be applied (see Appendix 2.A.1) to yield the following expression for $\mathcal{Z}$ in terms of the dual variables:

$$\mathcal{Z} = \sum_j \left(\sum_i \prod_{v \in V} 18j^v(i_v, j_v) \prod_{e \in E} N^e(i_e, j_e)^{-1} \right) \left(\prod_{p \in P} e^{-\frac{2}{\beta} j_p (j_p+1)} (2j_p + 1) \right). \tag{2.7}$$

Here V denotes the vertex set of the lattice, while the summations over i and j range over all possible edge and plaquette labellings, respectively. A plaquette labelling j assigns an irreducible representation of $SU(2)$ to each element of P. These representations are labelled by non-negative half-integers (we will denote this set by $\frac{1}{2}\mathbb{N}$) and are referred to as *spins*; a labelling j is thus a map $j\colon P \to \frac{1}{2}\mathbb{N}$. An edge labelling i, on the other hand, is valued in a basis of maps that intertwine the representations of the plaquettes incident on the same edge. In our present case, the choice of basis corresponds to a grouping of the four incident plaquette spins into two pairs. When such an edge splitting has been made, the intertwiners may also be labelled by spins, as described in Appendix 2.A.2. Different choices of splitting can be made, but some are more computationally efficient than others. In writing (2.7), we assume a fixed choice of splitting has been made and so an edge labelling is a map $i\colon E \to \frac{1}{2}\mathbb{N}$.

In the first pair of parentheses of (2.7), there is a product of $18j$ *symbols*, each of which is a function of the 18 spins which label the 12 plaquettes and 6 edges incident to a vertex v; we denote the spins which appear by j_v and i_v. Next to it is a product of edge normalizations N^e depending on the edge spin i_e and on the four spins j_e labelling the plaquettes incident on e. It is important to recognize that the $18j$ symbol and the normalization factors N^e are purely representation-theoretic quantities (independent of the action chosen) and that, from a computational viewpoint, they represent the non-trivial part of the amplitude evaluation. Efficient algorithms can be found (using diagrammatic techniques similar to those used in [5]) for computing the $18j$ symbols and edge normalizations. Two of these are reviewed in Appendix 2.A.2.

2.A The dual model and $18j$ symbol algorithms

2.A.1 Derivation of the dual model

This section sketches some of the steps of the transformation from the conventional to the dual form of the lattice Yang-Mills partition function, (2.4) and (2.7) respectively. Our approach is inspired by the spin foam picture, and is closest to that found in [6]. Non-abelian dual models have also been analyzed from a spin foam perspective in [17, 18].

We begin by observing that, due to gauge invariance, the plaquette action $S(g_p)$ of (2.4) depends only on the conjugacy class of its argument. Thus, its exponential can be expanded in terms of group characters χ_j

$$e^{-S(g)} = \sum_j c_j \chi_j(g), \tag{2.8}$$

where j ranges over the equivalence classes of finite-dimensional irreducible unitary representations of the gauge group G. Substituting into (2.4) and interchanging the order of summation and integration yields

$$\mathcal{Z} = \sum_{\{j_p\}} \int \prod_{e \in E} dg_e \prod_{p \in P} c_{j_p} \chi_{j_p}(g_p). \tag{2.9}$$

At this point it is convenient to specialize to a $D = 3$ cubic lattice with periodic boundary conditions and to fix an orientation for the plaquettes and edges of the lattice. Choose a right-handed set of xyz axes for the lattice. Orient all of the edges in the positive coordinate directions. Every lattice cube is in the first octant of one of its vertices. Take each of the three plaquettes of the cube that are incident to this vertex and orient it in the counterclockwise direction, as seen from outside the cube. It is easy to see that this choice of orientations is translation invariant, that the orientation of each edge agrees with two of the four plaquettes incident on it and is opposite to the other two, and that every plaquette has two edges whose orientations agree with its own and two that do not.

With this choice of orientation, the holonomy around a plaquette p is $g_p = g_1 g_2 g_3^{-1} g_4^{-1}$, where g_1, g_2, g_3 and g_4 are the group elements associated to the edges of the plaquette p, starting with an appropriate edge and going cyclically. Recall that

the inverse g_i^{-1} is used if the orientation of edge i does not agree with that of p. Thus

$$\chi_{j_p}(g_p) = U_{j_p}(g_1)^b_a \, U_{j_p}(g_2)^c_b \, U_{j_p}(g_3^{-1})^d_c \, U_{j_p}(g_4^{-1})^a_d \,, \tag{2.10}$$

where $U_j(g)^b_a$ denotes a matrix element with respect to a basis of the j representation. If we insert (2.10) into (2.9) and collect together factors depending on the group element g_e, we get a product of independent integrals over the group, each of the form

$$\int dg_e \, U_{j_1}(g_e)^{b_1}_{a_1} \, U_{j_2}(g_e)^{b_2}_{a_2} \, U_{j_3}(g_e^{-1})^{b_3}_{a_3} \, U_{j_4}(g_e^{-1})^{b_4}_{a_4} = \int dg_e$$

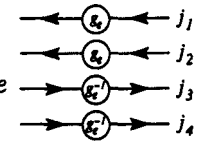

. (2.11)

Here and below we use a graphical notation for tensor contractions, defined as follows. Each *wire* represents a matrix element of the unitary representation labelling it. Parallel wires represent products of such matrix elements. The four matrix elements in (2.11) come from the characters associated to the four plaquettes incident on the edge e. The free ends of the wires represent the indices of these matrix elements. The wires can be joined together into loops, one for each plaquette. The joining corresponds to contracting with other matrix elements from different edge integrals to form the product of characters as in (2.10).

Equation (2.11) defines a projection operator on the space of linear maps $j_4 \otimes j_3 \to j_1 \otimes j_2$. It is the usual group averaging operator whose image is precisely the intertwiners. Since it is a projection operator, it can be resolved into a sum over a basis of intertwiners $I_i : j_4 \otimes j_3 \to j_1 \otimes j_2$,

$$\int dg_e$$

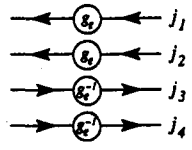

$$= \sum_i \frac{I_i I_i^*}{\langle I_i^*, I_i \rangle} =$$

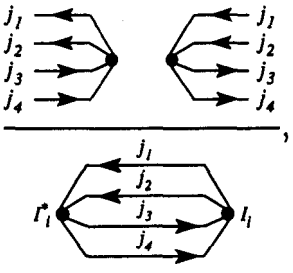

, (2.12)

where the intertwiners $I_i^* : j_1 \otimes j_2 \to j_4 \otimes j_3$ are chosen such that the trace $\langle I_{i'}^*, I_i \rangle$ of the composite $I_{i'}^* I_i$ is zero whenever $i' \neq i$ and non-zero if $i' = i$. The projection property is readily verified.

If, for each edge of the lattice, we fix a term i in the above summation, we can contract the intertwiners I_i and I_i^* with those coming from the other edges. At each

vertex of the lattice, there will be six such intertwiners, and their contraction can be graphically represented as an octahedral network that we call the $18j$ symbol:

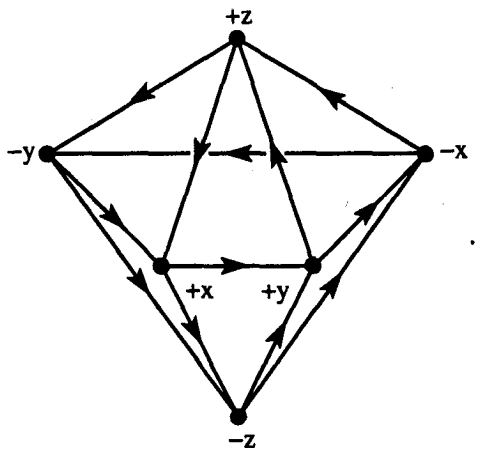

(2.13)

The vertices are labelled by the directions of the associated lattice edges emanating from the given lattice vertex, namely $\pm x$, $\pm y$, and $\pm z$. The value of the $18j$ symbol depends on the choice of basis elements I_i and $I_{i'}^*$ in (2.12), the six summation indices i labelling the edges, and the 12 incident plaquette labels j. Each normalization factor $N \equiv \langle I_i^*, I_i \rangle$ depends on the choice of basis elements at an edge, the summation index i on that edge, and the four plaquettes incident on that edge. Note that the choice of basis can be made independently at each edge.

The discussion up to this point has been quite general, assuming a 3-dimensional cubic lattice. Next, we specialize to $G = SU(2)$ and give the plaquette action character expansion coefficients. For the heat kernel (2.5), the expansion coefficients take the particularly simple form [15]

$$e^{-S(g)} = \frac{1}{K(I, \frac{\gamma^2}{2})} \sum_j (2j+1) e^{-\frac{\gamma^2}{2} j(j+1)} \chi_j(g), \quad j = 0, \tfrac{1}{2}, 1, \ldots, \tag{2.14}$$

where $K(g,t)$ is defined by (2.6). Putting these pieces together, we obtain the dual formula for the lattice Yang-Mills partition function

$$\mathcal{Z} = \sum_j \left(\sum_i \prod_{v \in V} 18j^v(j_v, i_v) \prod_{e \in E} N^e(i_e, j_e)^{-1} \right) \left(\prod_{p \in P} (2j_p + 1)\, e^{-\frac{\gamma^2}{2} j_p(j_p+1)} \right), \tag{2.15}$$

where an overall numerical factor of $K(I, \frac{\gamma^2}{2})$ per plaquette has been discarded. This precisely reproduces Equation (2.7), where we described the notation we are using

for the plaquette and edge labellings j and i.

2.A.2 Efficient algorithms for the $18j$ symbol via recoupling

In order to perform computations with (2.15), we first need to choose explicit basis elements I_i and I_i^* of the spaces of intertwiners that appear in (2.12). Below, we consider two patterns for choosing such bases for each edge of the lattice, one we call the ladder recoupling and one we call the tetrahedral recoupling. They lead to different $18j$ symbols and have different properties with respect to lattice translations.

2.A.2.1 The ladder recoupling

Recall that for compatible spins j, k and m, there is an intertwiner $j \otimes k \to m$ that is unique up to scale. To be explicit, we choose the specific intertwiner defined in [3, 2.5.4], and we denote it by

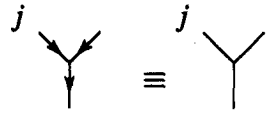

(2.16)

Similarly, we use the same reference[1] to define

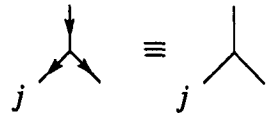

(2.17)

It is well-known that for fixed j_1, j_2, j_3 and j_4, the intertwiners

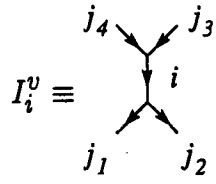

(2.18)

form a basis of the space of intertwiners $j_4 \otimes j_3 \to j_1 \otimes j_2$, as i varies over admissible spins. We call this the *vertical splitting.*

1. Note that our diagrams are read downwards, while those of [3] are read upwards.

There is also a second vertical splitting, given by interchanging j_3 and j_4, which changes the intertwiner by a factor of $(-1)^{j_3+j_4-i}$. The geometry of the lattice provides a natural way to choose between the two: we make sure that the plaquette labels on the left (j_4 and j_1 above) are part of the same lattice cube, and same for the labels on the right.

A convenient choice of dual basis is given by

$I_i^{v*} \equiv$ 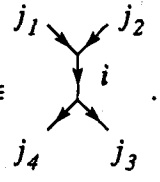

. (2.19)

One can check that $\langle I_{i'}^{v*}, I_i^v \rangle = 0$ for $i' \neq i$. We next need to evaluate the normalization factor

$N^v = \langle I_i^{v*}, I_i^v \rangle =$ 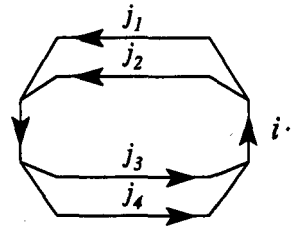

. (2.20)

In order to accomplish this, we now explain how to relate our tensor contraction diagrams to *spin networks*. While it would be possible to work entirely with tensor contraction diagrams, there are two reasons to switch to the spin network notation. First, spin networks do not require that the edges be directed, which relieves us of some complicated bookkeeping. Second, by using spin networks, we can take advantage of many existing formulas and software libraries for computing spin network evaluations.

Recall that a spin network is a trivalent undirected ribbon graph whose edges are labelled by spins. One assigns a value to a spin network in the following way. First, draw it in the plane, in general position, with the ribbon flat. Then, read it from top to bottom, interpreting the vertices as the trivalent intertwiners discussed above, and interpreting cups and caps as certain intertwiners which can introduce signs. If the spin network is closed, the resulting intertwiner is a map from the trivial representation to itself, and so can be identified with a complex number. The result is independent of the embedding in the plane, a fact that is quite useful in computations. In particular, the trivalent intertwiners are chosen carefully so that the evaluation remains unchanged when inputs are deformed into outputs and vice versa. We refer the reader to [3] for more details. While the starting point is different,

the formulas given in [12], with $A = 1$, also apply to these diagrams[2]. Note that some other authors have slightly different conventions, e.g. some take $A = -1$.

We will now work out how to compute tensor contractions using spin networks. Take a tensor contraction diagram involving just the trivalent intertwiners discussed above and draw it in the plane such that all edges are pointing downwards except for some edges which leave the bottom of the diagram and loop around to reenter at the top. If we erase the arrows, the resulting spin network will have the same interpretation as the tensor contraction diagram, except for the signs introduced in the cups and caps. One can show that the difference is exactly a factor of $(-1)^{2J}$, where J is the sum of the spins labelling the edges that loop around.

As a first example, the value of a loop labelled with j in the tensor notation is the dimension $2j + 1$ of the representation. However, in the spin network notation, the value of a loop is $\Delta_j = (-1)^{2j}(2j + 1)$.

Similarly, the value of the edge normalization factor is

$$N^v = \langle I_i^{v*}, I_i^v \rangle = \quad = (-1)^{2i} \quad = (-1)^{2i} \frac{\theta(j_1, j_2, i)\,\theta(j_3, j_4, i)}{\Delta_i},$$

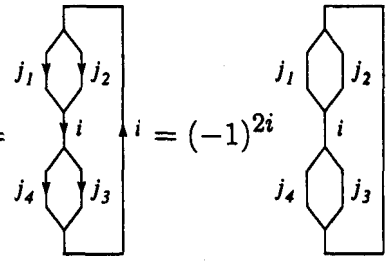

(2.21)

where $\theta(a, b, c)$ stands for the value of the following *theta network*:

$$\theta(a, b, c) \equiv$$

. (2.22)

Its value is given explicitly in [12, Chapter 9].

Note that the conversion sign factor $(-1)^{2i}$ from (2.21) can be expressed as $(-1)^{2(j_1+j_2)}$ by appealing to the parity constraints. Since each plaquette is "outgoing" from two edges, each plaquette spin contributes $(-1)^{4j} = 1$. In other words, the conversion sign factors from the edge normalizations N^v cancel. It can be shown that the conversion sign factor for the $18j$ symbol appearing in (2.13) is independent of the edge splitting and can be written as $(-1)^{2J}$, where, for instance, $J = j_{+x+y} + j_{+x-z} + j_{-y-z}$. Each plaquette spin shows up in exactly one such sign

2. Note that while we use half-integer spins, [12] uses twice-spins, which are always integers.

factor, so the signs combine to give $(-1)^{2J_{\text{tot}}}$, where J_{tot} is the sum of all plaquette spins. Note that on a lattice with two or more odd side-lengths, this sign factor can be non-trivial.

Next we must work out the value of the $18j$ symbols that arise using the vertical splitting. The corresponding spin network is obtained by applying this splitting to the vertices of the octahedron shown in (2.13) and erasing the arrows from its edges. A method for evaluating this spin network is shown in Figure 2.1. The calculation is similar to that of [5], where a "ladder" structure also appears. The recoupling move

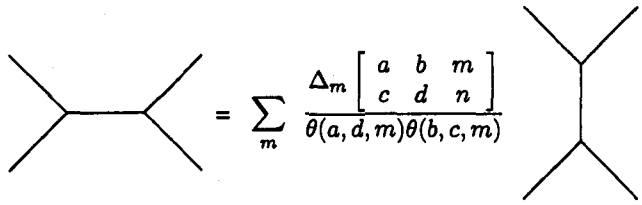

$$= \sum_m \frac{\Delta_m \begin{bmatrix} a & b & m \\ c & d & n \end{bmatrix}}{\theta(a,d,m)\theta(b,c,m)}$$

(2.23)

is applied to each of the six "rungs" of the ladder, producing a chain of bubbles. The function of six spin labels appearing in (2.23) is the tetrahedral network, shown in the last step of Figure 2.2. The value of the tetrahedral network is given explicitly in [12, Chapter 9] and is closely related to the Wigner-Racah $6j$ symbol of angular momentum theory [16, Appendix B], see (2.25).

Because of Schur's Lemma, the six independent sums from the recoupling moves become a single sum. The bubbles are proportional to the identity, weighted by a theta network divided by a loop. Six theta networks arising from the bubbles cancel against six of the twelve theta networks from the recoupling moves to give the six theta networks shown in the final line. The bubbles also contribute six loop factors (Δ_i) in the denominator, which exactly cancel the loop factors from the recoupling. The final result can be written as:

$$\sum_m \Delta_m \prod_{6 \text{ bubbles}} \begin{bmatrix} \cdots & \cdots & m \\ \cdots & \cdots & \cdots \end{bmatrix} \frac{1}{\theta(m, i_{+x}, j_{-y-z})\theta(m, i_{-x}, j_{+y+z})} \times \frac{1}{\theta(m, i_{+y}, j_{-x-z})\theta(m, i_{-y}, j_{+x+z})} \frac{1}{\theta(m, i_{+z}, j_{-x-y})\theta(m, i_{-z}, j_{+x+y})} \tag{2.24}$$

where the arguments of the six tetrahedral networks are those that appear in the last line of Figure 2.1. The explicit relation between the tetrahedral network and the

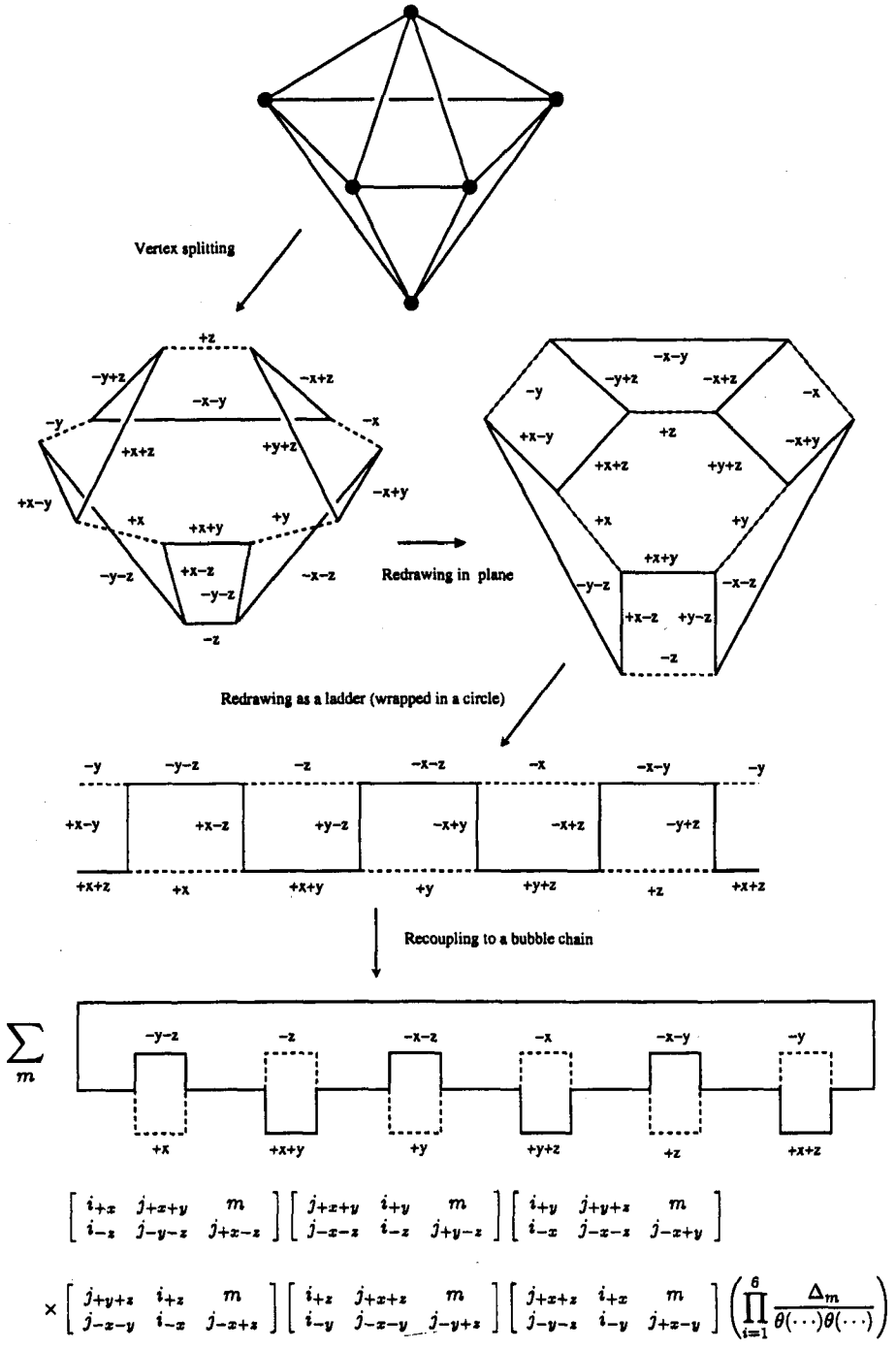

$$\left[\begin{matrix} i_{+x} & j_{+x+y} & m \\ i_{-z} & j_{-y-z} & j_{+x-z} \end{matrix}\right]\left[\begin{matrix} j_{+x+y} & i_{+y} & m \\ j_{-x-z} & i_{-z} & j_{+y-z} \end{matrix}\right]\left[\begin{matrix} i_{+y} & j_{+y+z} & m \\ i_{-x} & j_{-x-z} & j_{-x+y} \end{matrix}\right]$$

$$\times\left[\begin{matrix} j_{+y+z} & i_{+z} & m \\ j_{-x-y} & i_{-x} & j_{-x+z} \end{matrix}\right]\left[\begin{matrix} i_{+z} & j_{+x+z} & m \\ i_{-y} & j_{-x-y} & j_{-y+z} \end{matrix}\right]\left[\begin{matrix} j_{+x+z} & i_{+x} & m \\ j_{-y-z} & i_{-y} & j_{+x-y} \end{matrix}\right]\left(\prod_{i=1}^{6}\frac{\Delta_m}{\theta(\cdots)\theta(\cdots)}\right)$$

Figure 2.1: The ladder recoupling of the $18j$ symbol; a single sum.

Wigner-Racah $6j$ symbols is

$$\begin{bmatrix} J_1 & J_2 & J_3 \\ j_1 & j_2 & j_3 \end{bmatrix} = \sqrt{|\theta(J_1,J_2,j_3)\theta(j_1,j_2,j_3)\theta(J_1,j_2,J_3)\theta(j_1,J_2,J_3)|} \begin{Bmatrix} j_1 & j_2 & j_3 \\ J_1 & J_2 & J_3 \end{Bmatrix}. \quad (2.25)$$

Note the row swap and the fact that the four theta networks correspond to the four triples of spins from the $6j$'s arguments that must satisfy triangle inequalities. For reference, $|\theta(a,b,c)| = (-1)^{a+b+c}\theta(a,b,c)$.

The $18j$ symbol described in this section was used in computing the data appearing in Sections 3 and 4 of [4].

2.A.2.2 The tetrahedral recoupling

Next we consider a different splitting of the vertices of the octahedron, which we call the tetrahedral recoupling. The $18j$ symbol that arises here is more efficient to compute than the $18j$ symbol for the ladder recoupling, because it does not require a sum. However, the splitting is not translation invariant, which makes it slightly harder to work with. This section is not needed in the rest of the paper, but is useful as a comparison to other sources and will be important for future calculations.

We begin by considering a different basis for the space of intertwiners $j_4 \otimes j_3 \to j_1 \otimes j_2$. It is given by the *horizontal splitting*

$I_i^h \equiv$ 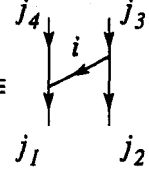

(2.26)

as i varies over admissible spins. Note that it makes no difference which way the arrow on the edge labelled by i points.

There is also a second horizontal splitting, given by interchanging j_3 and j_4. As we did for the vertical splitting, we choose between the two by requiring that j_4 and j_1 label plaquettes that are part of the same cube. Unlike the vertical splitting, the two horizontal splittings are not in general related by a sign.

A convenient dual basis is given by

$I_i^{h*} \equiv$ 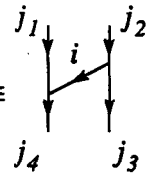

. (2.27)

The traces $\langle I_{i'}^{h*}, I_i^h \rangle$ work out to be

$$N^h = \langle I_{i'}^{h*}, I_i^h \rangle = (-1)^{2(j_1+j_2)} \frac{\theta(j_1, j_4, i)\,\theta(j_2, j_3, i)}{\Delta_i}. \tag{2.28}$$

For the tetrahedral recoupling, we use the vertical splitting (2.18) on three edges and the horizontal splitting on the opposite edges. The pattern we use is indicated in the first step of Figure 2.2. The result is a planar network consisting of four triangles connected to one another in a tetrahedral pattern.

For this recoupling, a minor complication arises because the intertwiner splittings are different on opposite edges. This means that a simple translation of the given tetrahedral $18j$ symbol to neighboring vertices does not correspond to a consistent choice of basis for the intertwiners. This is easily overcome by dividing the lattice into a checkerboard of odd and even sites, and alternately using the original and reflected versions of the $18j$ symbol. For periodic boundary conditions, this does limit one to lattices with even side-lengths, but this constraint is not serious in practice.

As was the case with the ladder recoupling, the conversion sign factors from the normalization factors cancel, and the conversion sign factors from the $18j$ symbols give a factor of $(-1)^{2J_{\text{tot}}}$. In this case, because the checkerboard pattern forces even side-lengths, one can show that $(-1)^{2J_{\text{tot}}} = 1$.

The diagrammatic relation

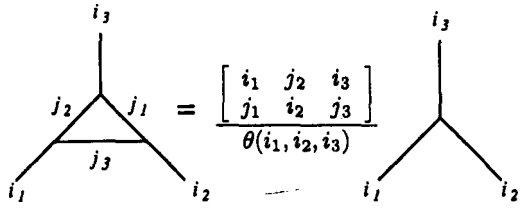

(2.29)

can be used to collapse each of the four triangles into 3-valent vertices, as shown in the last step of Figure 2.2. The final result is simply:

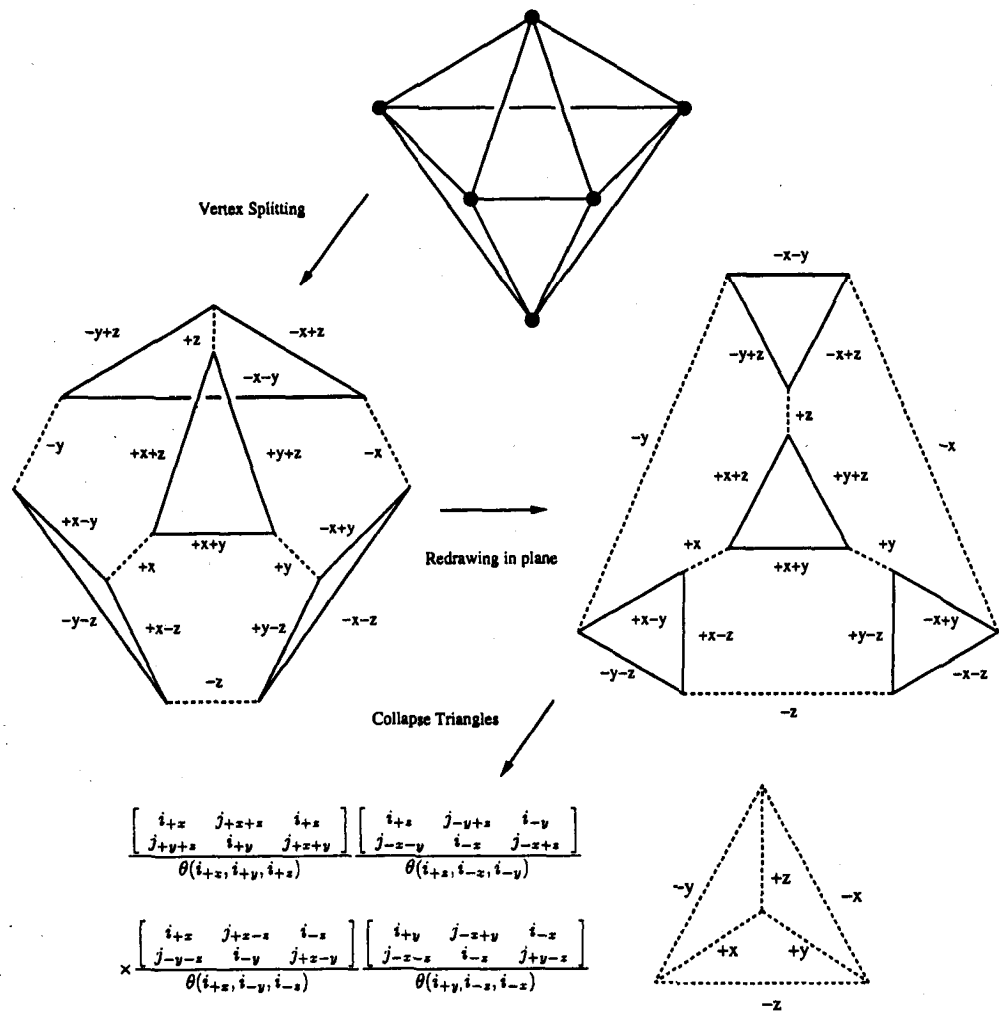

Figure 2.2: The tetrahedral recoupling of the $18j$ symbol; no sum.

$$\frac{\begin{bmatrix} i_{+x} & j_{+x+z} & i_{+z} \\ j_{+y+z} & i_{+y} & j_{+x+y} \end{bmatrix} \begin{bmatrix} i_{+z} & j_{-y+z} & i_{-y} \\ j_{-x-y} & i_{-x} & j_{-x+z} \end{bmatrix}}{\theta(i_{+x}, i_{+y}, i_{+z})\theta(i_{+z}, i_{-x}, i_{-y})} \times \frac{\begin{bmatrix} i_{+x} & j_{+x-z} & i_{-z} \\ j_{-y-z} & i_{-y} & j_{+x-y} \end{bmatrix} \begin{bmatrix} i_{+y} & j_{-x+y} & i_{-x} \\ j_{-x-z} & i_{-z} & j_{+y-z} \end{bmatrix}}{\theta(i_{+x}, i_{-y}, i_{-z})\theta(i_{+y}, i_{-z}, i_{-x})} \begin{bmatrix} i_{-x} & i_{-y} & i_{-z} \\ i_{+x} & i_{+y} & i_{+z} \end{bmatrix} \quad (2.30)$$

Because this formula is essentially a product of tetrahedral networks with no auxiliary summations, it is highly efficient to compute.

The tetrahedral recoupling is easy to express in terms of Wigner-Racah $6j$ symbols using relation (2.25). In order to compare our work to other work, we give some of the details. Ignoring signs for the moment, the theta networks from the edge normalizations (2.21) and (2.28), the conversion formula (2.25), and the vertex amplitude (2.30) all cancel. Now we collect the signs of the theta networks. The theta networks from the edge normalizations contribute a sign of $(-1)^{2i}(-1)^{j_1+j_2+j_3+j_4}$, where i labels the edge and the j_k label the incident plaquettes. Since each plaquette is shared by four edges, the factors $(-1)^{j_1+j_2+j_3+j_4}$ cancel. Thus the edge normalizations become $(-1)^{2i}/\Delta_i = 1/(2i+1)$. Since this is positive, we can multiply each vertex amplitude by $\sqrt{2i+1}$ to take this into account. The theta networks from (2.30) contribute a sign of $(-1)^{\sum_{k=1}^{6} 2i_k}$, where the i_k label the edges incident on the vertex. Since each edge is shared by two vertices, the vertex signs also cancel. The final answer is that the vertex amplitude (2.30) becomes a product of five Wigner-Racah $6j$ symbols multiplied by a product of six factors of the form $\sqrt{2i+1}$.

We observe that in this form the tetrahedral recoupling is equivalent to the dual amplitude formula first proposed by Anishetty et al. [1,2] and later used by Diakonov and Petrov [7]. The same formula was used in the computational work of Dass [8–10]. It should be emphasized that previous derivations of this formula did not make use of the spin foam formalism. As such, the identification of extra labels (those not coming from original plaquettes) with intertwiners was not explicit. We found this distinction between plaquette and intertwiner labels to be a crucial one in constructing our dual gauge theory simulation algorithm (see sections 2.2 and 2.3 of [4]).

Bibliography

[1] Anishetty R, Gadiyar G H, Mathur M, and Sharatchandra H S 1991 Color invariant additive fluxes for $SU(3)$ gauge theory *Physics Letters B* **271** 391–394

[2] Anishetty R, Cheluvaraja S, Sharatchandra H S, and Mathur M 1993 Dual of 3-dimensional pure $SU(2)$ lattice gauge theory and the Ponzano-Regge model *Physics Letters B* **314** 387–390

[3] Carter J S, Flath D E, and Saito M 1995 The classical and quantum $6j$-symbols (*Mathematical Notes* vol 43) (Princeton, NJ: Princeton University Press)

[4] Cherrington J W, Christensen J D, and Khavkine I 2007 Dual computations of non-abelian Yang-Mills on the lattice *Physics Review D* **76** 094503–094519 (*Preprint* arXiv:0705.2629)

[5] Christensen J D and Egan G 2002 An efficient algorithm for the Riemannian $10j$ symbols *Classical and Quantum Gravity* **19** 1184–93 (*Preprint* arXiv:gr-qc/0110045)

[6] Conrady F 2005 Geometric spin foams, Yang-Mills theory, and background-independent models (*Preprint* arXiv:gr-qc/0504059)

[7] Diakonov D and Petrov V 2000 Yang-Mills theory in three dimensions as quantum gravity theory *Journal of Experimental and Theoretical Physics* **91** 873–893

[8] Hari Dass N D 2000 Numerical simulations of $d = 3$ $SU(2)$ LGT in the dual formulation *Nuclear Physics B Proceedings Supplements* **83** 950–952

[9] Hari Dass N D 2001 Quasi-local update algorithms for numerical simulations of $d = 3$ $SU(2)$ LGT in the dual formulation *Nuclear Physics B Proceedings Supplements* **94** 665–669

[10] Hari Dass N D and Shin D 2001 Current status of the numerical simulations of $d = 3$ $SU(2)$ LGT in the dual formulation *Nuclear Physics B Proceedings Supplements* **94** 670–674

[11] Horn D and Zachos C K 1984 Lattice action forms stable under renormalization *Physical Review D* **29** 1202–1206

[12] Kauffman L H and Lins S L 1994 Temperley-Lieb recoupling theory and invariants of 3-manifolds (*Annals of Mathematics Studies* vol 134) (Princeton, NJ: Princeton University Press)

[13] Lang C B, Rebbi C, Salomonson P, and Skagerstam B-S 1981 The transition from strong coupling to weak coupling in the $SU(2)$ lattice gauge theory *Physics Letters B* **101** 173–179

[14] Lang C B, Rebbi C, Salomonson P, and Skagerstam B-S 1982 Definitions of the gauge-theory coupling in lattice and continuum quantum chromodynamics: Implications of change in the lattice action *Physical Review D* **26** 2028–2037

[15] Menotti P and Onofri E 1981 The action of $SU(N)$ lattice gauge theory in terms of the heat kernel on the group manifold *Nuclear Physics B* **190** 288–300

[16] Messiah A. 1962 Quantum Mechanics, Vol. 2 (Amsterdam, Netherlands: North-Holland) pp 1061–1066

[17] Oeckl R and Pfeiffer H 2001 The dual of pure non-Abelian lattice gauge theory as a spin foam model *Nuclear Physics B* **598** 400–426

[18] Oeckl R 2005 Discrete Gauge Theory: From Lattices to TQFT (London, UK: Imperial College Press)

[19] Wilson K G 1974 Confinement of quarks *Physical Review D* **10** 2445–2459

Chapter 3
q-deformed spin foam models of quantum gravity

3.1 Introduction

Spin foam models were first introduced as a space-time alternative to the spin network description of states in loop quantum gravity [3]. The most studied spin foam models are due to Barrett and Crane [8, 9]. A spin foam is a discretization of space-time where the fundamental degrees of freedom are the areas labelling its 2-dimensional faces.

An important goal in the investigation of spin foam models is to obtain predictions that can be compared to the large scale, classical, or semiclassical behavior of gravity. This work continues the numerical investigation of the physical properties of spin foam models of Riemannian quantum gravity begun in [5–7, 13]. In this paper, we extend the computations to the q-deformed Barrett-Crane model and to larger space-time triangulations.

The main applications of q-deformation are two-fold. On the one hand, it can act as a regulator for divergent models, as is apparent in the link between the Ponzano-Regge [27] and Turaev-Viro [31] models. On the other hand, Smolin [30] has argued that q-deformation is necessary to account for a positive cosmological constant. Both of these aspects are explored in more detail in section 3.2.2. A surprising result of our work is evidence that the limit, as the cosmological constant is taken to zero through positive values, is discontinuous.

Large triangulations are necessary to approximate semiclassical space-times. The possibility of obtaining numerical results from larger triangulations takes us one step closer to that goal and increases the number of facets from which the physical properties of a spin foam model may be examined. As an example, we are able to study how the spin-spin correlation varies with the distance between faces in the triangulation.

This paper is structured as follows. We begin in section 3.2 by reviewing the basics of q-deformation and discussing in detail its aforementioned applications. Section 3.3 reviews the details of the Barrett-Crane model, summarizes the necessary changes for its q-deformation, and defines several observables associated to spin foams. In section 3.4, we review the existing numerical simulation techniques and how they need to be generalized to handle q-deformation and larger triangulations. Section 3.5 presents the results of our numerical simulations. In section 3.6, we give our conclusions and list some avenues for future research. The Appendix briefly summarizes our notational conventions and useful formulas.

3.2 Deformation of $\mathfrak{su}(2)$

In this section, we describe the q-deformation of the Lie algebra $\mathfrak{su}(2)$ into the algebra $\mathfrak{su}_q(2)$ (also denoted $U_q(\mathfrak{su}(2))$), the representations of $\mathfrak{su}_q(2)$, and the applications of q-deformation. The deformations of $\mathfrak{spin}(4)$ are then obtained through the isomorphism $\mathfrak{spin}(4) \cong \mathfrak{su}(2) \oplus \mathfrak{su}(2)$.

The following is part of the general subject of *quantum groups* [21]. Here we shall concentrate solely on the $\mathfrak{su}(2)$ and $\mathfrak{spin}(4)$ cases.

3.2.1 The algebra $\mathfrak{su}_q(2)$ and its representations

The Lie algebra $\mathfrak{su}(2)$ is generated by the well known Pauli matrices σ_i, which obey the commutation relations

$$[\sigma_+, \sigma_-] = 4\sigma_3, \quad [\sigma_3, \sigma_+] = 2\sigma_+, \quad [\sigma_3, \sigma_-] = -2\sigma_-, \tag{3.1}$$

where $\sigma_\pm = \sigma_1 \pm i\sigma_2$. The universal enveloping algebra of $\mathfrak{su}(2)$ is the associative algebra generated by $\sigma_\pm$ and σ_3 subject to the above identities, with the Lie bracket being interpreted as $[A, B] = AB - BA$.

The q-deformed algebra $\mathfrak{su}_q(2)$ is constructed by replacing σ_3 with another generator. Formally, it is thought of as $\Sigma = q^{\frac{1}{2}\sigma_3}$, where $q \in \mathbb{C}$ with the exceptions $q \neq 0, 1, -1$. The Lie bracket relations are replaced by the identities

$$[\sigma_+, \sigma_-] = 4\frac{\Sigma^2 - \Sigma^{-2}}{q - q^{-1}}, \quad \Sigma\sigma_+ = q\sigma_+\Sigma, \quad \Sigma\sigma_- = -q\sigma_-\Sigma. \tag{3.2}$$

We can rewrite $q = 1 + 2\varepsilon$ and think of ε as a small complex number. Then, formally at leading order in ε, the substitution $\Sigma = q^{\frac{1}{2}\sigma_3} = 1 + \varepsilon\sigma_3 + O(\varepsilon^2)$ reduces the

deformed identities (3.2) to the standard Lie algebra relations (3.1). The associative algebra generated by $\sigma_\pm$ and σ_3 subject to the deformed identities (3.2) is the algebra $\mathfrak{su}_q(2)$.

For generic q, that is, when q is not a root of unity, the finite-dimensional irreducible representations of $\mathfrak{su}_q(2)$ are classified by a half-integer, $j = 0, 1/2, 1, 3/2, \ldots$, referred to as the *spin*, in direct analogy with the representations of $\mathfrak{su}(2)$ and the theory of angular momentum. The dimension of the representation j is $2j+1$. When $q = \exp(i\pi/r)$ is a $2r$th root of unity (ROU), where $r > 2$ is an integer called the ROU parameter, the representations j are still defined, but become reducible for $j > (r-2)/2$. They decompose into a sum of representations with spin at most $(r-2)/2$ and so-called *trace 0* ones, whose nature will be explained below.

For the purposes of this paper we are concerned only with intertwiners between representations of $\mathfrak{su}_q(2)$, i.e., linear maps commuting with the action of the algebra, and their (quantum) traces[1].

Any such intertwiner can be constructed from a small set of generators and elementary operations on them. These constructions, as well as traces, can be represented graphically. Such graphs are called *(abstract) spin networks*. Their calculus is well developed and is described in [18], whose conventions we follow throughout the paper with one exception: we use spins (half-integers) instead of twice-spins (integers). A brief review of our notation and conventions can be found in the Appendix.

Trace 0 representations of $\mathfrak{su}_q(2)$ are so called because the trace of an intertwiner from such a representation to itself is always zero. Thus, they can be freely discarded, as they do not contribute to the evaluation of q-deformed spin networks.

3.2.2 Applications of q-deformation

Deformation, especially with $q = \exp(i\pi/r)$ a $2r$th primitive ROU, is important for spin foam models for at least two reasons. Replacing $q = 1$ by some ROU can act as a regulator for a model whose partition function and observable values are otherwise divergent. Also, $\mathfrak{su}_q(2)$ spin networks[2] naturally appear when considering a positive cosmological constant in loop quantum gravity.

---

1. When $q = 1$, this notion of trace reduces up to sign to the usual trace of a linear map, but is slightly different otherwise, cf. [10, Chapter 4].

2. These are graphs embedded in a 3-manifold, labelled by representations of $\mathfrak{su}_q(2)$. They are similar to but distinct from the abstract spin networks referred to above. See [4] for the distinction.

The original Ponzano-Regge model [27] attempts to express the path integral for 3-dimensional Riemannian general relativity as a sum over labelled triangulations of a 3-manifold. The edges of the triangulation are labelled by discrete lengths, identified with spin labels of irreducible $SU(2)$ representations. Each tetrahedron contributes a $6j$-symbol factor to the summand, normalized to ensure invariance of the overall sum under change of triangulation. Unfortunately, the Ponzano-Regge model turned out to be divergent. Motivated by the construction of 3-manifold invariants, Turaev and Viro were able to regularize the Ponzano-Regge model [1,31] by replacing the $SU(2)$ $6j$-symbols with their q-deformed analogs at a ROU q. The key feature of the regularization is the truncation of the summation to only the irreducible representations of $\mathfrak{su}_q(2)$ of non-zero trace, which leaves only a finite number of terms in the model's partition function.

A version of the Barrett-Crane model, derived from a group field theory by De Pietri, Freidel, Krasnov and Rovelli [16] (DFKR for short), was also found to be divergent. A q-deformed version of the same model at a ROU q is similarly regularized (see section 3.3.2). Some numerical results for the regularized version of this model are given in section 3.5.2.

The argument linking q-deformation to the presence of a positive cosmological constant is due to Smolin [29] and is given in more refined form in [30]. It is briefly summarized as follows. Loop quantum gravity begins by writing the degrees of freedom of general relativity in terms of an $SU(2)$ connection on a spatial slice and the slice's extrinsic curvature. A state in the Schrödinger picture, a wave function on the space of connections, can be constructed by integrating the Chern-Simons 3-form over the spatial slice. This state, known as the Kodama state, simultaneously satisfies all the canonical constraints of the theory and semiclassically approximates de Sitter spacetime, which is a solution of the vacuum Einstein equations with a positive cosmological constant. The requirement that the Kodama state also be invariant under large gauge transformations implies discretization of the cosmological constant, $\Lambda \sim 1/r$, with r a positive integer. The coefficients of the Kodama state in the spin network basis are obtained by evaluating the labelled graph, associated to a basis state, as an abstract $\mathfrak{su}_q(2)$ spin network. Here the deformation parameter q is a ROU, $q = \exp(i\pi/r)$, where the ROU parameter r is identified with the discretization parameter of the cosmological constant.

Given the heuristic link [4] between spin networks of loop quantum gravity and spin foams, it is natural to q-deform a spin foam model as an attempt to account for a positive cosmological constant. With this aim, Noui and Roche [23] have given

a q-deformed version of the Lorentzian Barrett-Crane model. The possibility of q-deformation has been with the Riemannian Barrett-Crane model since its inception [8] and all the necessary ingredients have been present in the literature for some time. In the next section these details are collected in a form ready for numerical investigation.

3.3 Deformation of the Barrett-Crane model

Consider a triangulated 4-manifold. Let Δ_n denote the set of n-dimensional simplices of the triangulation. The dual 2-skeleton is formed by associating a dual vertex, edge and polygonal face to each 4-simplex, tetrahedron, and triangle of the triangulation, respectively. A *spin foam* is an assignment of labels, usually called spins, to the dual faces of the dual 2-skeleton. Each dual edge has 4 spins incident on it, while each dual vertex has 10. A *spin foam model* assigns amplitudes A_F, A_E and A_V, that depend on all the incident spins, to each dual face, edge and vertex, respectively. The amplitude $Z(F)$ assigned to a spin foam F is the product of the amplitudes for individual cells of the 2-complex, while the total amplitude Z_{tot} assigned to a triangulation is obtained by summing over all spin foams based on the triangulation:

$$Z(F) = \prod_{f \in \Delta_2} A_F(f) \prod_{e \in \Delta_3} A_E(e) \prod_{v \in \Delta_4} A_V(v), \quad Z_{\text{tot}} = \sum_F Z(F). \tag{3.3}$$

Some models, such as those based on group field theory [16, 17, 24], also include a sum over triangulations in the definition of the total partition function.

3.3.1 Review of the undeformed model

The Riemannian Barrett-Crane model was first proposed in [8]. Its relation to the Crane-Yetter [15] spin foam model is analogous to the relation of the Plebanski [26] formulation of general relativity (GR) to 4-dimensional BF theory with Spin(4) as the structure group. Both BF theory and the Crane-Yetter model are topological and the latter is considered a quantization of the former [2]. In the Plebanski formulation, GR is a constrained version of BF theory. Similarly, the Barrett-Crane model restricts the spin labels summed over in the Crane-Yetter model. With this restriction, Barrett and Crane hoped to produce a discrete model of quantum (Riemannian) GR.

3.3.1.1 Dual vertex amplitude

All amplitudes are defined in terms of $\mathfrak{spin}(4)$ spin networks. However, given the isomorphism $\mathfrak{spin}(4) \cong \mathfrak{su}(2) \oplus \mathfrak{su}(2)$, all irreducible representations of $\mathfrak{spin}(4)$ can be written as tensor products of irreducible representations of $\mathfrak{su}(2)$. The Barrett-Crane model specifically limits itself to *balanced* representations, which are of the form $j \otimes j$, where j is the irreducible representation of $\mathfrak{su}(2)$ of spin j. Since the tensor product corresponds to a juxtaposition of edges in a spin network, any $\mathfrak{spin}(4)$ spin network may be written as an $\mathfrak{su}(2)$ spin network where an edge labelled $j \otimes j$ is replaced by two parallel edges, each labelled j. To avoid redundancy of notation, we use a single j instead of $j \otimes j$ to label $\mathfrak{spin}(4)$ spin network edges. We then distinguish them from $\mathfrak{su}(2)$ networks by placing a bold dot at every vertex.

The Barrett-Crane vertex is an intertwiner between four balanced representations:

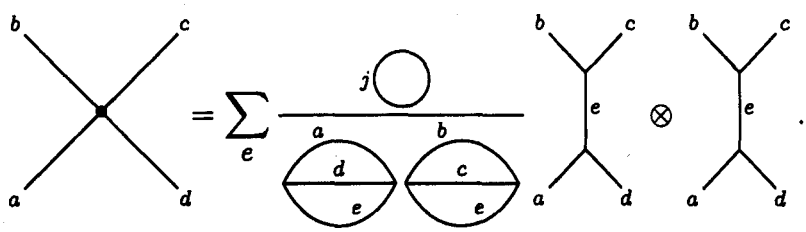

(3.4)

The graphs on the right hand side of the definition are $\mathfrak{su}(2)$ spin networks and the sum runs over all admissible labels e. The graphical notation and the conditions for admissibility are defined in the Appendix.

The above expression defines the Barrett-Crane vertex in a way that breaks rotational symmetry. However, it can be shown that the vertex is in fact rotationally symmetric. Up to normalization, this property makes the Barrett-Crane vertex unique [28]. The above formula defines a *vertical splitting* of the vertex. A ninety degree rotation will define an analogous *horizontal splitting*. Both possibilities are important in the derivation of the algorithm presented in section 3.4.1.

Given a 4-simplex v of a triangulation, the corresponding vertex of the dual 2-complex is assigned the amplitude

$A_V(v) =$

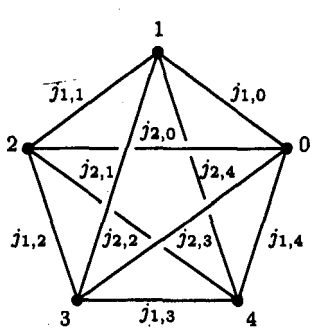

(3.5)

This spin network is called the $10j$-*symbol.* The 4-simplex v is bounded by five tetrahedra, which correspond to the vertices of the $10j$ graph. The four edges incident on a vertex correspond to the four faces of the corresponding tetrahedron; the spin labels are assigned accordingly. The edge joining two vertices corresponds to the face shared by corresponding tetrahedra. Evaluation of the $10j$-symbol is discussed in section 3.4.1. While the crossing structure depicted above is immaterial in the undeformed case, it is essential at nontrivial values of q. It is given here for reference.

3.3.1.2 Dual edge and face amplitudes

The original paper of Barrett and Crane did not specify dual edge and face amplitudes. Three different dual edge and face amplitude assignments were considered in a previous paper [7]. We concentrate on the same possibilities.

For the Perez-Rovelli model [25], we have

$$A_F(f) = j\bigcirc, \qquad A_E(e) = \frac{\overset{j_1}{\underset{j_4}{\overset{j_2}{\underset{j_3}{\bigcirc}}}}}{j_1\bigcirc\, j_2\bigcirc\, j_3\bigcirc\, j_4\bigcirc}. \tag{3.6}$$

For the DFKR model [16], we have

$$A_F(f) = j\bigcirc, \qquad A_E(e) = \frac{1}{\overset{j_1}{\underset{j_4}{\overset{j_2}{\underset{j_3}{\bigcirc}}}}}. \tag{3.7}$$

For the Baez-Christensen model [7], we have

$$A_F(f) = 1, \qquad A_E(e) = \frac{1}{\overset{j_1}{\underset{j_4}{\overset{j_2}{\underset{j_3}{\bigcirc}}}}}. \tag{3.8}$$

The bubble diagram, when translated into $su(2)$ spin networks, corresponds to

two bubbles (see Appendix)

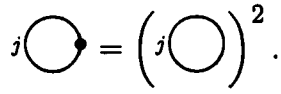

(3.9)

and evaluates to $(2j+1)^2$.

The so-called *eye diagram* simply counts the dimension of the space of 4-valent intertwiners, which is also the number of admissible e-edges summed over in equation (3.4). In symmetric form, it is given by

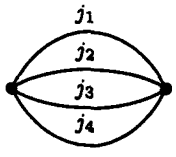

$$= \begin{cases} 1 + \min\{2j, s - 2J\} & \text{if positive and } s \text{ is integral,} \\ 0 & \text{otherwise,} \end{cases} \tag{3.10}$$

where $s = \sum_k j_k$, $j = \min_k j_k$, and $J = \max_k j_k$.

3.3.2 The q-deformed model

Thanks to graphical notation, the q-deformation of the spin foam amplitudes described above is straightforward, with only a few subtleties. The main distinction is that q-deformed graphs are actually ribbon (framed) graphs with braiding. Thus, any undeformed spin network has to be supplemented with information about twists and crossings before evaluation.

In [32], Yetter generalized the Barrett-Crane 4-vertex for a q-deformed version of $\mathfrak{spin}(4)$. Since $\mathfrak{spin}(4) \cong \mathfrak{su}(2) \oplus \mathfrak{su}(2)$, there is a two parameter family of possible deformations of the Lie algebra, $\mathfrak{spin}_{q,q'}(4) \cong \mathfrak{su}_q(2) \oplus \mathfrak{su}_{q'}(2)$. Yetter singles out the one parameter family $q' = q^{-1}$, restricted to balanced representations, since it preserves the invariance of the Barrett-Crane vertex under rotations. This family also has especially simple curl and twist identities:

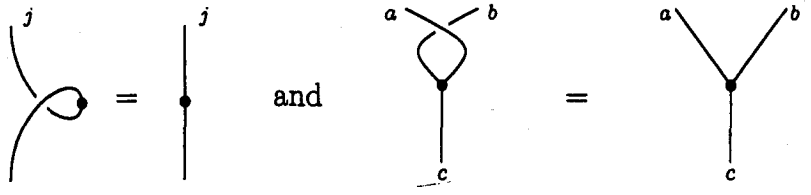

, (3.11)

where the left factor of $j \otimes j$ corresponds to $\mathfrak{su}_q(2)$ and the right one to $\mathfrak{su}_{q^{-1}}(2)$, and the 3-vertex is the obvious juxtaposition of two $\mathfrak{su}_q(2)$ and $\mathfrak{su}_{q^{-1}}(2)$ 3-vertices. Once this deformation is adopted, the ribbon structure can be ignored [32], so one

only needs to specify the crossing structure for a given $\mathfrak{spin}(4)$ spin network to obtain a well-defined q-evaluation.

There are three basic graphs needed to define the Barrett-Crane simplex amplitudes: the bubble, the eye, and the $10j$-symbol. The evaluation of the bubble graph, equation (3.9), is $[2j+1]^2$, where the quantum integer $[2j+1]$ is defined in the Appendix. Remarkably, the value of the eye diagram turns out not to depend on q and its value is still given by equation (3.10). The only exception is when q is a ROU with parameter r. Then, the dimension of the space of 4-valent intertwiners changes to

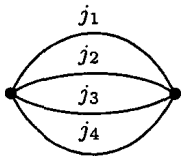

$$= \begin{cases} \min \left\{ \begin{array}{r} 1 + \min\{2j, s-2J\} \\ r - 1 - \max\{2J, s-2j\} \end{array} \right\} & \text{if positive and} \\ & s \text{ is integral,} \\ 0 & \text{otherwise,} \end{cases} \tag{3.12}$$

where again $s = \sum_k j_k$, $j = \min_k j_k$, and $J = \max_k j_k$.

The $10j$-symbol is the only network with a non-planar graph. Originally, it was defined in terms of the $15j$-symbol from the Crane-Yetter model. This $15j$-symbol was defined with q-deformation in mind, so its crossing and ribbon structure was fully specified [14, section 3]. Adapted to the $10j$-graph, it can be summarized as follows: *Consider a 4-simplex. The dual 1-skeleton of the boundary has five dual vertices and ten dual edges, and is the complete graph K_5 on these five dual vertices. If we remove one of the (non-dual) vertices from the boundary of the 4-simplex, what remains is homeomorphic to $\mathbb{R}^3$. For any such homeomorphism, the embedding of K_5 into $\mathbb{R}^3$ can be projected onto a 2-dimensional plane. The crossing structure of the $10j$ graph is defined by such a projection.* It is illustrated in equation (3.5). Although, with crossings, the $10j$ graph is no longer manifestly invariant under permutations of its vertices, it can be shown to be so.

3.3.3 Observables

The definition of observables in a spin foam model of quantum gravity is still open to interpretation (see section 6 of [7] for a brief discussion). For a fixed spin foam, the half-integer spin labels of its faces are the fundamental variables of the model. Practically speaking, any observable of a spin foam model should be an expectation value of some function $O(F)$ of the spin labels of a spin foam F, averaged over all

spin foams with amplitudes specified by equation (3.3):

$$\langle O \rangle = \sum_F \frac{O(F)Z(F)}{Z_{\text{tot}}}. \tag{3.13}$$

In this paper we choose to concentrate on a few observables representative of the kind of quantities computable in a spin foam model. As before, fix a triangulation of a 4-manifold, let Δ_2 represent the set of its faces and let $j\colon \Delta_2 \to \{0, 1/2, 1, \ldots\}$ be the spin labelling. We define:

$$J(F) = \frac{1}{|\Delta_2|} \sum_{f \in \Delta_2} \lfloor j(f) \rceil\,, \tag{3.14}$$

$$(\delta J)^2(F) = \frac{1}{|\Delta_2|} \sum_{f \in \Delta_2} (\lfloor j(f) \rceil - \langle J \rangle)^2\,, \tag{3.15}$$

$$A(F) = \frac{1}{|\Delta_2|} \sum_{f \in \Delta_2} \sqrt{\lfloor j(f) \rceil \, \lfloor j(f) + 1 \rceil}, \tag{3.16}$$

$$C_d(F) = \frac{1}{N_d} \sum_{\substack{f, f' \in \Delta_2 \\ \text{dist}(f,f')=d}} \frac{\lfloor j(f) \rceil \, \lfloor j(f') \rceil - \langle J \rangle^2}{\langle (\delta J)^2 \rangle}. \tag{3.17}$$

where $\lfloor n \rceil$ denotes a quantum half-integer (see Appendix), $|\cdot|$ denotes cardinality, $\text{dist}(f, f')$ denotes the distance between faces, and N_d is a normalization factor (see below for the definition of distance and N_d). These observables represent *average spin per face*, *variance of spin per face*, *average area per face*, and *spin-spin correlation* as a function of d.

The choice of observables given above is somewhat arbitrary. For instance, there are several subtly distinct choices for the expression for $(\delta J)^2$. Fortunately, they all yield expectation values that are nearly identical. The expression given above has the technical advantage of falling into the class of so-called *single spin observables*. These are observables whose expectation value can be directly obtained from the knowledge of probability with which spin j occurs on any face of a spin foam. All of J, $(\delta J)^2$, and A are single spin observables, while C_d is not.

Note that on a fixed triangulation with no other background geometry, there is no physical notion of distance. We can, instead, define a combinatorial analog. For any two faces f and f' of a given triangulation, let $\text{dist}(f, f')$ be the smallest number of face-sharing tetrahedra that connect f to f'. Given the discrete structure of our spacetime model, it is conceivable that this combinatorial distance, multiplied by a

fundamental unit of length, approximates some notion of distance derived from the dynamical geometry of the spin foam model.

The correlation function C_d may be thought of as analogous to a normalized 2-point function of quantum field theory. The *d-degree* of face f is the number of faces f' such that $\mathrm{dist}(f, f') = d$. If the d-degree of every face is the same, the normalization factor N_d can be taken to be the number of terms in the sum (3.17), that is, the number of face pairs separated by distance d. This choice ensures the inequality $|C_d| \leq 1$. If not all faces have the same d-degree, then the normalization factor has to be modified to

$$N_d = |\Delta_2| D_d, \tag{3.18}$$

where D_d is the maximum d-degree of a face, which reduces to the simpler definition in the case of uniform d-degree.

The choice of the q-dependent expression $\lfloor j \rceil$, instead of simply using the half-integer j, is motivated in section 3.5.1. For some q, the argument of the square root in $A(F)$ may be negative or even complex. In that case, a branch choice will have to be made. Luckily, if $q = 1$, q is a ROU, or q is real, the expression under the square root is always non-negative.

3.4 Numerical simulation

The key development that made possible numerical simulation of variations of the (undeformed) Barrett-Crane model [6, 7] is the development by Christensen and Egan of a fast algorithm for evaluating $10j$-symbols [13]. In this section, we show how this algorithm generalizes to the q-deformed case and discuss numerical evaluation of observables for the previously described spin foam models.

3.4.1 The q-deformation of the fast $10j$ algorithm

The derivation of the Christensen-Egan algorithm given in [13] is contingent on the possibility of splitting the Barrett-Crane 4-vertex as in equation (3.4) and on the recoupling identity, equation (3.43) of the Appendix. Both identities still hold in the q-deformed case. The validity of the 4-vertex splitting was proved by Yetter [32] and the recoupling identity is a standard part of $\mathfrak{su}_q(2)$ representation theory.

The only remaining detail of the algorithm's generalization is the crossing structure of the $10j$ graph, which was established in section 3.3.2. However, its only consequence is an extra factor from the twist implicit in the bubble diagram of section 4

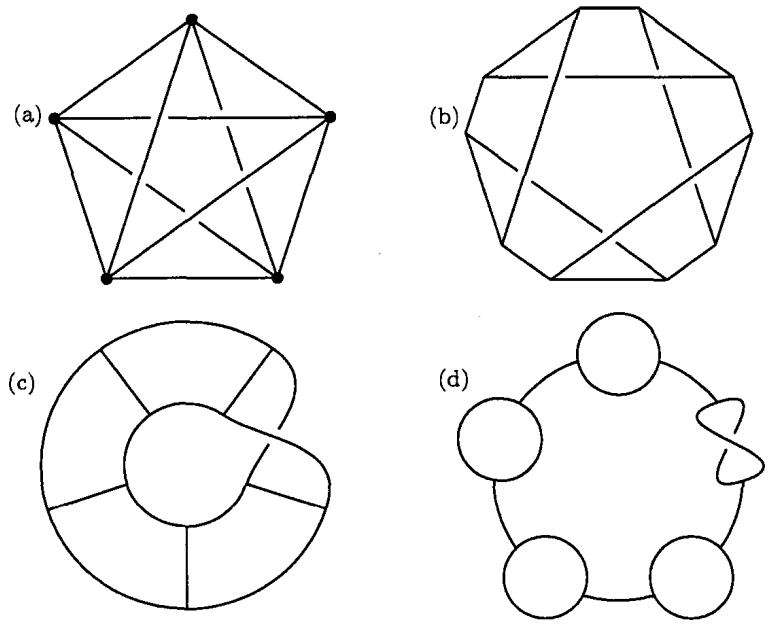

Figure 3.1: In reference to [13], (a) corresponds to equation (1), (b) corresponds to equation (2), while (c) and (d) correspond to the "ladder" and "bubble" diagrams of section 4, respectively. The illustrated twist introduces the explicitly q-dependent factor into equation (3.20).

of [13], cf. equation (3.50) of the Appendix. We will not reproduce the derivation of the algorithm here. However, the way in which the twist arises is schematically illustrated in figure 3.1. Note that the triviality of the twist for Yetter's balanced representations, equation (3.11), does not apply here since the twist occurs separately in distinct $\mathfrak{su}_q(2)$ networks.

The algorithm itself can be summarized in the following form:

$$\{10j\} = (-)^{2S} \sum_{m_1,m_2} \phi \,\mathrm{tr}[M_4 M_3 M_2 M_1 M_0]. \tag{3.19}$$

The $10j$-symbol depends on the ten spins $j_{i,k}$, $(i = 1, 2,\ k = 0, \ldots, 4)$ specified in equation (3.5). The overall prefactor depends on the total spin $S = \sum_{i,k} j_{i,k}$ and the per-term prefactor is

$$\phi = (-)^{m_1 - m_2}[2m_1 + 1][2m_2 + 1]q^{m_1(m_1+1) - m_2(m_2+1)}. \tag{3.20}$$

The exponents of $(-)$ and q are always integers. The M_k are matrices (not all of the same size) of dimensions compatible with the five-fold product and trace. Their

matrix elements are

$$(M_k)_{l_k}^{l_{k+1}} = \frac{[2l_k+1](T_1)_{l_k}^{l_{k+1}}(T_2)_{l_k}^{l_{k+1}}}{\theta(j_{2,k-1}, l_{k+1}, j_{1,k})\,\theta(j_{2,k+1}, l_{k+1}, j_{1,k+1})}, \tag{3.21}$$

$$(T_i)_{l_k}^{l_{k+1}} = \frac{\mathrm{Tet}\begin{bmatrix} l_k & j_{2,k} & m_i \\ l_{k+1} & j_{2,k-1} & j_{1,k} \end{bmatrix}}{\theta(j_{2,k}, l_{k+1}, m_i)}. \tag{3.22}$$

The quantum integers $[n]$, as well as the theta $\theta(a,b,c)$ and tetrahedral $\mathrm{Tet}[\cdots]$ $\mathfrak{su}_q(2)$ spin networks are defined in the Appendix.

The quantities l_k and m_i are spin labels (half-integers). They are constrained by admissibility conditions (parity conditions and triangle inequalities). The parity of each index is determined by the conditions

$$l_k \equiv j_{1,k} + j_{2,k} \equiv j_{1,k-1} + j_{2,k-2}, \tag{3.23}$$

$$m_i \equiv l_k + j_{2,k-1}, \tag{3.24}$$

for $i = 1,2$ and $k = 0,\ldots,4$, where $\equiv$ denotes equivalence mod 1 and the second subscript of j is taken mod 5. Summation bounds are determined by the triangle inequalities, which must be checked for each trivalent vertex introduced in the derivation of the algorithm. They boil down to

$$\mathrm{lb}_3(j_{1,k}, j_{2,k}, j_{2,k-1}) \le m_i \le j_{1,k} + j_{2,k} + j_{2,k-1}, \tag{3.25}$$

$$|j_{1,k-1} - j_{2,k-2}| \le l_k \le j_{1,k-1} + j_{2,k-2}, \tag{3.26}$$

$$|j_{1,k} - j_{2,k}| \le l_k \le j_{1,k} + j_{2,k}, \tag{3.27}$$

$$|m_i - j_{2,k-1}| \le l_k \le m_i + j_{2,k-1}, \tag{3.28}$$

for $i = 1,2$ and $k = 0,\ldots,4$, where we have used the notation

$$\mathrm{lb}_3(a,b,c) = 2\max\{a,b,c\} - (a+b+c). \tag{3.29}$$

When $q = \exp(i\pi/r)$ is a ROU, extra inequalities must be taken into account to

exclude summation over reducible representations. These are

$$m_i \geq j_{1,k} + j_{2,k} + j_{2,k-1} - (r-2), \tag{3.30}$$

$$m_i \leq \mathrm{ub}_3(j_{1,k}, j_{2,k}, j_{2,k-1}) + (r-2), \tag{3.31}$$

$$l_k \leq (r-2) - (j_{1,k} + j_{2,k}), \tag{3.32}$$

$$l_k \leq (r-2) - (j_{1,k-1} + j_{2,k-2}), \tag{3.33}$$

$$l_k \leq (r-2) - (m + j_{2,k-1}), \tag{3.34}$$

where now

$$\mathrm{ub}_3(a,b,c) = 2\min\{a,b,c\} - (a+b+c).$$

If any of the parity constraints or inequalities cannot be satisfied, the $10j$-symbol evaluates to zero.

This algorithm has been implemented and tested in the $q = 1$ and ROU cases, for both j and r up to several hundreds. Unfortunately, for generic q, when $Q = \max\{|q|, |q|^{-1}\} > 1$, the quantum integers grow exponentially as $|[n]| \sim Q^n$. Such a rapid growth makes the sums involved in this algorithm numerically unstable. It is still possible to use this algorithm with Q close to 1 or symbolically, using rational functions of q instead of limited precision floating point numbers. Symbolic computation is, however, significantly slower (by up to a factor of 10^6) than its floating point counterpart. The software library `spinnet` which implements these and other spin network evaluations is available from the authors and will be described in a future publication.

3.4.2 Positivity and statistical methods

The sums involved in evaluating expectation values of observables, as in equation (3.13), are very high-dimensional. For instance, a minimal triangulation of the 4-sphere (seen as the boundary of a 5-simplex) contains 20 faces. Hence, any brute force evaluation of an expectation value, even on such a small lattice, involves a sum over the 20-dimensional space of half-integer spin labels.

Fortunately, in the undeformed case, the total amplitude $Z(F)$ for a closed spin foam is never negative[3] [5]. The proof for the $q = 1$ case generalizes to the ROU case. One need only realize two facts. The first is that, in the ROU case, quantum integers are non-negative. The second is that, for q a ROU, an $\mathfrak{su}_{q^{-1}}(2)$ spin network

3. We expect the same thing to hold in Lorentzian signature [5, 12].

evaluates to the complex conjugate of the corresponding $su_q(2)$ spin network. The disjoint union of any two such spin networks evaluates to their product, the absolute value squared of either of them, and hence is non-negative. Then, the same positivity result follows as from equation (1) of [5]. This positivity allows us to treat $Z(F)$ as a statistical distribution and use Monte Carlo methods to extract expectation values with much greater efficiency than brute force summation.

The main tool for evaluating expectation values is the Metropolis algorithm [20, 22]. The algorithm consists of a walk on the space of spin labellings. Each step is randomly picked from a set of *elementary moves* and is either accepted or rejected based on the relative amplitudes of spin foam configurations before and after the move. An expectation value is extracted as the average of the observable over the configurations constituting the walk. Elementary moves for spin foam simulations are discussed in the next section.

A Metropolis-like algorithm is possible even if individual spin foam amplitudes $Z(F)$ are negative or even complex. However, if the total partition function Z_{tot} sums to zero, then the expectation values in equation (3.13) become ill defined. Moreover, in numerical simulations, if Z_{tot} is even close to zero, expectation value estimates may exhibit great loss of precision and slow convergence. In the path-integral Monte Carlo literature, this situation is known as the *sign problem* [11]. Still, the sign problem need not occur or, depending on the severity of the problem, there may be ways of effectively dealing with it.

Independent Metropolis runs can be thought of as providing independent estimates of a given expectation value. Thus, the error in the computed value of an observable can be estimated through the standard deviation of the results of many independent simulation runs [19].

3.4.3 Elementary moves for spin foams

The choice of elementary moves for spin foam simulations must satisfy several criteria. Theoretically, the most important one is ergodicity. That is, any spin foam must be able to transform into any other one through a sequence of elementary moves which avoid configurations with zero amplitude. Practically, it is important that these moves usually preserve admissibility. A spin foam F is called *admissible* if the associated amplitude $Z(F)$ is non-zero. If, starting with an admissible spin foam, most elementary moves produce an inadmissible spin foam, the simulation will spend a lot of time rejecting such moves without any practical benefit.

As before, consider a fixed triangulation of a compact 4-manifold. The parity conditions (3.23) imposed on the $j_{i,k}$,

$$j_{1,k} + j_{2,k} \equiv j_{1,k-1} + j_{2,k-2}, \quad 0 \leq k \leq 4,$$

when taken together with the total spin foam amplitude (3.3), provide strong constraints on admissible spin foams. One can show that a move that changes spin labels by $\pm 1/2 \pmod 1$ on each face of a closed surface in the dual 2-skeleton preserves the parity constraint. Essentially, the problem of finding a set of ergodic moves for the space of admissible spin foams boils down to finding a basis for the space of closed 2-chains with integer coefficients on the dual 2-skeleton. We take as the elementary moves the moves that change the spin labels by $\pm 1/2$ on the boundaries of the dual 3-cells of the dual 3-complex; the dual 3-cells correspond to the edges of the triangulation. If the manifold has non-trivial mod 2 homology in dimension 2, additional moves would be necessary for ergodicity, but for the examples we consider the moves above suffice. From a practical point of view, extra moves might improve the simulation's equilibration time. For instance, in the ROU case, parity preserving moves that change the spins from 0 to $(r-2)/2$ or $(r-3)/2$ were introduced, since spins close to either admissible extreme may have large amplitudes. This property of the Perez-Rovelli and Baez-Christensen models is illustrated in the following section.

Unfortunately, the inequalities constraining spin labels do not have a similar geometric interpretation and cannot be used to easily restrict the set of elementary moves in advance.

3.5 Results

Using methods described in the previous section, we ran simulations of the three variations of the Barrett-Crane model described in section 3.3 and obtained expectation values for observables listed in section 3.3.3. While previous work [7] performed simulations only on the minimal triangulation of the 4-sphere, which we will refer to simply as the *minimal triangulation*, we have extended the same techniques to arbitrary triangulations of closed manifolds.

3.5.1 Discontinuity of the $r \to \infty$ limit

The most striking result we can report is a discontinuity in the transition to the limit $r \to \infty$, where r, a positive integer, is the ROU parameter with $q = \exp(i\pi/r)$. As

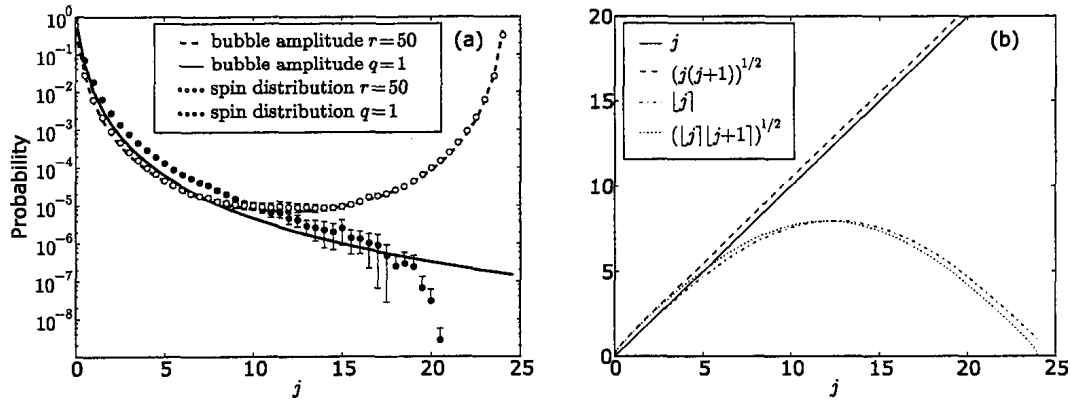

Figure 3.2: (a) Single spin distribution and single bubble amplitude for the Baez-Christensen model. The distribution was obtained from 10^9 steps of Metropolis simulation on a triangulation with 202 faces (cf. section 3.5.3). (b) Some single spin observables as functions of j, with $r = 50$.

$r \to \infty$, the deformation parameter q tends to its classical value 1. If we interpret the cosmological constant as inversely proportional to r, $\Lambda \sim 1/r$, this limit also corresponds to $\Lambda \to 0$, through positive values. For a fixed spin foam, the amplitudes and observables we study tend continuously to their undeformed values as $r \to \infty$. However, we find that observable *expectation values* do not tend to their undeformed values in the same limit, that is, $\langle O \rangle_r \not\to \langle O \rangle_{q=1}$ as $r \to \infty$.

The discontinuity is most simply illustrated with the *single spin distribution*, that is the probability of finding spin j at any spin foam face. This probability can be estimated from the histogram of all spin labels that have occurred during a Monte Carlo simulation. The points in figure 3.2(a) show the single spin distributions for the Baez-Christensen model with $r = 50$ and $q = 1$. The curves show the corresponding *single bubble* amplitude. It is the amplitude $Z(F_j)$ of a spin foam F_j with all spin labels zero, except for the boundary of an elementary dual 3-cell, whose faces are all labelled with spin j. The amplitudes and distributions are normalized as probability distributions so their sums over j yield 1. The similarity between the points and the continuous curves is consistent with the hypothesis that spin foams with isolated bubbles dominate the partition function sum. The behavior of the single spin distribution for the Perez-Rovelli model is very similar, except that its peaks are much more pronounced.

Note that the undeformed single spin distribution has a single peak at $j = 0$, while the $r = 50$ case has two peaks, one at $j = 0$ and the other at $j = (r-2)/2$, the largest non-trace 0 irreducible representation. The bimodal nature of the single spin distribution has an important impact on the large r behavior of observable expectation

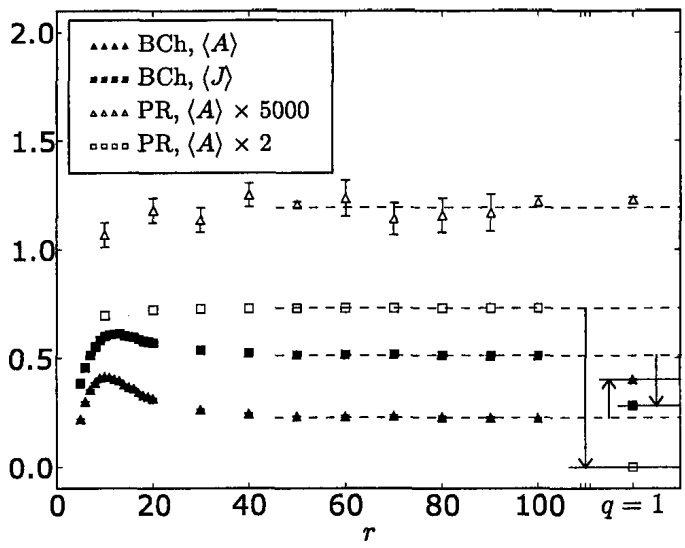

Figure 3.3: Observables for the Baez-Christensen (BCh) and Perez-Rovelli (PR) models as functions of the ROU parameter r. For large r, observables do not in general tend to their undeformed, $q = 1$, values; arrows show the deviation. Some observables were scaled to fit on the graph. Data is from Metropolis simulations on the minimal triangulation.

values, as is most easily seen with single spin observables (section 3.3.3). For instance, if we consider the average, $\bar{j}$, of the half-integers j, the large j peak would dominate the expectation value and $\langle \bar{j} \rangle$ would diverge linearly in r, as $r \to \infty$. On the other hand, since J is the average of the quantum half-integers $\lfloor j \rceil$, $\langle J \rangle$ at least approaches a constant in the same limit. This is illustrated in figure 3.2(b).

However, as shown in figure 3.3, this limit is not the same as the undeformed expectation value. At the same time, as can be seen from the plot of the Perez-Rovelli average area in the same figure, there are some observables whose large r limits are at least very close to the undeformed values. The area observable summand $A_j = \sqrt{\lfloor j \rceil \lfloor j+1 \rceil}$ is exactly zero at both $j = 0$ and $j = (r-2)/2$, while the spin observable summand $J_j = \lfloor j \rceil$ is zero at $j = 0$ but still positive at $j = (r-2)/2$, figure 3.2(b). The large j peak of the Perez-Rovelli model is very narrow and thus the expectation value of a single spin observable is strongly influenced by its value at $j = (r-2)/2$.

The data for larger triangulations is qualitatively similar.

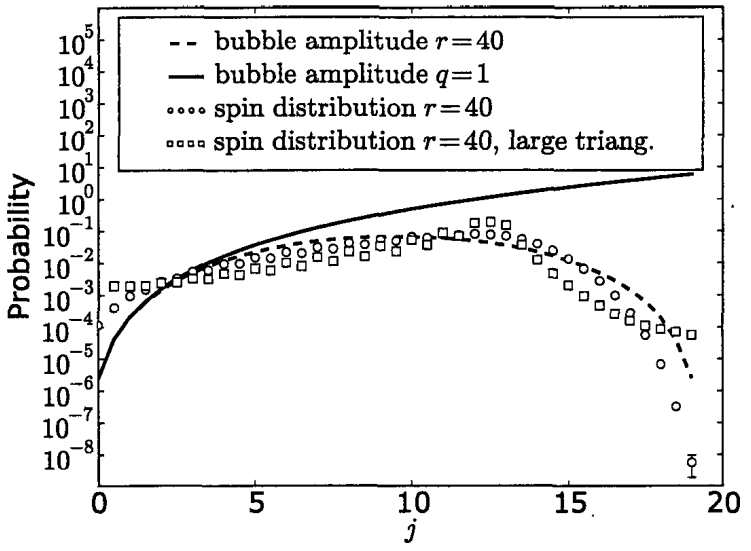

Figure 3.4: Single spin distributions and single bubble amplitudes for the DFKR model. The distributions were obtained from 10^9 steps of Metropolis simulation on the minimal triangulation and on a triangulation with 202 faces (cf. section 3.5.3).

3.5.2 Regularization of the DFKR model

As expected, the ROU deformation of the DFKR model yields a finite partition function and finite expectation values. For instance, its single spin distribution for $r = 40$ is illustrated in figure 3.4. The divergence of the amplitude for large spins in the undeformed, $q = 1$, case makes numerical simulation impossible without an artificial spin cutoff. Thus, we do not have an undeformed analog of the single spin distribution. For the minimal triangulation, the ROU spin distribution deviates slightly from the single bubble amplitude close to the boundaries of admissible j. For the larger triangulation, the deviation is much more pronounced and is not restricted to the edges. This suggests that there are other significant contributions to the partition function besides single bubble spin foams.

Note the large weight associated with spins around $j = r/4$. Around this value of j, both the area $A_j = \sqrt{\lfloor j \rfloor \lfloor j+1 \rfloor}$ and the spin $J_j = \lfloor j \rfloor$ attain their maximal values and are proportional to r. Thus, it is natural to expect their expectation values to grow linearly in r, which is consistent with the divergent nature of the undeformed DFKR model. This is precisely the behavior shown in figure 3.5. On the minimal triangulation, the best linear fits for the average spin expectation value and for the

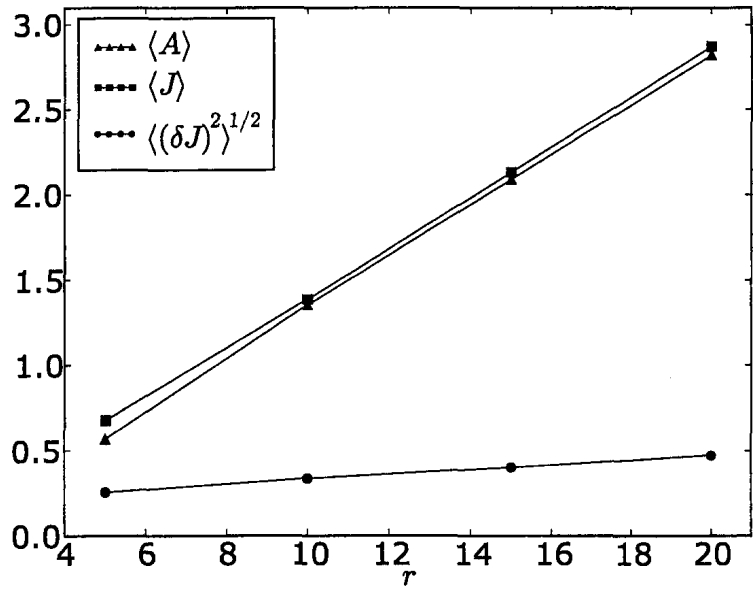

Figure 3.5: Observables for the DFKR model: area $\langle A \rangle$, average spin $\langle J \rangle$, spin standard deviation $\sqrt{\langle (\delta J)^2 \rangle}$. Metropolis simulation, minimal triangulation. Error bars are smaller than the data points.

square root of the average spin variance are

$$\langle J \rangle_r = 0.146\, r - 0.064, \tag{3.35}$$

$$\left\langle (\delta J)^2 \right\rangle_r^{1/2} = 0.014\, r + 0.187. \tag{3.36}$$

For larger triangulations, the dependence of these observables is also approximately linear in r, with only slight variation in the effective slope.

3.5.3 Spin-spin correlation

The ability to work with larger lattices allows us to explore a broader range of observables. One of them is the spin-spin correlation function C_d defined in section 3.3.3. In general $\langle C_0 \rangle = 1$ and $\langle C_d \rangle \to 0$ for large d. The decay of the correlation shows how quickly the spin labels on different spin foam faces become independent. A positive value of $\langle C_d \rangle$ indicates that, on average, any two faces distance d apart both have spins above (or both below) the mean $\langle J \rangle$. On the other hand, a negative value of $\langle C_d \rangle$ indicates that, on average, any two faces distance d apart have one spin above and one below the mean $\langle J \rangle$.

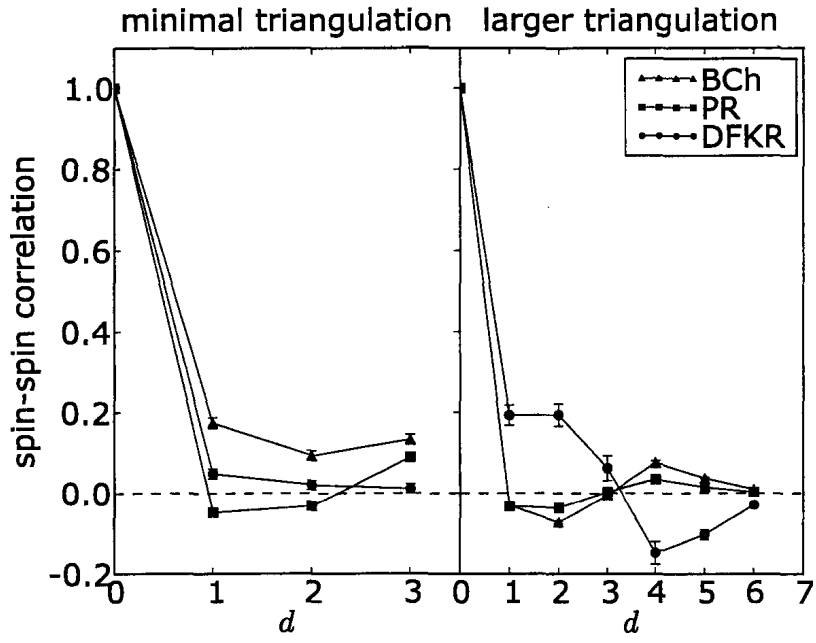

Figure 3.6: Spin-spin correlation functions for the Baez-Christensen (BCh), Perez-Rovelli (PR) and DFKR models, on the minimal triangulation (6 vertices, 15 edges, 20 faces, 15 tetrahedra, and 6 4-simplices) as well as a larger triangulation (23 vertices, 103 edges, 202 faces, 200 tetrahedra, and 80 4-simplices). ROU parameter $r = 10$.

A small triangulation limits the maximum distance between faces. For example, the minimal triangulation has maximum distance $d = 3$. Larger triangulations of the 4-sphere were obtained by refining the minimal one by applying Pachner moves randomly and uniformly over the whole triangulation. We restricted the Pachner moves to those that did not decrease the number of simplices.

The largest triangulation we have used has maximum distance $d = 6$. Its correlations for different models are shown in figure 3.6 along with those from the minimal triangulation. Correlation functions for different values of ROU parameter r (including the $q = 1$ case) and other triangulations are qualitatively similar.

Notice the small negative dip for small values of d for the Perez-Rovelli and Baez-Christensen models. As discussed in previous sections, the partition functions of these models are dominated by spin foams with isolated bubbles. The correlation data is consistent with this hypothesis. The values of the spins assigned to faces of the bubble will be strongly correlated, while the values of the spins on two faces, one of which lies on the bubble and the other does not, should be strongly anti-correlated. Since a given face usually has fewer nearest neighbors that lie on the same bubble than that do not, on average, the short distance correlation is expected to be negative. At slightly larger distances, the correlation function turns positive again. This indicates

that on a larger triangulations, spin foams with several isolated bubbles contribute strongly to the partition function. Although, with so few data points, it is difficult to extrapolate the behavior of the correlation function to larger triangulations and distances, its features are qualitatively similar to that of a condensed fluid, where the density-density correlation function exhibits oscillations on the scale of the molecular dimensions.

Note that the behavior of the DFKR correlation function is significantly different from the other two. This is also consistent with the already observed fact that its partition function has strong contributions from other than single or isolated bubble spin foams.

3.6 Conclusion

We have numerically investigated the behavior of physical observables for the Perez-Rovelli, DFKR, and Baez-Christensen versions of the Barrett-Crane spin foam model. Each version assigns different dual edge and face amplitudes to a spin foam, and these choices greatly affect the behavior of the resulting model. The behavior of the models was also greatly affected by q-deformation.

The limiting behavior of observables was found to be discontinuous in the limit of large ROU parameter r, i.e., $q = \exp(i\pi/r)$ close to its undeformed value of 1. This result is at odds with the physical interpretation of the relation $\Lambda \sim 1/r$ between the cosmological constant Λ and the ROU parameter. Finally, the behavior of the examined physical observables, especially of the spin-spin correlation function, indicates the dominance of isolated bubble spin foams in the Perez-Rovelli and Baez-Christensen partition functions, while less so for the the DFKR one.

Some questions raised by these results deserve attention. For instance, it is not known whether the same $q \to 1$ limit behavior will be observed when q is taken through non-ROU values. While calculations with $\max\{|q|, |q|^{-1}\} > 1$ are numerically unstable, they should still be possible for $|q| \sim 1$.

Another important project is to perform a more extensive study of the effects of triangulation size in order to better understand the semi-classical limit.

Finally, all of this work should also be carried out for the Lorentzian models, which are physically much more interesting but computationally much more difficult.

These and other questions will be the subject of future investigations.

Acknowledgements

The authors would like to thank Wade Cherrington for helpful discussions. The first author was supported by NSERC and FQRNT postgraduate scholarships and the second author by an NSERC grant. Computational resources for this project were provided by SHARCNET.

3.A Spin network notation and conventions

Quantum integers are a q-deformation of integers. For an integer n, the corresponding quantum integer is denoted by $[n]$ and is given by

$$[n] = \frac{q^n - q^{-n}}{q - q^{-1}}. \tag{3.37}$$

In the limit $q \to 1$, we recover the regular integers, $[n] \to n$. Note that $[n]$ is invariant under the transformation $q \mapsto q^{-1}$. When $q = \exp(i\pi/r)$ is a root of unity (ROU), for some integer $r > 1$, an equivalent definition is

$$[n] = \frac{\sin(n\pi/r)}{\sin(\pi/r)}. \tag{3.38}$$

This expression is non-negative in the range $0 \leq n \leq r$. *Quantum factorials* are defined as

$$[n]! = [1][2]\cdots[n]. \tag{3.39}$$

In many cases, q-deformed spin network evaluations can be obtained from their undeformed counterparts by simply replacing factorials with quantum factorials. For convenience, when dealing with half-integral spins, we also define *quantum half-integers* as

$$\lfloor j \rceil = \frac{[2j]}{2} \tag{3.40}$$

when j is a half-integer.

Abstract $\mathfrak{su}_q(2)$ spin networks can be approached from two different directions. They can represent contractions and compositions of $\mathfrak{su}_q(2)$-invariant tensors and intertwiners [10]. At the same time, they can represent traces of tangles evaluated according to the rules of the Kauffman bracket [18]. Either way, the computations turn out to be the same. We present here formulas for the evaluation of a few spin networks of interest.

The *single bubble* network evaluates to what is sometimes called the *superdimension* of the spin-j representation:

$$= (-)^{2j}[2j+1]. \tag{3.41}$$

(As in the rest of the paper, the spin labels are half-integers.)

Up to a constant, there is a unique 3-valent vertex (corresponding to the Clebsch-Gordan intertwiner) whose normalization is fixed up to sign by the value of the *θ-network*:

$$\theta(a,b,c) = \quad = \frac{(-)^s[s+1]![s-2a]![s-2b]![s-2c]!}{[2a]![2b]![2c]!}, \tag{3.42}$$

where $s = a+b+c$. The θ-network is non-vanishing, together with the three-vertex itself, if and only if s is an integer and the triangle inequalities are satisfied: $a \leq b+c$, $b \leq c+a$, and $c \leq a+b$. In addition, when q is a ROU, one extra inequality must be satisfied: $s \leq r-2$. The triple (a,b,c) of spin labels is called *admissible* if $\theta(a,b,c)$ is non-zero.

The recoupling identity gives the transformation between different bases for the linear space of 4-valent tangles (or intertwiners):

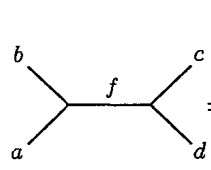

$$= \sum_e \frac{(-)^{2e}[2e+1]\,\mathrm{Tet}\begin{bmatrix} a & b & e \\ c & d & f \end{bmatrix}}{\theta(a,d,e)\,\theta(c,b,e)}$$

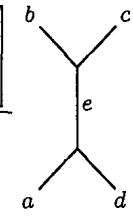

, (3.43)

where the sum is over all admissible labels e and the value of the *tetrahedral network* is

$$\mathrm{Tet}\begin{bmatrix} a & b & e \\ c & d & f \end{bmatrix} =$$

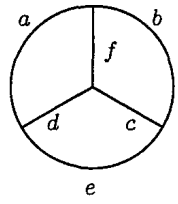

$$= \frac{\mathcal{I}!}{\mathcal{E}!} \sum_{m \leq S \leq M} \frac{(-)^S[S+1]!}{\prod_i [S-a_i]! \prod_j [b_j - S]!}, \tag{3.44}$$

where

$$\mathcal{I}! = \prod_{i,j}[b_j - a_i]! \qquad \mathcal{E}! = [2A]![2B]![2C]![2D]![2E]![2F]! \tag{3.45}$$

$$a_1 = (a+d+e) \qquad b_1 = (b+d+e+f) \tag{3.46}$$

$$a_2 = (b+c+e) \qquad b_2 = (a+c+e+f) \tag{3.47}$$

$$a_3 = (a+b+f) \qquad b_3 = (a+b+c+d) \tag{3.48}$$

$$a_4 = (c+d+f) \qquad m = \max\{a_i\} \quad M = \min\{b_j\}. \tag{3.49}$$

Due to parity constraints, the a_i, b_j, m, M, and S are all integers.

Since the three-vertex is unique up to scale, its composition with with a braiding applied to two incoming legs yields a multiplicative factor:

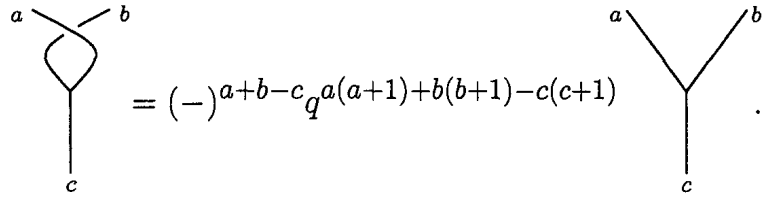

(3.50)

Note that the above braiding factor is not invariant under the transformation $q \mapsto q^{-1}$, while the bubble, tetrahedral and θ-networks are all invariant under this transformation, by virtue of their expressions in terms of quantum integers.

Bibliography

[1] Archer F and Williams R M 1991 The Turaev-Viro state sum model and three-dimensional quantum gravity *Physics Letters B* **273** 438–44

[2] Baez J C 1996 4-dimensional BF theory as a topological quantum field theory *Letters in Mathematical Physics* **38** 129–43 (*Preprint* arXiv:q-alg/9507006)

[3] Baez J C 1998 Spin foam models *Classical and Quantum Gravity* **15** 1827–58 (*Preprint* arXiv:gr-qc/9709052)

[4] Baez J C 2000 An introduction to spin foam models of quantum gravity and BF theory *Lecture Notes in Physics* **543** 25–94 (*Preprint* arXiv:gr-qc/9904025)

[5] Baez J C and Christensen J D 2002 Positivity of spin foam amplitudes *Classical and Quantum Gravity* **19** 2291–306 (*Preprint* arXiv:gr-qc/0110044)

[6] Baez J C, Christensen J D, and Egan G 2002 Asymptotics of $10j$ symbols *Classical and Quantum Gravity* **19** 6489–513 (*Preprint* arXiv:gr-qc/0208010)

[7] Baez J C, Christensen J D, Halford T R, and Tsang D C 2002 Spin foam models of Riemannian quantum gravity *Classical and Quantum Gravity* **19** 4627–48 (*Preprint* arXiv:gr-qc/0202017)

[8] Barrett J W and Crane L 1998 Relativistic spin networks and quantum gravity *Journal of Mathematical Physics* **39** 3296–302 (*Preprint* arXiv:gr-qc/9709028)

[9] Barrett J W and Crane L 2000 A Lorentzian signature model for quantum general relativity *Classical and Quantum Gravity* **17** 3101–18 (*Preprint* arXiv:gr-qc/9904025)

[10] Carter J S, Flath D E, and Saito M. 1995 The classical and quantum $6j$-symbols (*Mathematical Notes* vol 43) (Princeton, New Jersey: Princeton University Press)

[11] Ceperley D and Alder B 1986 Quantum Monte Carlo *Science* **231** 555–60

[12] Cherrington J W and Christensen J D 2006 Positivity in Lorentzian Barrett-Crane models of quantum gravity *Classical and Quantum Gravity* **23** 721–36 (*Preprint* arXiv:gr-qc/0509080)

[13] Christensen J D and Egan G 2002 An efficient algorithm for the Riemannian $10j$ symbols *Classical and Quantum Gravity* **19** 1184–93 (*Preprint* arXiv:gr-qc/0110045)

[14] Crane L, Kauffman L H, and Yetter D N 1997 State-Sum Invariants of 4-Manifolds *Journal of Knot Theory and Its Ramifications* **6** 177–234 (*Preprint* arXiv:hep-th/9409167)

[15] Crane L and Yetter D N 1993 A categorical construction of 4D topological quantum field theories *Quantum topology* ed Kauffman L H and Baadhio R A (Singapore: World Scientific Press) pp 120–30

[16] De Pietri R, Freidel L, Krasnov K, and Rovelli C 2000 Barrett-Crane model from a Boulatov-Ooguri field theory over a homogeneous space *Nuclear Physics B* **574** 785–806 (*Preprint* arXiv:hep-th/9907154)

[17] Freidel L 2005 Group field theory: an overview *International Journal of Theoretical Physics* **44** 1769–83 (*Preprint* arXiv:hep-th/0505016)

[18] Kauffman L H and Lins S L 1994 Temperley-Lieb recoupling theory and invariants of 3-manifolds (*Annals of Mathematics Studies* vol 134) (Princeton, New Jersey: Princeton University Press)

[19] Kikuchi M and Ito N 1993 Statistical dependence time and its application to dynamical critical exponent *Journal of the Physical Society of Japan* **62** 3052

[20] Landau D P and Binder K 2005 A guide to Monte Carlo simulations in statistical physics 2nd ed (Cambridge: Cambridge University Press)

[21] Majid S 2000 Foundations of quantum group theory (Cambridge: Cambridge University Press)

[22] Metropolis N, Rosenbluth A W, Rosenbluth M N, Teller A H, and Teller E 1953 Equation of state calculations by fast computing machines *Journal of Chemical Physics* **21** 1087–92

[23] Noui K and Roche P 2003 Cosmological deformation of Lorentzian spin foam models *Classical and Quantum Gravity* **20** 3175–214 (*Preprint* arXiv:gr-qc/0211109)

[24] Perez A 2003 Spin foam models for quantum gravity *Classical and Quantum Gravity* **20** R043–104 (*Preprint* arXiv:gr-qc/0301113)

[25] Perez A and Rovelli C 2001 A spin foam model without bubble divergences *Nuclear Physics B* **599** 255–82 (*Preprint* arXiv:gr-qc/0006107)

[26] Plebański J F 1977 On the separation of Einsteinian substructures *Journal of Mathematical Physics* **18** 2511–20

[27] Ponzano G and Regge T 1968 Semiclassical limit of Racah coefficients *Spectroscopic and group theoretical methods in physics* ed Bloch F, Cohen S G, De-Shalit A, Sambursky S, and Talmi I (Amsterdam: North-Holland) pp 1–98

[28] Reisenberger M P 1999 On relativistic spin network vertices *Journal of Mathematical Physics* **40** 2046–54 (*Preprint* arXiv:gr-qc/9809067)

[29] Smolin L 1995 Linking topological quantum field theory and nonperturbative quantum gravity *Journal of Mathematical Physics* **36** 6417–55 (*Preprint* arXiv:gr-qc/9505028)

[30] Smolin L 2002 Quantum gravity with a positive cosmological constant *Preprint* arXiv:hep-th/0209079

[31] Turaev V G and Viro O Y 1992 State sum invariants of 3-manifolds and quantum $6j$-symbols *Topology* **31** 865–902

[32] Yetter D N 1999 Generalized Barrett-Crane vertices and invariants of embedded graphs *Journal of Knot Theory and Its Ramifications* **8** 815–29 (*Preprint* arXiv:math.QA/9801131)

Chapter 4
Evaluation of new spin foam vertex amplitudes

4.1 Introduction

Spin foam models are an attempt to produce a theory of quantum gravity starting from a discrete, path integral-like approach. They were first defined a decade ago [4, 8]. More recently, we have seen significant progress toward extraction of their semiclassical behavior and its favorable comparison to the expected weak field limit of gravity, starting with Rovelli and collaborators' calculation of the graviton propagator [25, 29]. Unfortunately, further calculations have revealed that the standard spin foam model due to Barrett and Crane produced incorrect results for some of the propagator matrix elements [1, 2]. This result has motivated several proposals to replace the Barrett-Crane (BC) spin foam vertex amplitude [8] for quantum gravity. The first proposal, by Engle, Pereira and Rovelli (EPR) [16, 17], aimed also to identify the spin foam boundary state space with that of loop quantum gravity spin networks; this model is also referred to as the "flipped" vertex model. Another proposal, by Livine and Speziale [23, 24], used $SU(2)$-coherent states to define the spin foam amplitudes and reproduced the EPR proposal up to an edge normalization factor. Finally, a paper by Freidel and Krasnov [18], suggested that the EPR model corresponds to a topological theory related to gravity and proposed a generalization thereof corresponding to gravity itself (the FK model). The present paper, along with most previous work, concerns only the Riemannian signature models of gravity.

Section 4.2 briefly introduces spin foam models and presents the three models described above in a unified framework. Section 4.3 describes an efficient algorithm for numerical evaluation of vertex amplitudes of the new models, extending the existing Christensen-Egan algorithm for the BC model. In section 4.4, the different spin foam models are compared at the level of effective vertex amplitudes. Finally, section 4.5 briefly discusses the results of section 4.4 and future work.

4.2 BF theory

The new spin foam models of gravity may be presented in a way similar to the original BC model. Following Freidel and Krasnov [18], we define them within a unified framework. See also the more recent paper [14].

The starting point is BF theory. It is a 4-dimensional field theory with two fields: a gauge connection 1-form A and an auxiliary 2-form B. The action is given by

$$S = \int \mathrm{tr}[B \wedge F], \tag{4.1}$$

where $F = dA$ is the curvature of the connection. If the gauge group is taken to be $Spin(4)$, the double cover of $SO(4)$ and a constraint is imposed, ensuring simplicity[1] of the B 2-form, this theory becomes equivalent to the Plebanski formulation of general relativity in Riemannian signature [8].

BF theory is in a sense topological. Particularly, its underlying manifold may be freely changed from a smooth one to a discretized (piecewise linear) one. Moreover, for BF theory, quantization and discretization commute [3]. Spin foam models aim to reproduce gravity by heuristically imposing simplicity constraints on BF theory after the discretization and quantization steps have been performed [5]. The connection between spin foams and gravity is motivated by results from loop quantum gravity [28].

Consider BF theory defined on a simplicial complex, also referred to as a *triangulation*. It is convenient to introduce the *dual 2-complex*. Each 4-simplex is identified with a *dual vertex*, each tetrahedron is identified with a *dual edge*, and each triangle is identified with a *dual face*. Discretizing the A and B fields and integrating out the B field, the theory's path integral yields the following expression for its partition function:

$$Z = \text{“}\int \mathrm{d}A\,\mathrm{d}B\, e^{iS}\ \text{”} = \int \mathrm{d}g \prod_f \delta(g_f), \tag{4.2}$$

where the connection A has been replaced by group elements g associated to every dual edge, and g_f represents the holonomy around a dual face. This form of the partition function manifestly shows that only flat geometries (with trivial holonomies) contribute to the BF theory path integral. See [26] for details.

The δ-functions can be expanded in terms of gauge group characters and the group integrations can be performed at each dual edge. What remains is a discrete

1. *Simplicity* means that there exists a 1-form e such that $B = e \wedge e$.

sum of the form

$$Z = \sum_F \prod_f A_f(F) \prod_e A_e(F) \prod_v A_v(F), \tag{4.3}$$

where F ranges over all spin foams, while f, e, and v range respectively over dual faces, dual edges, and dual vertices. In this context, a *spin foam* is a labelling of the dual faces of the triangulation by irreducible representations of the gauge group. These representation labels come from the character expansion described above. This definition of spin foams will have to be augmented with extra labels for the purpose of introducing the new models.

Irreducible representations of $\mathrm{Spin}(4) \cong SU(2) \times SU(2)$ are labelled by a pair of integers $\mathbf{j} = (j^-, j^+)$, where each j is a spin, corresponding to an irreducible representation of $SU(2)$. Hence forth, all representation labels will be referred to as spins, unless otherwise specified.

For pure BF theory, face amplitudes are determined by the character expansion of δ-functions and are given by the dimension of the irrep j labelling a given face

$$A_f(F) = \dim \mathbf{j}_f = (j_f^- + 1)(j_f^+ + 1). \tag{4.4}$$

Edge and vertex amplitudes are determined by evaluating the group integrals in equation (4.2). The basic identities we use are

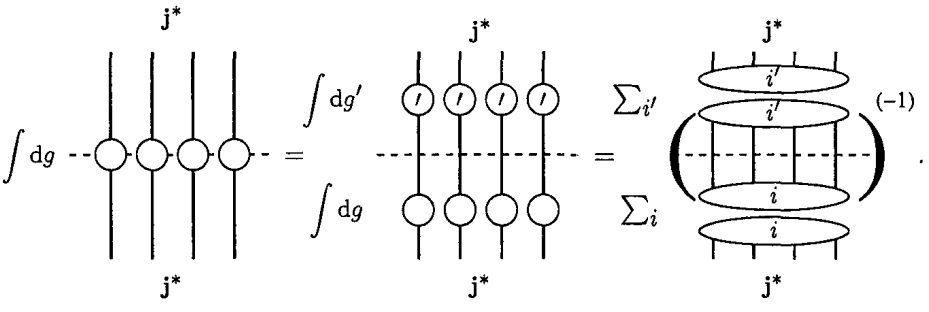

(4.5)

The above graphical notation requires some explanation. See [26] and the Appendix of [11] (also chapter 2 of this thesis) for full details. Briefly, a vertical strand represents a matrix element of a particular representation of the gauge group. Most of the representation and basis labels have been omitted for conciseness. Instead, some spins will be marked as collective labels with an asterisk. Their expanded meaning should be clear from context. Concatenation of strands corresponds to matrix multiplication, or equivalently to contracting basis indices of matrix elements. Juxtaposition of strands corresponds to the Kronecker product of the associated matrix elements, or

equivalently to the tensor product of the given representations. The blank and primed circles convey whether it is the group element g or g' that is taken in the given representation. The horizontal dotted line represents the triangulation tetrahedron dual to the dual edge to which the given group element is associated.

The first equality in (4.5) follows directly from the normalization of the Haar group measure, its invariance under translations and the multiplicative property of representation matrix elements. In this context, group integration is also known to produce a projection operator onto the space of intertwiners among the representations given by the four strands. The last equality in (4.5) illustrates this identity by expanding this projector in a basis of normalized intertwiners; the bracketed spin network provides correct normalization in the denominator of the expression. The summation over the new intertwiner basis labels i and i' make up the sums over dual edge labels (part of the summation over spin foams), part of the sum over spin foams in (4.3). Performing the same group integration and intertwiner expansion over all dual edges of the triangulation, we can read off the edge and vertex amplitudes of equation (4.3).

Thus, for discrete BF theory, writing all tensor contractions in terms of spin networks we find these amplitudes to be

$A_e(F) =$ 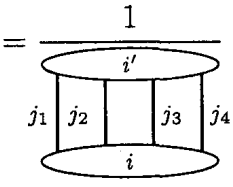

and $A_v(F) =$ 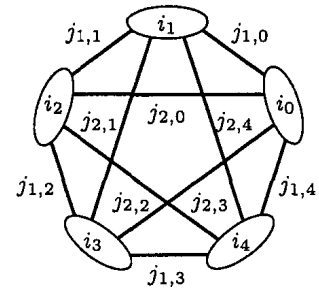

. (4.6)

The topology of the contraction graph corresponding to A_v above follows directly from the adjacency structure of the dual 2-complex. We shall refer to this graph as the *pent graph*; it will appear in the vertex amplitude definition of each spin foam model discussed later in this section. Both the edge and vertex amplitudes, A_e and A_v, appear with full spin labelling. For conciseness, most of the spin labels will be suppressed or represented schematically, as in equation (4.5), in the rest of the paper.

Starting from this basic setup, new models may be obtained by modifying the partition function directly, by changing amplitudes at the level of equation (4.3), or at an intermediate level, by modifying the integrand in equation (4.5). We present the new models following the last approach.

4.2.1 Gravity, Barrett-Crane and new models

The Barrett-Crane (BC) model starts with the quantized BF theory path integral (4.3) and imposes restrictions on the spin foam summation in equation (4.3). These restrictions heuristically correspond to imposing the simplicity constraints on the B field [8]. The restriction is twofold. First, the Spin(4) representations are restricted to balanced ones $\mathbf{j} = (j, j)$, where $j^- = j^+ = j$. Second, the intertwiner summation and edge weights of equation (4.5) are modified such that the i-sums contain only a single term corresponding to the so-called BC 4-valent intertwiner.

The BC model amplitudes are given in section 4.2.2.1. The evaluation of this vertex amplitude is discussed in several papers [6, 7, 12, 21], where variations on the face and edge amplitudes have also been considered.

Recently, shortcomings of the BC model have been identified by several authors. Specifically, while this vertex amplitude correctly reproduced the asymptotic behavior of some graviton propagator matrix elements, it does not do so for all of them [1, 2, 29]. Modified spin foam models, referred to here as *new models*, have been subsequently proposed with the hope of overcoming these difficulties. The model proposed by Engle, Pereira, and Rovelli (EPR) [16, 17] and by Livine and Speziale [23, 24] had the common motivation of identifying its boundary state space with the space of spin network states of loop quantum gravity. The model proposed by Freidel and Krasnov (FK) [18] was derived in a similar fashion, but made different choices while imposing the simplicity constraints. As a result, the FK model's boundary state space is different from that of the EPR one. More recently, Conrady and Freidel have discussed in more detail the boundary state space of the FK model [14].

4.2.2 Model framework

The BC, EPR, and FK models may be presented within the same framework, following [18]. We briefly present this framework and how each model is realized in it.

The first step, compared to BF theory, as above, is to restrict the Spin(4) representations to balanced ones, $\mathbf{j} = (j, j)$.

Consider a single strand from the double integral in equation (4.5). It depicts the product of two linear operators, corresponding to group elements g and g', in the Spin(4) irrep j. One could always insert the identity operator between g and g' without changing anything. On the other hand, inserting a different linear operator in the same place will produce different results. Keeping with the goal of identifying

the i-intertwiners in (4.5) with the $SU(2)$ intertwiners in loop quantum gravity spin networks, instead of inserting an arbitrary linear operator, we insert only an arbitrary $SU(2)$ intertwiner, in the following sense.

Because of the decomposition Spin(4) $\cong SU(2) \times SU(2)$, a balanced irrep of Spin(4) can be written as the tensor product of two copies of an $SU(2)$ irrep, $\mathbf{j} = j \otimes j$. Seen as a tensor product of two $SU(2)$ reps, using Clebsch-Gordan rules, it can be decomposed into a direct sum of $SU(2)$ representations 0, 2, ..., $2j$. This decomposition is not unique, since one is possible for each diagonal $SU(2)$-subgroup of Spin(4). However, each such choice is equivalent because of the group integrals surrounding the operator insertion; ultimately, spin foam amplitudes are independent of the choice. By inserting an $SU(2)$ intertwiner, $j \otimes j \longrightarrow j \otimes j$, between g and g', we essentially insert a linear combination of projections onto the $SU(2)$ irreducible invariant subspaces:

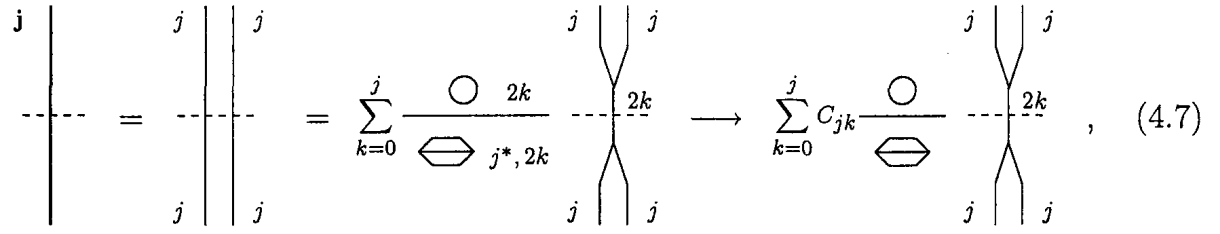

(4.7)

where the C_{jk} are arbitrary weight factors, the trivalent vertex corresponds to the Clebsch-Gordan tensor. The extra coefficients are necessary, in our choice of normalization, for the Clebsch-Gordan decomposition of the $j \otimes j$ representation. The spin network conventions and normalizations used in this paper are those of [10, 20]. Their relation to $SU(2)$-tensor contractions is presented in detail in the Appendix of [11] (also chapter 2 of this thesis). Note that the intermediate spin[2] is always even and so can be written as $2k$ for integer k.

Consider just a single Clebsch-Gordan projector insertion for each of the strands in (4.5), as show in (4.7), and concentrate only on the part of that equation below the dotted line. The same calculation will have to be done above the dotted line, that is on both sides of each tetrahedron in the triangulation. The Spin(4) group integral can be written as an integral over two copies of $SU(2)$, where $g = (g^-, g^+)$. The matrix elements of g in a balanced representation $\mathbf{j}$ will be an outer product of

2. The notation of this paper differs from reference [18], as Freidel and Krasnov use half-integral spins, while we use integral twice-spins to label $SU(2)$ irreps. In the present notation, their j becomes $j/2$, but their k does coincide numerically with our k. Also, their l corresponds to i introduced in equation (4.8).

matrix elements of g^- and g^+ in representation j (circles with $-$ and $+$, respectively):

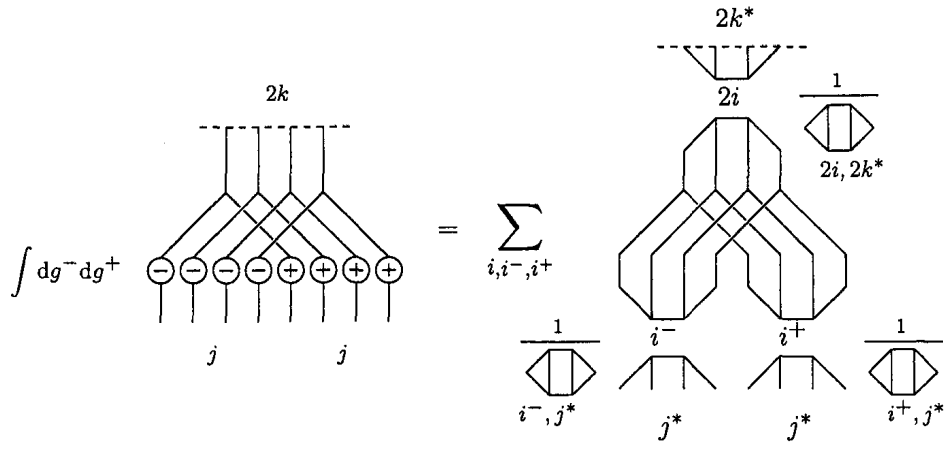

(4.8)

Summations over the $i^{\pm}$ intertwiners again follow directly from the property that group integration is equivalent to projection onto the space of intertwiners between the four j representations (*j-spins*). The extra summation over the i intertwiners can be inserted because the Clebsch-Gordan projectors map each pair of $i^{\pm}$ intertwiners into the subspace of intertwiners between the four $2k$ representations (*k-spins*). These intertwiners can be conveniently parametrized, as depicted, by an even integer $2i$ (*i-spins*)[3].

The open spin networks at the bottom of the right hand side of (4.8) join with other similar spin networks and form left ($-$) and right ($+$) pent networks, which will contribute to the corresponding vertex amplitude. These are spin networks with topology shown in (4.13), obtained by substitution of i^- and i^+ intertwiners into the pent graph of equation (4.6). The open spin network at the top of the same expression joins with its mirror image above the dotted line and contributes to the corresponding edge amplitude. With the exception of the *tripetal spin network*[4] located at the center of the diagram on the right of (4.8), all spin networks appearing so far have known evaluations. They have come up in the evaluation of the BC vertex amplitude and have been explicitly computed using recoupling techniques from [10, 20]. The tripetal spin network will be evaluated in section 4.3.

To completely define each of the three models under consideration, it remains only to specify the dual 2-skeleton spin foam labelling and the weight factors C_{jk}

3. It should be noted that reference [16] uses half-integral spins, while we use integral twice-spins to label $SU(2)$ irreps. However, Engle, Pereira and Rovelli's definitions for i- and j-spins numerically coincide with ours.

4. This spin network was first introduced in equation (5) of [16].

in (4.7). The face, edge and vertex amplitudes are then specified by the preceding construction (see section 4.3 for an important caveat). Most generally, in this framework, the spin foams summed over in the partition function (4.3) assign a j-spin to each dual faces, an i-spin to each dual edges, and a k-spin to each dual edge-dual face pair. However, the number of labels may be reduced in special cases.

While this presentation is convenient for computational purposes, it hides some of the motivation from the derivation of these models. More physical insight for each model can be found in the original references.

4.2.2.1 BC model

In the Barrett-Crane model, the faces of the dual 2-complex are labelled by j-spins. The choice of intertwiner insertion weights are $C_{jk} = 0$ $(k \neq 0)$, and $C_{j0} = (-)^j(j+1)$, which is the value of the j-loop spin network. Each dual edge is shared by 4 dual faces, while each dual vertex is shared by 10 dual faces. The preceding construction specifies the following dual face, edge and vertex amplitudes:

$$A_f(F) = (j_f + 1)^2, \quad A_e(F) = 1, \quad \text{and} \quad A_v(F) = \quad , \tag{4.9a}$$

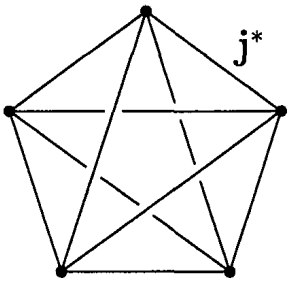

where

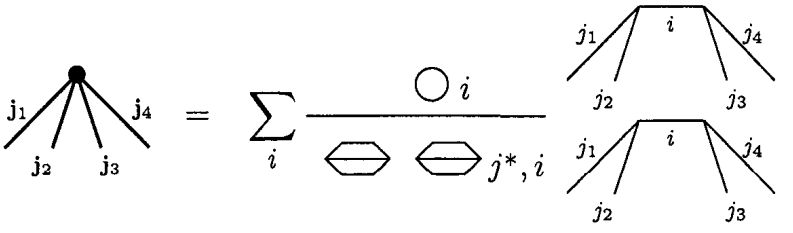

. (4.9b)

Here the spin arguments are determined by the dual faces sharing the given cell of the 2-skeleton. Specifically, the vertex amplitude depends on 10 spins, hence its name, the BC 10j-symbol. It is important to note that different edge and face amplitudes have been proposed for the BC model as well [7, 15, 27].

4.2.2.2 EPR model

In the Engle-Pereira-Rovelli model, the dual faces are labelled by j-spins, and dual edges are labelled by i-spins [cf. (4.8)]. The weights are $C_{jj} = 1$ and $C_{jk} = 0$ for $k \neq j$. Each dual edge is shared by 4 dual faces, while each dual vertex is shared by 10 dual faces and 5 dual edges. The preceding construction specifies the following dual face, edge and vertex amplitudes:

$$A_f(F) = (j_f + 1)^2, \quad A_e(F) = \frac{\bigcirc\, 2i_e}{\Theta\quad\Theta\; 2j^*, 2i_e}, \tag{4.10a}$$

and

$$A_v(F) = \quad , \tag{4.10b}$$

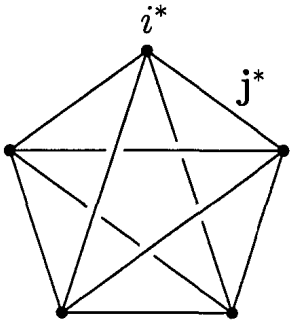

where

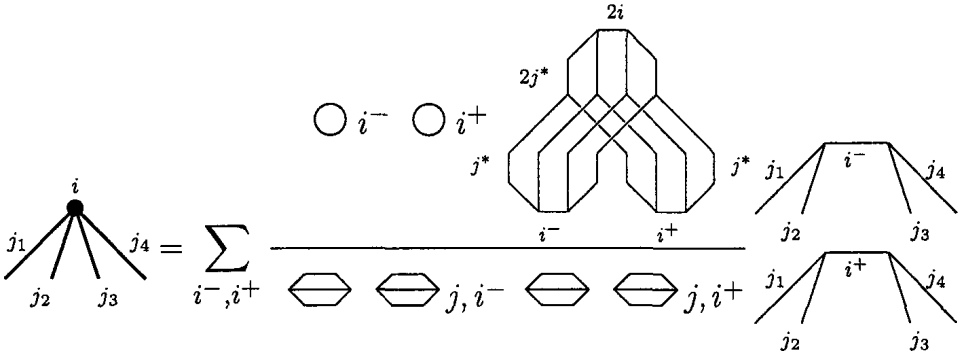

(4.10c)

Here the spin arguments are determined by the dual faces and edges sharing the given cell of the 2-skeleton. Specifically, the vertex amplitude depends on the 10 j-spins from the dual faces sharing it, as well as the 5 i-spins from the incident dual edges, hence it may be called the EPR $15j$-symbol. The same vertex amplitude was derived in [16] and [24], although the former reference was not specific about face and edge amplitudes.

4.2.2.3 FK model

In the Freidel-Krasnov model, the dual faces are again labelled by spins, denoted j, and dual edges are also labelled by intertwiners, denoted i, and finally each dual edge-face pair contributes an independent spin, denoted k [cf. (4.8)]. The weight factor is more complex than for the other two models and is given by

$$C_{jk} = \frac{[(j+1)!]^2}{(j-k)!(j+k+1)!}. \tag{4.11}$$

Each dual edge is shared by 4 dual faces, while each dual vertex is shared by 10 dual faces and 5 dual edges, as well as 20 individual dual edge-face pairs. The preceding construction specifies the following dual face, edge and vertex amplitudes:

$$A_f(F) = (j_f+1)^2, \quad A_e(F) = \frac{\bigcirc\, 2i_e}{\Theta\ \Theta\ 2k^*, 2i_e} \prod_{f \supset e} C_{j_f k_f} \frac{\bigcirc\, 2k_f}{\Theta\ j_f^*, 2k_f}, \tag{4.12a}$$

and

$A_v(F) =$ 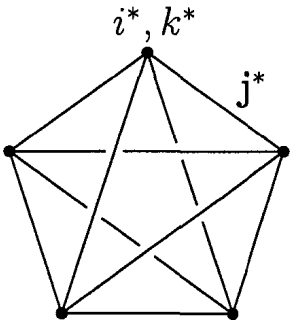

, (4.12b)

where

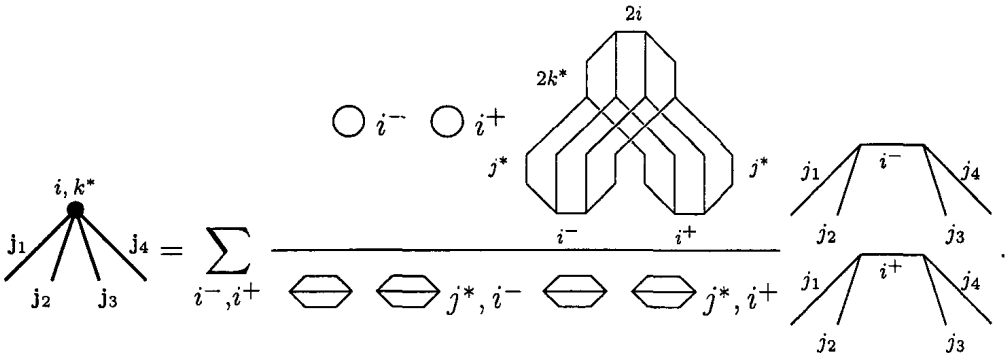

. (4.12c)

Here the spin arguments are determined by the dual faces and edges sharing the given cell of the 2-skeleton. Specifically, the vertex amplitude depends on the 10 j-spins from the dual faces sharing it, as well as the 5 i-spins from the incident dual edges, and on the 20 k-spins from the dual edge-face pairs sharing it. Thus it may be called

the FK $35j$-symbol. Setting all k-spins, and necessarily all i-spins, to 0, this model exactly reproduces the BC spin foam amplitudes. Also, setting all k-spins equal to the corresponding j-spins exactly reproduces the EPR vertex amplitude $A_v(F)$. However, in that case, the EPR edge amplitude $A_e(F)$ is reproduced with the extra factor $\prod_{f\supset e}[(j_f+1)!]^2/(2j_f+1)!$.

4.3 Evaluating new vertex amplitudes

The second group integration identity in (4.5) requires a choice of basis in the space of intertwiners between four Spin(4) representations. This choice is arbitrary; however, some choices are more convenient than others. For example, the normalization factor in (4.5) is simplest when the i'-basis is the same as the i-basis. On the other hand, the choice of intertwiner basis in the EPR model, equation (4.10c), is made such that when the intertwiner networks are substituted into the vertex amplitude pent graph, equation (4.6), the amplitude is resolved as a sum over $15j$-symbols with the following topology:

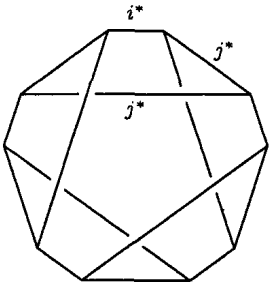

(4.13)

A similar choice is made for the BC and FK models, equations (4.9b) and (4.12c). This topology is required for the numerical algorithm described in section 4.3.2.

Unfortunately, the requirements of simple edge normalization factors and the above topology requirement for each vertex amplitude are not always compatible. For example, they are not compatible for the minimal triangulation of the 4-sphere. With the current formulation of the vertex amplitude evaluation algorithm, preference must be given to the topology requirement. A similar issue, referred to as "edge splitting," was encountered for spin foams on a cubic lattice in [11] (also chapter 2 of this thesis).

Throughout this paper, we have assumed that the topology and simplicity of dual edge normalization requirements can be simultaneously satisfied. This assumption is justified in the case of a single 4-simplex, and other simple arrangements of a small number of 4-simplices. If this assumption is not justified, then the dual edge amplitudes given in the previous section will have to be modified, with the important

exception of the BC model. The edge normalization requirement for the BC model is trivial.

4.3.1 Tripetal network evaluation

The tripetal spin network, defined in equation (4.8), is evaluated as follows. It is first written as a contraction of two trivalent networks, along the strands labelled i^-, i^+ and $2i$.

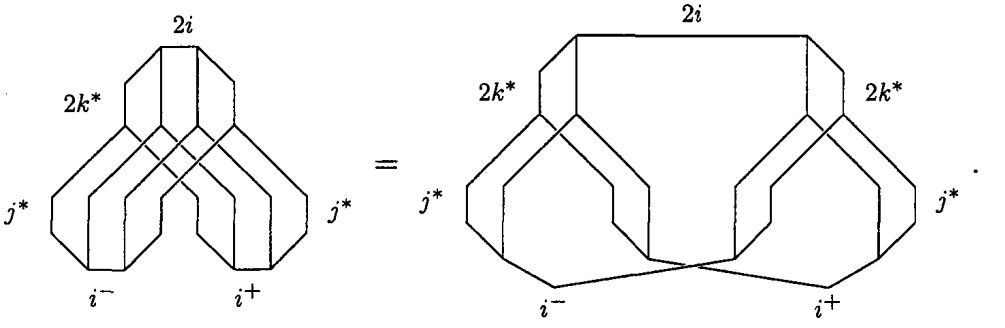

(4.14)

Each of these trivalent networks must be proportional to the unique $SU(2)$ 3-valent intertwiner. The proportionality constant is computed explicitly through recoupling:

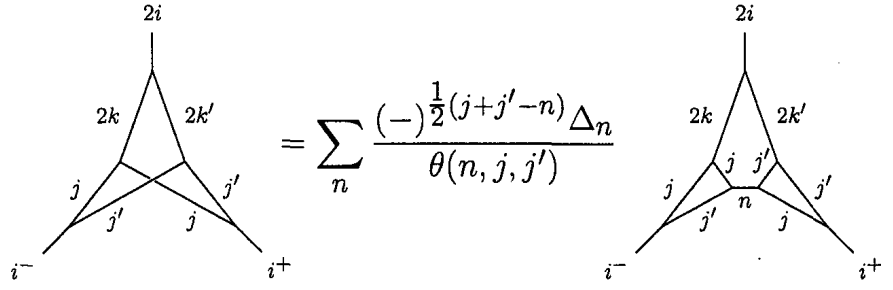

$$= \sum_n \frac{(-)^{\frac{1}{2}(j+j'-n)}\Delta_n}{\theta(n,j,j')} \qquad (4.15)$$

$$= \sum_n \frac{(-)^{\frac{1}{2}(j+j'-n)}\Delta_n}{\theta(n,j,j')} \frac{\begin{bmatrix} j & j & j' \\ i^- & n & 2k \end{bmatrix}}{\theta(i^-,n,2k)} \frac{\begin{bmatrix} j' & j' & j \\ i^+ & n & 2k' \end{bmatrix}}{\theta(i^+,n,2k')} \qquad (4.16)$$

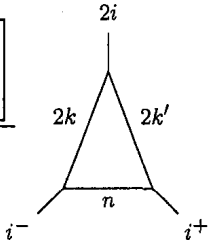

$$= \sum_n \frac{(-)^{\frac{1}{2}(j+j'-n)}\Delta_n}{\theta(n,j,j')} \frac{\begin{bmatrix} j & j & j' \\ i^- & n & 2k \end{bmatrix}}{\theta(i^-,n,2k)} \frac{\begin{bmatrix} j' & j' & j \\ i^+ & n & 2k' \end{bmatrix}}{\theta(i^+,n,2k')} \frac{\begin{bmatrix} 2k' & 2k & n \\ i^- & i^+ & 2i \end{bmatrix}}{\theta(i^-,i^+,2i)} \qquad (4.17)$$

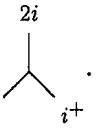

The first equality recouples the crossing strands through the auxiliary spin n. Other steps correspond to collapsing triangles to 3-valent vertices. The square brackets denote the evaluation of a tetrahedral spin network, while θ and Δ denote the eval-

uations of the theta-like and loop spin networks seen in (4.7) and elsewhere. For full details, see [20] and the Appendix of [21].

After this simplification, the tripetal network is proportional to the theta network, where we write the left copy of the above coefficient as $P_{i^-i^+}$ and the right copy as $Q_{i^-i^+}$:

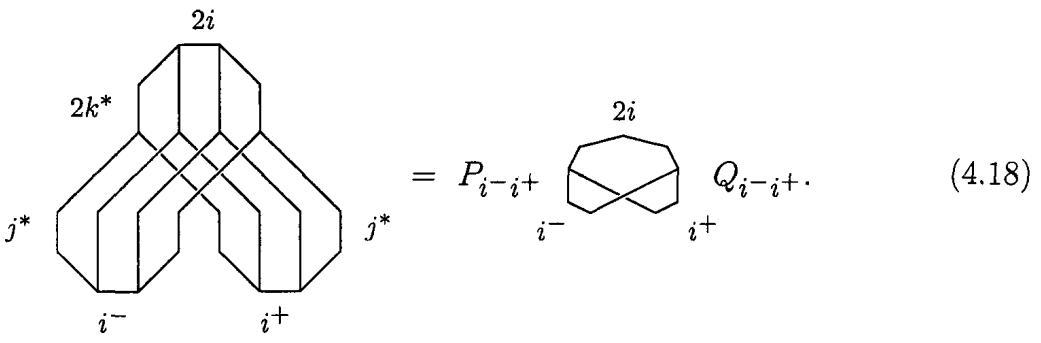

(4.18)

The network on the right hand side of the above equation is equal to the theta network up to sign, which is specified in (4.19a). Both $P_{i^-i^+}$ and $Q_{i^-i^+}$ depend on many spins. The displayed indices are those that will be important in section 4.3.2.

To obtain the final formulas for each vertex e of the pent graph, we make appropriate substitutions into the above expression, from each half of the tripetal network. We replace i and $i^\pm$ by i_e and $i_e^\pm$ respectively. In the P coefficient, the spin k becomes $k^p_{1,e}$, while k' becomes $k^p_{2,e}$. At the same time, the spin j becomes $j_{1,e}$, while j' becomes $j_{2,e}$. Similarly, in Q, the spin k becomes $k^q_{2,e-2}$, k' becomes $k^q_{1,e-1}$, j becomes $j_{2,e-2}$ and j' becomes $j_{1,e-1}$. The final formula for the tripetal network is

$$R^e_{i_e^- i_e^+} = (-)^{\frac{1}{2}(i_e^- + i_e^+ - 2i_e)} \frac{P^e_{i_e^- i_e^+} Q^e_{i_e^- i_e^+}}{\theta(i_e^-, i_e^+, 2i_e)}, \tag{4.19a}$$

$$P^e_{i_e^- i_e^+} = \sum_{n_p} (-)^{\frac{1}{2}(j_{1,e}+j_{2,e}-n_p)} \Delta_{n_p} \frac{\begin{bmatrix} 2k^p_{2,e} & 2k^p_{1,e} & n_p \\ i_e^- & i_e^+ & 2i_e \end{bmatrix}}{\theta(n_p, j_{1,e}, j_{2,e})} \frac{\begin{bmatrix} j_{1,e} & j_{1,e} & j_{2,e} \\ i_e^- & n_p & 2k^p_{1,e} \end{bmatrix}}{\theta(i_e^-, n_p, 2k^p_{1,e})} \frac{\begin{bmatrix} j_{2,e} & j_{2,e} & j_{1,e} \\ i_e^+ & n_p & 2k^p_{2,e} \end{bmatrix}}{\theta(i_e^+, n_p, 2k^p_{2,e})}, \tag{4.19b}$$

$$Q^{e}_{i_e^- i_e^+} = \sum_{n_q} (-)^{\frac{1}{2}(j_{2,e-2}+j_{1,e-1}-n_q)} \Delta_{n_q} \frac{\begin{bmatrix} 2k^q_{1,e-1} & 2k^q_{2,e-2} & n_q \\ i_e^- & i_e^+ & 2i_e \end{bmatrix}}{\theta(n_q, j_{2,e-2}, j_{1,e-1})} \frac{\begin{bmatrix} j_{2,e-2} & j_{2,e-2} & j_{1,e-1} \\ i_e^- & n_q & 2k^q_{2,e-2} \end{bmatrix}}{\theta(i_e^-, n_q, 2k^q_{2,e-2})} \frac{\begin{bmatrix} j_{1,e-1} & j_{1,e-1} & j_{2,e-2} \\ i_e^+ & n_q & 2k^q_{1,e-1} \end{bmatrix}}{\theta(i_e^+, n_q, 2k^q_{1,e-1})}. \tag{4.19c}$$

Notation for the j- and k-spins is explained in the next section.

4.3.2 Numerical algorithm

The results of the previous section can be used to extend the Christensen-Egan (CE) algorithm [12, 21] to evaluate the new vertex amplitude.

First, we set up some notation. Most generically, the new vertex is a function of 10 spins $j_{c,e}$, 5 intertwiner spins i_e, and 20 more auxiliary spins $k^x_{c,e}$. The index e refers to a particular vertex of the pent graph in (4.6) (corresponding to a particular dual edge incident on the given dual vertex). The c subscript corresponds to either the inner (star) or outer (pentagon) 5-cycle of the pent graph, with $j_{c,e}$ denoting the graph edge belonging to cycle c and emanating anticlockwise from vertex e. The x superscript indicates whether the corresponding k-spin belongs to the P- or to the Q-side of the pent vertex e. The e index is always taken mod 5.

Consider the formulas[5] (19)–(22) from [21]. They completely describe the evaluation of the BC vertex amplitude. We now explicitly write out the evaluation of the new vertex amplitude A_v, using current conventions:

$$A_v = (-)^S \sum_{m^-, m^+} \phi \, \mathrm{tr}[M_4 M_3 M_2 M_1 M_0], \tag{4.20}$$

where $S = \sum_{c,e} j_{c,e}$ and the per-term multiplicative factor is

$$\phi = (-)^{\frac{1}{2}(m^- - m^+)} (m^- + 1)(m^+ + 1). \tag{4.21}$$

The rows and columns of the matrices M_e are indexed by pairs of integers $\mathbf{i} = (i^-, i^+)$.

5. Note, that reference [21] uses half-integral spins, while the current paper uses integer twice-spins to label $SU(2)$ irreps, following [20].

Their components are

$$(M_e)_{\mathbf{i}_e}^{\mathbf{i}_{e+1}} = R^e_{i_e^- i_e^+} N^e_{i_e^-} N^e_{i_e^+} (T^e_-)_{i_e^-}^{i_{e+1}^-} (T^e_+)_{i_e^+}^{i_{e+1}^+}, \tag{4.22}$$

where $R^e_{i_e^- i_e^+}$ was defined in (4.19), while

$$N^e_{i_e^\pm} = \frac{\Delta_{i_e^\pm}}{\theta(i_e^\pm, j_{1,e}, j_{2,e})\theta(i_e^\pm, j_{2,e-2}, j_{1,e-1})}, \tag{4.23}$$

and

$$(T^e_\pm)_{i_e^\pm}^{i_{e+1}^\pm} = \frac{\begin{bmatrix} i_e^\pm & j_{1,e} & j_{2,e-1} \\ i_{e+1}^\pm & m^\pm & j_{2,e} \end{bmatrix}}{\theta(i_{e+1}^\pm, m^\pm, j_{2,e})}. \tag{4.24}$$

T is taken directly from equation (22) of [21].

For an implementation of the above algorithm, it is important to compute the precise range of the $m^\pm$ summations, the size of each M_e matrix, that is, the allowed ranges of the $i_e^\pm$ spins, and the ranges of the $n_{p,q}$ summations in the definitions of P and Q in (4.19). Whenever the arguments of either the theta or tetrahedral spin networks fail to satisfy certain conditions, these networks evaluate to zero. Therefore, the $m^\pm$, $i_e^\pm$, and $n_{p,q}$ ranges are taken to be the largest such that all necessary conditions are satisfied. These conditions are

$$\theta(a,b,c): \ \mathrm{tri}(a,b,c), \tag{4.25}$$

$$\text{and} \quad \begin{bmatrix} a & b & e \\ c & d & f \end{bmatrix}: \ \mathrm{tri}(c,d,f), \ \mathrm{tri}(a,b,f), \ \mathrm{tri}(a,d,e), \ \mathrm{tri}(c,b,e), \tag{4.26}$$

where the abbreviation stands for the triangle inequality and parity constraint

$$\mathrm{tri}(a,b,c): \ a \le b+c, b \le c+a, c \le a+b, \text{ and } a+b+c = 0 \pmod 2. \tag{4.27}$$

It can be shown that these conditions, once collected from equations (4.19), (4.23) and (4.24), are sufficient to make all summations involved in the algorithm finite. The linearity of the triangle inequalities also implies that the upper bound on all sums grows linearly with the magnitude of the input i-, j-, and k-spins. However, it is important for an efficient implementation to obtain the tightest possible bounds on

each of the summation indices.

The most computationally intensive steps in the algorithm are filling the matrices in (4.22) and computing their product-trace in (4.20). The efficiency of the evaluation algorithm can be expressed in terms of the magnitudes of input spins. Suppose that the $j_{c,e}$, i_e, and $k^x_{c,e}$ spins are roughly of magnitude j. Then, various triangle inequalities restrict the $m^\pm$ and $i^\pm_e$ summations to ranges of size $O(j)$. The $\mathbf{i}_e = (i^+_e, i^-_e)$ double index then spans a range of size $O(j^2)$. The R, N and T matrices take respectively $O(j^{2+1+1})$, $O(j^1)$ and $O(j^{2+1})$ time, yielding an overall $O(j^4)$ estimate. The each tetrahedral network may be evaluated in $O(j)$ time, which can be improved to $O(1)$ time using recurrence relations [30] or hashing techniques. With such improvements, the R and T filling times reduce to $O(j^{2+1+0})$ and $O(j^{2+0})$, lowering the overall estimate to $O(j^3)$. Although, in practice, matrix filling contributes significantly to the algorithms run time complexity, we will show that the product-trace operation dominates the evaluation in the large j limit. In order to compute the trace, we need to accumulate $O(j^2)$ diagonal matrix elements of the five-fold matrix product. Naively, each matrix product takes $O(j^{2+2+2}) = O(j^6)$ operations. However, the structure of the M_e matrices shown in (4.22) allows a simplification. Each of the R and N multiplications takes $O(j^{2+2+0}) = O(j^4)$ operations, since the matrices are diagonal, while the T multiplications take $O(j^{2+2+1}) = O(j^5)$ operations, since each involves only one of i^-_e or i^+_e. The matrix products are performed serially, so the asymptotic complexity of the trace-product is thus $O(j^5)$ and, including the outer $m^\pm$ sums, the vertex amplitude evaluation has asymptotic complexity of $O(j^7)$ [cf. the Christensen-Egan algorithm for the Barrett-Crane vertex [12], whose asymptotic complexity is $O(j^5)$].

4.4 Comparison with Barrett-Crane vertex

One of the motivations for constructing new vertex amplitudes is the recently discovered inadequacy of the BC model in reproducing semiclassical graviton propagator behavior in the large spin limit. Some of the propagator matrix elements show the expected behavior, while others do not [1, 2, 29]. Thus, it is important to identify where the new vertex models differ from the BC one and whether they have better semiclassical limits.

The comparison should ultimately be done at the level of physical observables computed within each model. An important class of observables, already mentioned above, are matrix elements of the graviton propagator. However, their calculation

requires a contraction of the vertex amplitude with an appropriately chosen boundary state. This contraction introduces a large number of extra summations, which, if implemented naively, make the calculation prohibitively expensive. A further generalization of the evaluation algorithm is necessary to make the implementation computationally efficient [22] (chapter 5 of this thesis).

A simpler comparison can be done at the level of amplitudes and can already reveal important behaviors of the new vertices. One complication is the difference in the spin argument structures: the BC vertex has 10 spin arguments, the EPR vertex has 15 spin arguments, while the FK vertex has a total of 35 independent spin arguments. This complication may be overcome by fixing the 10 common j-spin arguments and maximizing the vertex amplitude over the remaining spins. This effective vertex amplitude can be substituted into the partition function (4.3) where the summation is then performed over spin foams which only assign j-spin labels to the dual 2-complex. This simplification allows the comparison of amplitudes for individual spin foams.

It is important to note that the amplitudes in (4.3) have contributions from faces and edges as well as vertices. The face amplitudes are the same for all models and are easily factored out. The edge amplitudes, on the other hand, also differ from model to model and thus must be included in the amplitude comparison. To make the comparison on a vertex by vertex basis, the edge amplitudes are split between the vertices they connect as follows:

$$A_v^{\text{eff}}(j) \sim \max_{i,k} A_v(j,k,i) \sqrt{\prod_{e \supset v} |A_e(j,k,i)|}. \tag{4.28}$$

For simplicity, we consider only spin inputs where each of the $j_{c,e}$, i_e and $k^x_{c,e}$ sets of spins have equal values, respectively denoted by j, i, and k. Our assumption is that vertex amplitudes for these spin inputs behave generically. Small scale numerical tests support this assumption. Otherwise, maximizing the expression in (4.28) over a larger i,k-parameter space quickly becomes impractical.

For the EPR model, we found that the maximum allowed value $i = 2j$ maximizes the amplitude. This behavior is illustrated in figure 4.1 for $j = 30$.

For the FK model, we found that, for fixed j and k, the amplitude is again maximized by the extreme value $i = 2k$. See figure 4.2 for the case $j = 30$ and $k = 15$. While keeping i at the dominant value $2k$, for fixed j, the amplitude is maximized by $k = 1$, although $k = 0$ dominates slightly for very small values of j. This k dependence is illustrated in figure 4.3 for the case $j = 30$.

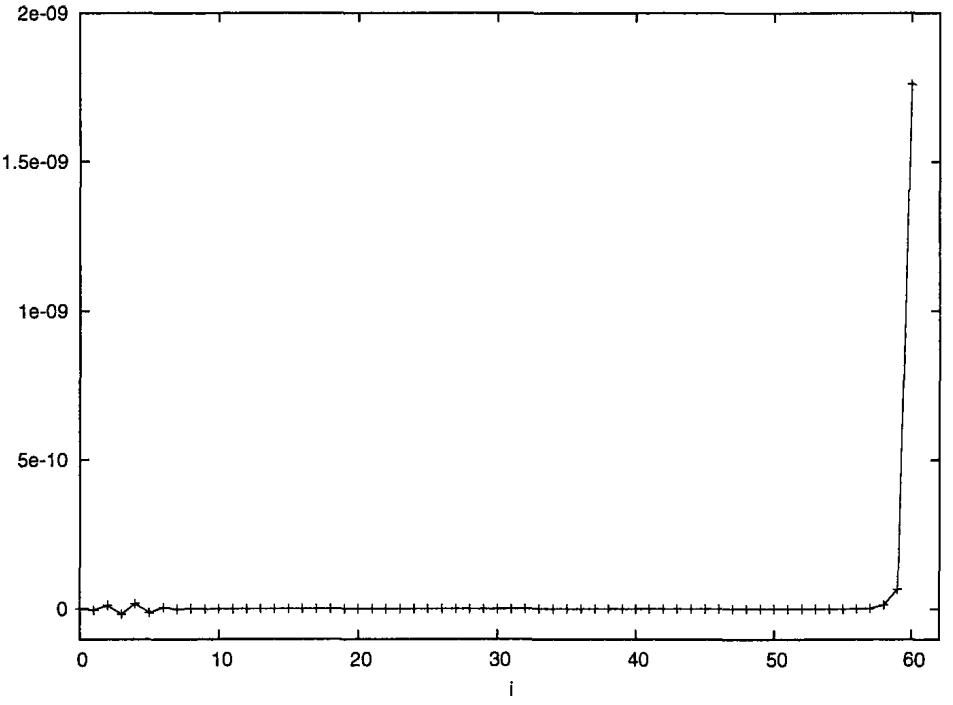

Figure 4.1: Effective EPR vertex amplitude: all $j = 30$, all i equal, satisfying $0 \leq i \leq 2j$.

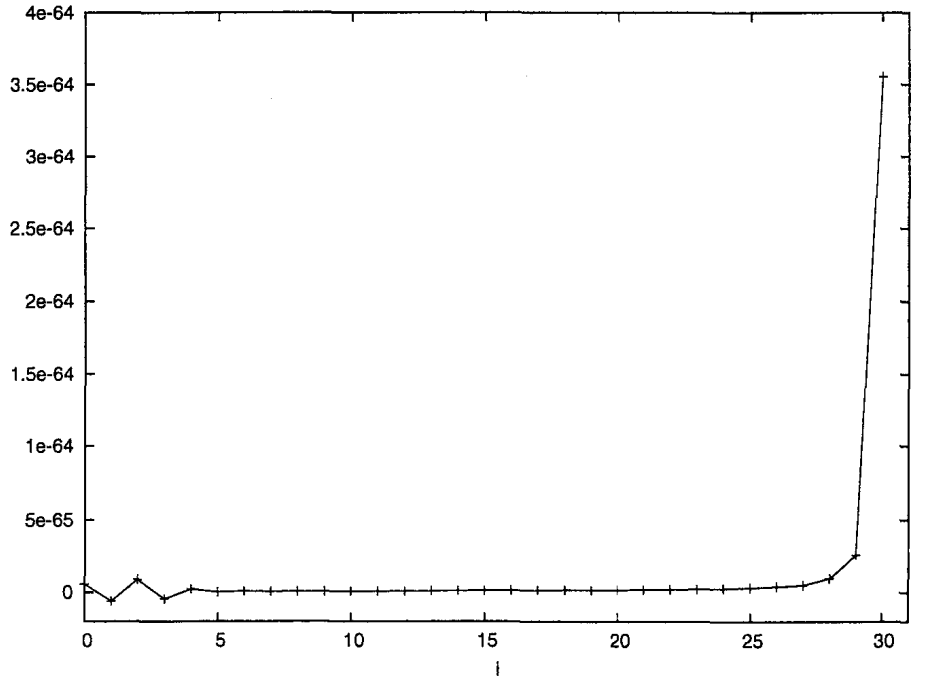

Figure 4.2: Effective FK vertex amplitude: all $j = 30$, all $k = 15$, all i equal, satisfying $0 \leq i \leq 2k$.

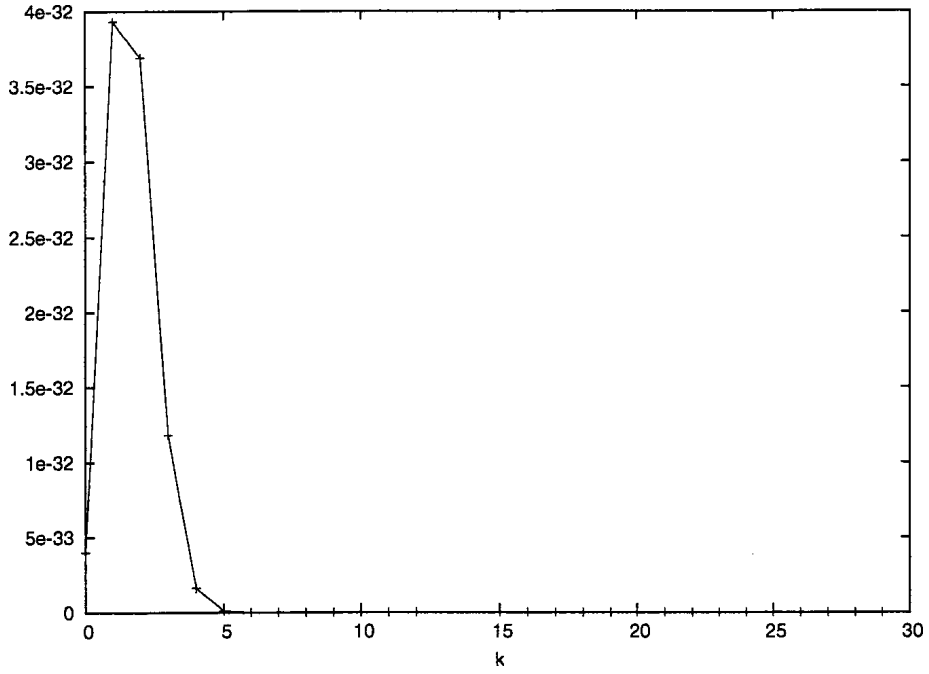

Figure 4.3: Effective FK vertex amplitude: all $j = 30$, all $i = 2k$, all k equal, satisfying $0 \leq k \leq j$.

4.4.1 Amplitude asymptotics

Spin foam quantization is similar in spirit to the discretized path integral approach to gravity. As such, the spin foam vertex amplitude is often compared to the gravitational path integral amplitude:

$$A_v(j) \sim \exp[iS_R], \tag{4.29}$$

where S_R is the Regge action for gravity evaluated on a discrete geometry described by the spins j in the large spin limit. For the BC vertex, this view has turned out to be overly simplistic. The relation predicted by careful asymptotic analysis is

$$A_v(j) \sim D(j) + \mu(j)[\exp(iS_R) + \exp(-iS_R)] + \cdots, \tag{4.30}$$

where $D(j)$ and $\mu(j)$ are non-oscillating functions decaying as j^{-2} and $j^{-9/2}$ respectively, with $(\cdots)$ representing higher order terms. The dominant asymptotic $D(j)$, understood to be due to the contribution of degenerate geometries, masks the desired Regge action amplitude [6, 9, 19].

A natural question is whether the new vertices share the same asymptotic behavior. Numerical evaluation of the BC vertex is only sensitive to the dominant

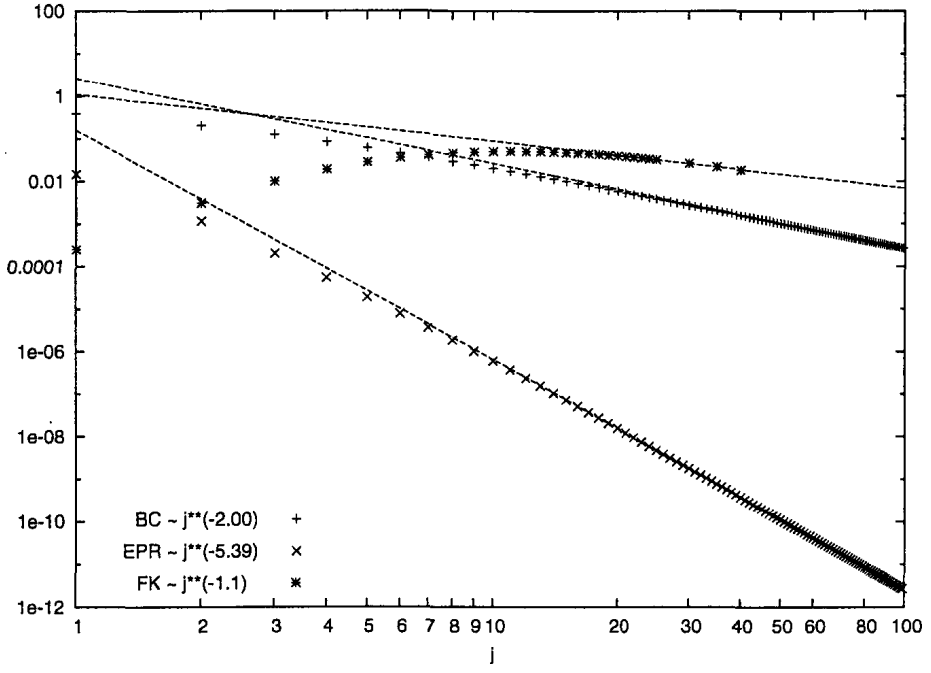

Figure 4.4: Large j behavior of the effective vertex amplitudes for the BC, EPR and FK models.

asymptotic contribution $D(j)$. The subdominant oscillating Regge action term would become important only if $D(j)$ is subtracted or if the vertex amplitude is averaged against another oscillatory function, in phase with one of the Regge action terms, as done in the graviton propagator calculations [13, 29]. While analytical asymptotics for the EPR and FK vertices are still missing, we can straightforwardly compare the numerical asymptotics of the dominant effective vertex amplitudes of all three models. This comparison is made in figure 4.4. For all models, the data shows no oscillations, which means that we are most likely seeing only the $D(j)$ asymptotic term. Note that the power laws shown in the figure will change if, for whatever reason, the edge amplitudes given in section 4.2 are modified by j-dependent factors.

4.5 Conclusion and Outlook

We have presented three spin foam models in a unified framework: the standard Barrett-Crane (BC) model and two more recent proposals, the Engle-Pereira-Rovelli (EPR) and Freidel-Krasnov (FK) models. Their vertex amplitudes were simplified using spin network recoupling techniques. A fast numerical evaluation algorithm for the new vertex amplitudes was developed by extending the Christensen-Egan

algorithm for the BC model.

Despite the different spin argument structure, we have extracted effective vertex amplitudes that can be directly compared from model to model. Figure 4.4 shows a comparison of their asymptotics. It is clear that the dominant asymptotic behavior of the new vertex amplitudes is non-oscillatory and displays power-law decay very similar to the BC model. The same figure shows the estimated power-law exponents. It seems likely that analytical asymptotics will reveal structure similar to (4.30).

A generalization of the vertex evaluation algorithm to efficiently incorporate contraction with a spin-factored boundary state will be presented elsewhere [22] (chapter 5 of this thesis). This improvement simplifies numerical investigation of the graviton propagator and other observables in these models.

Acknowledgments

The author would like to thank Dan Christensen for suggesting this project. Also, Wade Cherrington, Carlo Rovelli, and Elena Magliaro have contributed through helpful discussions. The author was supported by an Ontario Graduate Scholarship and a SHARCNET Fellowship. Computational resources for this project were provided by SHARCNET.

Bibliography

[1] Alesci E and Rovelli C 2007 Complete LQG propagator: Difficulties with the Barrett-Crane vertex *Physical Review D* **76** 104012–104033 (*Preprint* arXiv:0708.0883)

[2] Alesci E and Rovelli C 2008 Complete LQG propagator. II. Asymptotic behavior of the vertex *Physical Review D* **77** 044024–044034 (*Preprint* arXiv:0711.1284)

[3] Baez J C 1996 4-dimensional BF theory as a topological quantum field theory *Letters in Mathematical Physics* **38** 129–43 (*Preprint* arXiv:q-alg/9507006)

[4] Baez J C 1998 Spin foam models *Classical and Quantum Gravity* **15** 1827–58 (*Preprint* arXiv:gr-qc/9709052)

[5] Baez J C 2000 An introduction to spin foam models of quantum gravity and BF theory *Lecture Notes in Physics* **543** 25–94 (*Preprint* arXiv:gr-qc/9904025)

[6] Baez J C, Christensen J D, and Egan G 2002 Asymptotics of $10j$ symbols *Classical and Quantum Gravity* **19** 6489–513 (*Preprint* arXiv:gr-qc/0208010)

[7] Baez J C, Christensen J D, Halford T R, and Tsang D C 2002 Spin foam models of Riemannian quantum gravity *Classical and Quantum Gravity* **19** 4627–48 (*Preprint* arXiv:gr-qc/0202017)

[8] Barrett J W and Crane L 1998 Relativistic spin networks and quantum gravity *Journal of Mathematical Physics* **39** 3296–302 (*Preprint* arXiv:gr-qc/9709028)

[9] Barrett J W and Steele C M 2003 Asymptotics of Relativistic Spin Networks *Classical and Quantum Gravity* **20** 1341–1362 (*Preprint* arXiv:gr-qc/0209023)

[10] Carter J S, Flath D E, and Saito M 1995 The classical and quantum $6j$-symbols (*Mathematical Notes* vol 43) (Princeton, NJ: Princeton University Press)

[11] Cherrington J W, Christensen J D, and Khavkine I 2007 Dual computations of non-abelian Yang-Mills on the lattice *Physics Review D* **76** 094503–094519 (*Preprint* arXiv:0705.2629)

[12] Christensen J D and Egan G 2002 An efficient algorithm for the Riemannian $10j$ symbols *Classical and Quantum Gravity* **19** 1184–93 (*Preprint* arXiv:gr-qc/0110045)

[13] Christensen J D, Livine E R, and Speziale S 2007 Numerical evidence of regularized correlations in spin foam gravity (*Preprint* arXiv:0710.0617)

[14] Conrady F and Freidel L 2008 Path integral representation of spin foam models of 4d gravity (*Preprint* arXiv:0806.4640)

[15] De Pietri R, Freidel L, Krasnov K, and Rovelli C 2000 Barrett-Crane model from a Boulatov-Ooguri field theory over a homogeneous space *Nuclear Physics B* **574** 785–806 (*Preprint* arXiv:hep-th/9907154)

[16] Engle J, Pereira R, and Rovelli C 2007 The loop-quantum-gravity vertex-amplitude *Physical Review Letters* **99** 161301–161304 (*Preprint* arXiv:0705.2388)

[17] Engle J, Pereira R, and Rovelli C 2008 Flipped spinfoam vertex and loop gravity *Nuclear Physics B* **798** 251–290 (*Preprint* arXiv:0705.1236)

[18] Freidel L and Krasnov K 2008 A new spin foam model for 4d gravity *Classical and Quantum Gravity* **25** 125018–125053 (*Preprint* arXiv:0708.1595)

[19] Freidel L and Louapre D 2003 Asymptotics of $6j$ and $10j$ symbols *Classical and Quantum Gravity* **20** 1267–1294 (*Preprint* arXiv:hep-th/0209134)

[20] Kauffman L H and Lins S L 1994 Temperley-Lieb recoupling theory and invariants of 3-manifolds (*Annals of Mathematics Studies* vol 134) (Princeton, NJ: Princeton University Press)

[21] Khavkine I and Christensen J D 2007 q-deformed spin foam models of quantum gravity *Classical and Quantum Gravity* **24** 3271–3290 (*Preprint* arXiv:0704.0278)

[22] Khavkine I 2008 Evaluation of new spin foam vertex amplitudes with boundary states To appear.

[23] Livine E R and Speziale S 2007 New spinfoam vertex for quantum gravity *Physical Review D* **76** 084028–084041 (*Preprint* arXiv:0705.0674)

[24] Livine E R and Speziale S 2007 Consistently solving the simplicity constraints for spinfoam quantum gravity (*Preprint* arXiv:0708.1915)

[25] Modesto L and Rovelli C 2005 Particle scattering in loop quantum gravity *Physical Review Letters* **95** 191301–191304 (*Preprint* arXiv:gr-qc/0502036)

[26] Oeckl R 2005 Discrete Gauge Theory: From Lattices to TQFT (London, UK: Imperial College Press)

[27] Perez A and Rovelli C 2001 A spin foam model without bubble divergences *Nuclear Physics B* **599** 255–82 (*Preprint* arXiv:gr-qc/0006107)

[28] Rovelli C 2004 Quantum Gravity (Cambridge, UK: Cambridge University Press)

[29] Rovelli C 2006 Graviton propagator from background-independent quantum gravity *Physical Review Letters* **97** 151301–151304 (*Preprint* arXiv:gr-qc/0508124)

[30] Schulten K and Gordon R G 1975 Exact recursive evaluation of $3j$- and $6j$-coefficients for quantum mechanical coupling of angular momenta *Journal of Mathematical Physics* **16** 1961–1970

Chapter 5
Evaluation of new spin foam vertex amplitudes with boundary states

5.1 Introduction

Spin foam models are an attempt to produce a theory of quantum gravity starting from a discrete, path integral-like approach. For the last decade, the standard spin foam model has been the one due to Barrett and Crane [8]. More recently, some shortcomings of the Barrett-Crane (BC) model have been identified [2, 3] and alternative models were proposed. Two leading alternatives are the Engle-Pereira-Rovelli (EPR) model (also referred to as the "flipped" vertex model) [15, 16] and the Freidel-Krasnov (FK) model [14, 17]. Here, as in much of the spin foam literature, we only discuss gravity in Riemannian signature.

Having been defined, the new models must be tested to see whether their semiclassical behavior is an improvement over the BC model. So far, two test problems have been proposed: semiclassical wave packet propagation [22], and evaluation of the graviton 2-point function [9, 13, 24]. Both problems require the computation of large sums, where the spin foam vertex amplitude is contracted with a suitably defined boundary state. These computations, while important for extracting the physical content of the new spin foam models, have so far not been tractable.

In a previous paper [19] (chapter 4 of this thesis), the author has described an efficient numerical algorithm, based on the existing Christensen-Egan (CE) algorithm for the BC model, to evaluate the new spin foam vertex amplitudes. This algorithm was used to examine their asymptotic behavior. The present paper extends this algorithm to allow efficient contraction of the vertex amplitude with a large class of boundary states (so-called *factored* boundary states).

Application of this algorithm to the wave packet propagation problem shows that, under fairly general conditions, the shape of the propagated wave packet does not agree with the expected semiclassical result, unlike hypothesized in [22].

Section 5.2 reviews the two proposed calculations that require the introduction of boundary states. Also, the class of factored boundary states is defined. Section 5.3 describes the appropriate CE algorithm generalizations. Section 5.4 shows the results of applying the algorithms of section 5.3 to the problems of section 5.2. Finally, section 5.5 concludes with a discussion of the results and future work.

5.2 Spin foams with boundary states

Spin foam models in general are described in [4,5] and especially from a computational perspective in [6,7,20] and [19] (chapter 4 of this thesis). Briefly, a spin foam model of gravity starts with a triangulated 4-manifold (possibly with boundary). Its *dual 2-complex* consists of cells dual to simplices of the triangulation: a *dual vertex* for each 4-simplex, a *dual edge* for each tetrahedron, and a *dual face* for each triangle. A labelling of the dual 2-complex by *spins* constitutes a *spin foam.* The labelling of the dual 2-complex depends on the model, but at a minimum includes an integer label for each dual face, called a *spin*[1]. Besides specifying this labelling, a *spin foam model* also assigns an amplitude to a given spin foam. This amplitude for a spin foam F takes the form

$$A(F) = \prod_f A_f(F) \prod_e A_e(F) \prod_v A_v(F), \tag{5.1}$$

where f, e, and v range respectively over dual faces, dual edges, and dual vertices. Each of the amplitudes $A_f(F)$, $A_e(F)$, $A_v(F)$ may depend on its own label and on the labels of adjacent dual cells.

The BC model assigns integer labels only to dual faces (*j-spins*). The EPR model also assigns integer labels to dual edges (*i-spins*). The FK model additionally assigns integers to each dual edge-dual face pair (*k-spins*)[2].

The partition function for a spin foam model is defined to be

$$Z = \sum_F A(F), \tag{5.2}$$

---

1. Most of the time these integers identify representations of $SU(2)$, hence the name *spin.* Technically, they are *twice-spins*, since they do not take on half-integral values

2. It should be noted that the current paper uses integral twice-spins to label $SU(2)$ irreps, following [18], while the original references for the EPR [15] and FK [17] models use half-integral spins. However, the i and j labels of [15] coincide numerically with the current notation, while the l, j and k labels of [17] coincide respectively with i, $j/2$, and k in current notation.

where the summation ranges over all spin foams F. The expectation value of an observable O is calculated according to the formula

$$\langle O \rangle = \frac{1}{Z} \sum_F O(F) A(F). \tag{5.3}$$

If the underlying triangulated manifold is closed, then corresponding spin foams are also said to be *closed*. Similarly, if the underlying manifold has a boundary, the spin foams are said to be *open* and also have a boundary. Any open spin foam F_O can be decomposed into $F_O = F \cup F_B$, where F_B labels only cells dual to the boundary, while F labels only cells dual to triangulation simplices in the interior. For an open spin foam F_O, its amplitude may be naturally generalized to

$$A(F_O) = A(F, F_B)\Psi(F_B), \tag{5.4}$$

where the bulk amplitude $A(F, F_B)$ is the usual amplitude defined according to (5.1), and Ψ is referred to as the boundary state, which may be fixed separately from the bulk amplitude. The partition function and observables are then written as

$$Z_\Psi = \sum_{F,F_B} A(F, F_B)\Psi(F_B), \quad \text{and} \quad \langle O \rangle_\Psi = \frac{1}{Z_\Psi} \sum_{F,F_B} O(F, F_B) A(F, F_B)\Psi(F_B). \tag{5.5}$$

As an illustration, an open spin foam model with a boundary state may arise if we split a closed spin foam model in two parts and average over one of them. Suppose a close triangulated manifold can be decomposed into two bulk pieces and the codimension-1 boundary between them. Any closed spin foam F_C can then be decomposed as $F_C = F \cup F_B \cup F'$, where F_B corresponds to the boundary, F to the interior of the piece we are interested in and F' to the interior of the other piece. The partition function may be rewritten as follows:

$$\begin{aligned} Z &= \sum_{F_C} A(F, F_B) A(F_B) A(F', F_B) \\ &= \sum_{F,F_B} A(F, F_B) A(F_B) \sum_{F'} A(F', F_B) = \sum_{F,F_B} A(F, F_B)\Psi(F_B), \end{aligned} \tag{5.6}$$

where $\Psi(F_B)$ has been defined by averaging over all spin foams F'. This example is very similar to the separation of a large system into a subsystem and the environment in quantum statistical mechanics.

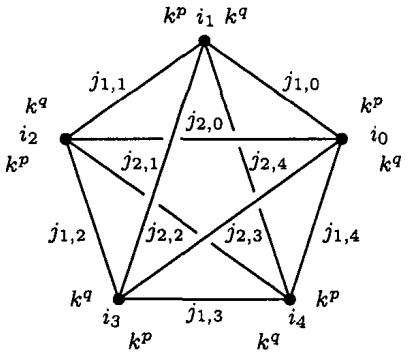

Figure 5.1: The *pent graph*, summarizing the indexing scheme for i-, j-, and k-spins.

The simplest example of a triangulation with boundary is a single 4-simplex, with the five tetrahedra forming its boundary. The 2-complex dual to the interior consists of a single dual vertex, corresponding to the 4-simplex itself. The dual 2-complex of the boundary consists of five dual edges, dual to the tetrahedra, and of ten dual faces, dual to the triangular faces of the tetrahedra. The problems described in sections 5.2.1 and 5.2.2, have previously only been considered for a single 4-simplex. This paper restricts attention to the same case.

The algorithms that will be described in section 5.3 are applicable only to a restricted class of states, *factored* states. Such a state must factor in a specific way with respect to the spins it depends on. The various spin labels of the dual complex of the 4-simplex and the corresponding notation are summarized in figure 5.1, referred to as the *pent graph*. The vertices of the pent graph correspond to the five boundary tetrahedra of the 4-simplex, while the ten edges connecting them correspond to its triangles. This graph is labelled by 35 spins, i_e, $j_{c,e}$, and $k^x_{c,e}$. The e subscript numbers the vertices of the pent graph; it is always taken mod 5. The spin $j_{c,e}$ labels the graph edge joining vertices e and $e+c$. The superscript x stands for either p or q; $k^p_{c,e}$ labells the vertex-edge pair e and (c,e), while $k^q_{c,e}$ labells the pair $e+c$ and (c,e). Again, all vertex indices are taken mod 5.

The class of factored states is somewhat different for each model. However, it contains at least all of the following:

$$\Psi(F_B) = \prod_{c,e} \psi_{c,e}(j_{c,e}) \prod_{e} \psi_e(i_e) \prod_{x,f,e} \psi_{x,f,e}(k^x_{f,e}), \tag{5.7}$$

where the products range over all i-, j-, and k-spins. Spins not part of a particular model may be dropped from the product. The ψs are arbitrary functions with finite support. For each model, the class of factored states is enlarged, as factors of $\Psi(F_B)$

may be allowed to depend on specific clusters of spins, instead of only individual ones. The details will be elaborated in section 5.3.

Nearly all previous work on the problems described in sections 5.2.1 and 5.2.2 have been considered only for factored boundary states. While this class of states is restrictive, its limitations may be overcome. Note that the expectation value $\langle O \rangle_\Psi$ in equation (5.5) is equal to the ratio of two quantities that are both linear in the boundary state Ψ. The numerical algorithm computes this numerator and denominator separately. Since any boundary state Ψ can be approximated by linear combinations of factored states with finite support, so can $\langle O \rangle_\Psi$ be approximated for any boundary state Ψ.

5.2.1 Semiclassical wave packets

The problem presented in this section was introduced in [22]. Consider a single 4-simplex. As shown in the preceding section, it is described by a spin foam with a single dual vertex and i-, j-, and k-spins labelling cells dual to its boundary. An arbitrary functional $\Psi(F_B)$ depending on these boundary spins, in general, corresponds to a statistical quantum state, that is, a density matrix.

This is analogous to the single point particle, where an arbitrary density matrix $\rho(x_f, x_i) = \langle x_f, t_f | \rho | x_i, t_i \rangle$ can be described in terms of its matrix elements between eigenstates of the Heisenberg position operator at different times[3], $x(t_i)|x_i, t_i\rangle = x_i|x_i, t_i\rangle$ and $x(t_f)|x_f, t_f\rangle = x_f|x_f, t_f\rangle$. The density matrix is pure only if it can be factored, $\rho(x_f, x_i) = \psi(x_f, t_f)^* \psi(x_i, t_i)$, where $\psi(x, t)$ denotes the time evolution of a given wave function.

Similarly, we can split the boundary of the 4-simplex into two pieces[4], the initial $(-)$ and the final $(+)$. Then, for a pure boundary state, we should be able to write

$$\Psi(F_B) = \Psi_+(F_B^+)^* \Psi_-(F_B^-), \tag{5.8}$$

where $F_B^\pm$ respectively depend only on spins labelling the dual complex of the corresponding piece of the boundary.

---

3. In this representation, the functional $\rho(x_f, x_i)$ is not necessarily symmetric, $\rho(x_i, x_f) \neq \rho(x_f, x_i)^*$.

4. Technically speaking, this decomposition is unique only in Lorentzian signature. In Riemannian signature, different choices of the decomposition should correspond to different possible Wick rotations.

The relationship of the two boundary state factors $\Psi_\pm(F_B^\pm)$ is constrained in two ways. On the one hand (in the limit of $\hbar \to 0$), the amplitude should be peaked on those geometries that correspond to the boundary of a classical 4-geometry satisfying Einstein's equations. On the other hand, Ψ_+ should be a time-evolved, "future" version of the "past" Ψ_-, which can be expressed as

$$\Psi_+(F_B^+) = \sum_{F, F_B^-} A(F, F_B)\Psi_-(F_B^-), \tag{5.9}$$

where the summation over the boundary spin foams keeps F_B^+ fixed and varies F_B^-.

Reference [22] has proposed an expression for $\Psi(F_B)$, in the context of the EPR model, which should reproduce a flat regular 4-simplex. This state has gaussian dependence on individual spins and hence is factorable in a convenient way. The problem is then to compute $\Psi_+(F_B^+)$ both from (5.8) and from (5.9), and to compare the two. Agreement is interpreted as evidence of a correct semiclassical limit for the EPR model.

A concrete expression for the proposed $\Psi(F_B)$ is

$$\Psi(F_B) = N \prod_{c,e} \psi_{c,e}(j_{c,e}) \prod_e \psi_e(i_e, \{j_{c,e}\}), \quad \text{with} \tag{5.10}$$

$$\psi_{c,e}(j_{c,e}) = e^{-\frac{1}{\tau}(j_{c,e}-j_0)^2 + i\Theta j_{c,e}}, \tag{5.11}$$

$$\psi_e(i_e, \{j_{c,e}\}) = \sqrt{\frac{2i_e+1}{\theta(2i_e, 2j_{1,e}, 2j_{2,e})\theta(2i_e, 2j_{1,e-1}, 2j_{2,e-2})}}\, e^{-\frac{3}{4j_0}(i-i_0)^2 + i\frac{\pi}{2}i_e}, \tag{5.12}$$

where N is a normalization factor, j_0 determines the size of the regular 4-simplex and $\cos\Theta = -1/4$. The parameter τ controls the size of quantum fluctuations about the classical values of j.

The wave packet propagation geometry given in [22] fixes $\tau = 0$ in the state (5.11), freezing all j-spins to the background value j_0. Effectively, only the dependence of $\Psi(F_B)$ on the i-spins was considered. A single vertex of the 4-simplex is labelled as "past", while the remaining four as "future". The four "future" vertices form a tetrahedron, whose dual is labelled by an i-spin. This labelled dual edge constitutes F_B^+, while the remaining four dual edges labelled by i-spins constitute F_B^-. This propagation geometry will be referred to as *EPR 4-1 propagation.*

An immediate generalization, feasible with the algorithm described in section 5.3, is to relax the $\tau = 0$ limitation. The choice of τ should be consistent

with the parameters used in the graviton propagator calculations. Thus, following[5] [13], we let the wave packet width depend on the background spin,

$$\tau = 4j_0/\alpha, \tag{5.13}$$

with α is a positive parameter.

Further, a uniform methodology should be constructed for each of the three models. As only j-spins are common among the models, we propose the following wave packet propagation geometry. One possibility is to propagate wave packets from one of the j-spins to the remaining nine. This configuration corresponds to fixing a single triangle (defined by three vertices of a 4-simplex) in the "past", while relegating the other nine triangles (containing at least one of the two remaining 4-simplex vertices) to the "future". Thus, the single j-labelled face dual to the "past" triangle will constitute F_B^-, while the rest of the boundary spin foam will constitute F_B^+, including all i- and k-spins, if any. This propagation geometry will be referred to as *1-9 propagation.*

Another alternative is to assign a vertex of the 4-simplex to the "future", together with the six triangles sharing sharing it. The remaining four triangles are relegated to the "past". Thus, F_B^+ consists of the six j-labelled faces dual to the "future" triangles, with the rest of the boundary spin foam constituting F_B^-. This propagation geometry will be referred to as *4-6 propagation.* There are numerous other possibilities. However, the two described above are sufficient to illustrate an application of the numerical algorithms and to show the qualitative behavior to be expected from propagated wave packets.

The boundary state (5.10) is valid only for the EPR model. For the BC model, we simply drop the ψ_e factors:

$$\Psi(F_B) = N \prod_{c,e} \psi_{c,e}(j_{c,e}). \tag{5.14}$$

And for the FK model we must add extra $\psi^x_{c,e}$ factors for each k-spin:

$$\Psi(F_B) = N \prod_{c,e} \psi_{c,e}(j_{c,e}) \prod_{e} \psi_e(i_e, \{j_{c,e}\}) \prod_{x,c,e} \psi^x_{c,e}(k^x_{c,e}, j_{c,e}). \tag{5.15}$$

---

5. It should be noted that reference [13] uses half-integral spins, while we use integral twice-spins to label $SU(2)$ irreps. A j label from Christensen, Livine and Speziale corresponds numerically to $j/2$ in current notation.

Because the k-spins are closely geometrically associated with j-spins, we use the same gaussian state parameters:

$$\psi^x_{c,e}(k^x_{c,e}, j_{c,e}) = \sqrt{\frac{2k^x_{c,e}+1}{\theta(j_{c,e}, j_{c,e}, 2k^x_{c,e})} C_{j_{c,e}k^x_{c,e}}} e^{-\frac{\alpha}{4j_0}(k^x_{c,e}-j_0)^2 + i\Theta k^x_{c,e}}, \tag{5.16}$$

$$C_{jk} = \frac{(j+1)!}{(j-k)!}\frac{(j+1)!}{(j+k+1)!}. \tag{5.17}$$

The square root factor includes the FK model edge normalization, as does (5.12) for the EPR model.

5.2.2 Graviton propagator

The graviton propagator is well defined in the perturbative quantization of gravity. It is computed as the 2-point function $G_{\mu\nu\rho\sigma}(x,y) = \langle 0|h_{\mu\nu}(x)h_{\rho\sigma}(y)|0\rangle$, where $|0\rangle$ is the Minkowski vacuum, and $h_{\mu\nu}(x)$ is the metric perturbation. General relativity requires that, in harmonic gauge [25], the decay rate of the 2-point function, for large separation between points x and y, is the same as for the Newtonian force of gravitational attraction: inverse distance squared. The framework for computing the equivalent of the graviton propagator in the spin foam formalism was elaborated in [9, 21, 23, 24]. The quantum area spectrum is $A = \ell_P^2(j+1)$, with j a dual face spin foam label and ℓ_P the Plank length. Dimensional arguments then give the expected decay of the propagator as $O(1/j)$, with j being the typical size for the chosen spin foam boundary state.

The expected asymptotic behavior of the graviton propagator has been checked for the BC model both analytically and numerically [13, 21, 24]. Unfortunately, the expected behavior was only reproduced for certain tensor components of $G_{\mu\nu\rho\sigma}(x,y)$, but not for others [2, 3]. This negative result has prompted the introduction of EPR and FK spin foam models as alternatives to the BC model. The challenge is to compute the graviton propagator for the new models and check that it has the expected asymptotic behavior.

Following [13], we show the computational set up for the BC model and then extend it to other models. Consider again a single 4-simplex with boundary and the corresponding spin foam. We associate the area $A = \ell_P^2(j+1)$ to each triangle, depending on the j-spin labelling its dual. The goal is to compute the correlation

between observables depending on the triangle areas [cf. (5.5)]:

$$W_{ce,c'e'} = \frac{1}{Z_\Psi} \sum_{F,F_B} A(F,F_B) h_{ce}(F_B) h_{c'e'}(F_B) \Psi(F_B), \tag{5.18}$$

where ce and $c'e'$ index the specific $j_{c,e}$ and $j_{c',e'}$ spins taking part in the correlation. Again following [13], the boundary state[6] is a semiclassical gaussian state peaked around a flat 4-simplex, whose scale is set by j_0:

$$\Psi(F_B) = \prod_{c,e} e^{-\frac{\alpha}{4j_0}(j_{c,e}-j_0)^2 + i\Theta j_{c,e}}, \tag{5.19}$$

where $\cos\Theta = -1/4$, and j_0 sets the scale for the background geometry, as in the previous section. The observables measure the fluctuation of areas squared:

$$h_{ce}(F_B) = \frac{(j_{c,e}+1)^2 - (j_0+1)^2}{(j_0+1)^2}. \tag{5.20}$$

Note that the product $\Psi'(F_B) = h_{ce}(F_B)\Psi(F_B)$ has exactly the same factorizability properties as $\Psi(F_B)$. This property allows both the numerator and denominator in (5.18) to be computed on the same footing.

Again, an important task here is the generalization of this calculation to the EPR and FK models. This generalization essentially requires the specification of a boundary state that describes a semiclassical state peaked around the flat regular 4-simplex. Since this is the same requirement used in picking out the boundary states in the section on wave packet propagation, simply choose the same ones. That is, the BC, EPR and FK boundary states are specified, respectively, by equations (5.14), (5.10), and (5.15).

5.3 Numerical algorithms

We will start by reviewing the spin foam vertex evaluation algorithms with fixed boundary spins. The dual face and edge amplitudes, A_f and A_e, are trivial to compute. The difficulty lies in evaluating the dual vertex amplitude A_v, which is where we will concentrate. All algorithms described in this section are extensions of the

6. We incorporate the "measure" discussed in [13] into the boundary state and pick the trivial case $k = 0$.

original CE algorithm for the BC model [12] and all fall into the same product-trace pattern:

$$A_v(\{j_{c,e}, i_e, k^x_{c,e}\}) = (-)^S \sum_{m^-,m^+} \phi \,\mathrm{tr}[M_4 M_3 M_2 M_1 M_0], \tag{5.21}$$

where $(-)^S$ is an overall sign factor, ϕ depends only on $m^\pm$ and M_e are matrices of compatible dimensions, collectively depending on all the spins. Each of these elements may be specified separately in any incarnation of this algorithm. In all cases presented below, we have

$$\phi = (-)^{\frac{1}{2}(m^- - m^+)}(m^- + 1)(m^+ + 1). \tag{5.22}$$

However, the M_e matrices will be redefined for each variation of the algorithm. The notation for various boundary spins is summarized with the pent graph in figure 5.1.

The run time complexity of a generalized CE algorithm may be estimated as follows. Suppose that the spin arguments to A_v in (5.21) are of average magnitude j. Then, generally, the dimensions of the matrices M_e scale as a power of j; say, each matrix is $O(j^d) \times O(j^d)$, for some integer d. The run time will be dominated by filling the M_e matrices and by the product-trace operation.

The product-trace may be implemented as follows: each of the $O(j^d)$ standard basis vectors is subjected to matrix-vector multiplies by the M_e and appropriate elements of the result vectors are accumulated into the trace. If the M_e are dense, then the cost of a matrix-vector multiply is $O(j^{2d})$. However, we shall see below that this complexity may be reduced by decomposing each M_e into sparse factors. Hence, we will parametrize the matrix-vector multiply complexity as $O(j^D)$, with D no greater than $2d$, and the product-trace complexity as $O(j^{d+D})$.

The upper bound on the time needed to fill an $O(j^d) \times O(j^d)$ matrix M_e is $O(j^{2d+f})$, if each matrix element is computed in $O(j^f)$ time. Sparse factorization improves this estimate as well, which we will parametrize as $O(j^{F+f})$, where F does not exceed $2d$. In all cases we have examined, $d + D > F + f$, which implies that the product-trace operation dominates matrix filling in run time for large spins. More detailed discussions of possible optimizations for matrix filling can be found in [20] and [19] (chapter 4 of this thesis). Below, we will give the best known value of f for each algorithm.

Finally, the outer $m^\pm$ sums in (5.21) also span ranges of size $O(j)$. Therefore, the run time complexity of a generalized CE algorithm may be expressed as $O(j^{2+d+D})$.

The matrix elements of the M_e (computed in the following sections), will contain spin network evaluations that require certain inequality and parity constraints on their arguments. Solving these constraints yields precise matrix dimensions and bounds for any intermediate summations. The details are described in section 3.2 of [19] (chapter 4 of this thesis). It can be shown that all matrix dimensions as well as intermediate summation bounds are finite. However, for that to be true in the presence of a boundary state, it is crucial that each factor of the boundary state (5.7) has finite support.

5.3.1 BC vertex

For the BC model, the vertex amplitude is only a function of the j-spins. As a slight abuse of notation, we will use the symbols i_e as indices (also referred to as spins, and directly analogous to the $i_e^{\pm}$ indices introduced for the other models) of the M_e matrices:

$$(M_e)_{i_e}^{i_{e+1}} = \frac{(i_e+1)\begin{bmatrix} i_e & j_{2,e} & m^- \\ i_{e+1} & j_{2,e-1} & j_{1,e} \end{bmatrix}\begin{bmatrix} i_e & j_{2,e} & m^+ \\ i_{e+1} & j_{2,e-1} & j_{1,e} \end{bmatrix}}{\theta(j_{2,e-1}, i_{e+1}, j_{1,e})\,\theta(j_{2,e}, i_e, j_{1,e})\,\theta(j_{2,e}, i_{e+1}, m^-)\,\theta(j_{2,e}, i_{e+1}, m^+)}. \tag{5.23}$$

The sign factor from (5.21) is given by $S = \sum_{c,e} j_{c,e}$. The ranges of the i_e and m spins are specified by triangle inequalities and parity constraints satisfied by various spins. For a detailed derivation and for notation, see the original reference [12], and also [20] (chapter 3 of this thesis) and its Appendix[7].

The structure of the M_e matrices will become increasingly important and will grow in sophistication in the algorithms presented below. Hence, it is convenient to introduce a graphical notation to represent this structure. In this simplest case we have:

$$M_e = \quad {}^{i_{e+1}} \text{---} \boxed{M_e} \text{---} {}^{i_e} . \tag{5.24}$$

Each strand represents an index. The incoming and outgoing strands correspond to the i_e and i_{e+1} indices of M_e and are labelled as such. The product-trace operation in (5.21) is effected by concatenating appropriately labelled strands. Further features of the notation will be elaborated as they are introduced.

---

7. Note however, that these references use half-integral spins, while the present paper uses integer twice-spins.

Each matrix M_e is dense and of size $O(j)\times O(j)$. According to the discussion at the beginning of this section, we have $d=1$, $D=2$, $f=0$, $F=2$, and $2+d+D=5$. Hence, we recover the well known $O(j^5)$ run time complexity of the original CE algorithm.

5.3.2 New vertices

For the EPR model, the amplitude is a function of both i- and j-spins, while the FK model is also a function of k-spins. Here, we give the explicit FK formula, with the EPR version obtained by setting $k^x_{c,e}=j_{c,e}$. The matrix elements of M_e are

$$(M_e)^{i^-_{e+1}i^+_{e+1}}_{i^-_e i^+_e}=Q^{e+1}_{i^-_{e+1}i^+_{e+1}}(T^e_-)^{i^-_{e+1}}_{i^-_e}(T^e_+)^{i^+_{e+1}}_{i^+_e}\left[P^e_{i^-_e i^+_e}N^e_{i^-_e}N^e_{i^+_e}\frac{(-)^{\frac{1}{2}(i^-_e+i^+_e-2i_e)}}{\theta(i^-_e,i^+_e,2i_e)}\right] \tag{5.25}$$

where

$$(T^e_\pm)^{i^\pm_{e+1}}_{i^\pm_e}=\frac{\begin{bmatrix} i^\pm_e & j_{1,e} & j_{2,e-1}\\ i^\pm_{e+1} & m^\pm & j_{2,e}\end{bmatrix}}{\theta(i^\pm_{e+1},m^\pm,j_{2,e})}, \tag{5.26}$$

$$N_{i^\pm_e}=\frac{\Delta_{i^\pm_e}}{\theta(i^\pm_e,j_{1,e},j_{2,e})\theta(i^\pm_e,j_{2,e-2},j_{1,e-1})}, \tag{5.27}$$

$$P^e_{i^-_e i^+_e}=\sum_{n_p}(-)^{\frac{1}{2}(j_{1,e}+j_{2,e}-n_p)}\Delta_{n_p}$$
$$\frac{\begin{bmatrix}2k^p_{2,e} & 2k^p_{1,e} & n_p\\ i^-_e & i^+_e & 2i_e\end{bmatrix}}{\theta(n_p,j_{1,e},j_{2,e})}\frac{\begin{bmatrix}j_{1,e} & j_{1,e} & j_{2,e}\\ i^-_e & n_p & 2k^p_{1,e}\end{bmatrix}}{\theta(i^-_e,n_p,2k^p_{1,e})}\frac{\begin{bmatrix}j_{2,e} & j_{2,e} & j_{1,e}\\ i^+_e & n_p & 2k^p_{2,e}\end{bmatrix}}{\theta(i^+_e,n_p,2k^p_{2,e})}, \tag{5.28}$$

and

$$Q^e_{i_e^- i_e^+} = \sum_{n_q} (-)^{\frac{1}{2}(j_{2,e-2}+j_{1,e-1}-n_q)} \Delta_{n_q} \frac{\begin{bmatrix} 2k^q_{1,e-1} & 2k^q_{2,e-2} & n_q \\ i_e^- & i_e^+ & 2i_e \end{bmatrix}}{\theta(n_q, j_{2,e-2}, j_{1,e-1})} \frac{\begin{bmatrix} j_{2,e-2} & j_{2,e-2} & j_{1,e-1} \\ i_e^- & n_q & 2k^q_{2,e-2} \end{bmatrix}}{\theta(i_e^-, n_q, 2k^q_{2,e-2})} \frac{\begin{bmatrix} j_{1,e-1} & j_{1,e-1} & j_{2,e-2} \\ i_e^+ & n_q & 2k^q_{1,e-1} \end{bmatrix}}{\theta(i_e^+, n_q, 2k^q_{1,e-1})}. \tag{5.29}$$

For a detailed derivation and for bounds on the various summations, see [19] (chapter 4 of this thesis).

The matrix elements of M_e are indexed by the pairs (i_e^-, i_e^+) and (i_{e+1}^-, i_{e+1}^+). In graphical notation, M_e has the following structured factorization.

$M_e =$ 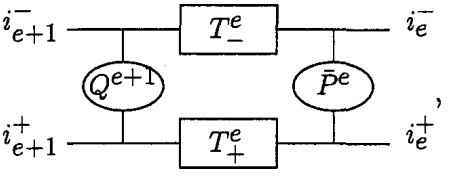

, (5.30)

where $\bar{P}^e$ stands for the entire bracketed term in (5.25). Unmarked vertices in the above diagram essentially correspond to Kronecker deltas. The notation is saying that both P^e and Q^{e+1} are diagonal matrices acting on the space of vectors indexed by (i_e^-, i_e^+) or (i_{e+1}^-, i_{e+1}^+). On the other hand, the $T^e_\pm$ matrices are block diagonal, acting separately on the $-$ and $+$ indices.

The dimension of each M_e is $O(j^2) \times O(j^2)$, implying $d = 2$. However, each M_e decomposes into sparse (diagonal or block diagonal) factors. The filling complexity parameters for the largest of these factors, $\bar{P}$ and Q, are $f = 1$, $F = 2$, and $F + f = 3$. Also, the cost of a matrix-vector multiply is parametrized by $D = 2 + 1 = 3$, giving $2 + d + D = 7$. Therefore, the run time complexity of evaluating an EPR or FK vertex amplitude is $O(j^7)$, as originally pointed out in [19] (chapter 4 of this thesis). This estimate compares favorably to simply treating M_e as a dense $O(j^2) \times O(j^2)$ matrix, which would imply an overall $O(j^8)$ run time complexity.

Contracting a boundary state, as described in section 5.2, with the vertex amplitude (5.21) gives the following partition function

$$Z_\Psi = \sum_{\{j_{c,e}, i_e, k^x_{c,e}\}} A_v(\{j_{c,e}, i_e, k^x_{c,e}\}) \Psi(\{j_{c,e}, i_e, k^x_{c,e}\}). \tag{5.31}$$

A naive approach to the problem of computing Z_Ψ would wrap an algorithm to compute A_v (as described so far in this section) in as many outer sums as there are spins in $\{j_{c,e}, i_e, k^x_{c,e}\}$. Namely, for the BC model, this would produce a calculation of run time complexity $O(j^{5+10}) = O(j^{15})$, with 10 outer spin sums. The EPR model would yield $O(j^{7+15}) = O(j^{22})$, with 15 outer spin sums, and the FK model $O(j^{7+35}) = O(j^{42})$, with 35 outer spin sums. Clearly, with the naive approach, these problems become intractable. Fortunately, when dealing with a factored state (as defined tentatively in section 5.2 and more precisely in the following sections), these summations may be absorbed into a redefinition of the M_e matrices, producing again a generalized CE algorithm:

$$Z_\Psi = \sum_{m^-,m^+} \phi \,\mathrm{tr}[M_4 M_3 M_2 M_1 M_0], \tag{5.32}$$

where ϕ is still defined by equation (5.22) and the sign factor is necessarily absorbed into the M_e. This approach is described in the next two sections.

It is important to note that the dimensions of the M_e matrices may be strongly impacted by the presence of a finitely supported boundary state. It is convenient for our purposes to keep the assumption that, even in the presence of a boundary state, the summation range for each spin is still of order $O(j)$. The run time complexity will be analyzed only for this case. However, the same analysis can be easily performed in other cases, where some of the spin summation ranges are significantly different.

5.3.3 BC vertex with boundary states

For the BC model, consider a factored boundary state of the form

$$\Psi(\{j_{c,e}\}) = \prod_{c,e} \psi_{c,e}(j_{c,e}). \tag{5.33}$$

The dependence of the matrices given in (5.23) on $\{j_{c,e}\}$ allows us to obtain the form (5.32) with the following redefinition:

$$(M_e)^{j_{2,e}i_{e+1}}_{j_{2,e-1}i_e} = \frac{(i_e+1)\,\psi_{2,e-1}(j_{2,e-1})}{\theta(j_{2,e},i_{e+1},m^-)\,\theta(j_{2,e},i_{e+1},m^+)} \sum_{j_{1,e}} \psi_{1,e}(j_{1,e}) \frac{\begin{bmatrix} i_e & j_{2,e} & m^- \\ i_{e+1} & j_{2,e-1} & j_{1,e} \end{bmatrix} \begin{bmatrix} i_e & j_{2,e} & m^+ \\ i_{e+1} & j_{2,e-1} & j_{1,e} \end{bmatrix}}{\theta(j_{2,e-1},i_{e+1},j_{1,e})\,\theta(j_{2,e},i_e,j_{1,e})}. \quad (5.34)$$

Graphically, we represent the above equation as

$M_e =$ 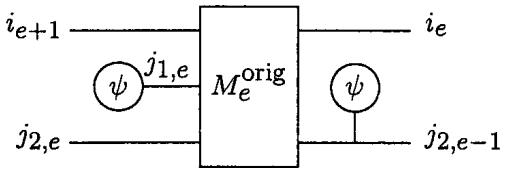

, (5.35)

where M_e^{orig} corresponds to the right hand side of equation (5.23) and ψ refer to the appropriate factors of the boundary state (5.33). The tadpole ψ shows an internal summation over $j_{1,e}$ necessary to form the matrix elements of M_e. It is shown here to highlight the location of the extra summation insertion and the possible relation of $\psi_{1,e}$ to other spins. Note that, without any modification to the evaluation algorithm, we can generalize the notion of factored boundary states to include factors of the form $\psi(j_{1,e}, j_{2,e}, j_{2,e-1})$.

Notice that in this case M_e is dense and of size $O(j^2) \times O(j^2)$. Hence, the algorithm's runtime complexity is $O(j^8)$, as $d = 2$, $D = 2+2$, and $2+d+D = 8$, while the filling parameters are $f = 1$ and $F = 4$. Interestingly enough, the *tets*[8] satisfy an identity which allows us to decompose M_e into sparse factors speeding up both the product-trace and matrix filling, thus reducing the run time complexity to $O(j^7)$. This identity is known as the Biedenharn-Elliot identity [10, 18]:

$$\frac{\begin{bmatrix} A & B & C \\ a & b & c \end{bmatrix} \begin{bmatrix} A' & B' & C' \\ a & b & c \end{bmatrix}}{\theta(a,b,c)} = \sum_s \Delta_s \frac{\begin{bmatrix} s & C' & B' \\ a & B & C \end{bmatrix}}{\theta(s,A,A')} \frac{\begin{bmatrix} s & A' & C' \\ b & C & A \end{bmatrix}}{\theta(s,B,B')} \frac{\begin{bmatrix} s & B' & A' \\ c & A & B \end{bmatrix}}{\theta(s,C,C')}. \quad (5.36)$$

8. The *tets* are the 2×3 arrays in square brackets, also called *tetrahedral networks*.

The product of two tets in equation (5.34) can be rewritten using this identity as

$$\frac{\begin{bmatrix} i_e & j_{2,e} & m^- \\ i_{e+1} & j_{2,e-1} & j_{1,e} \end{bmatrix} \begin{bmatrix} i_e & j_{2,e} & m^+ \\ i_{e+1} & j_{2,e-1} & j_{1,e} \end{bmatrix}}{\theta(j_{2,e-1}, i_{e+1}, j_{1,e})}$$
$$= \sum_{s_e} \Delta_{s_e} \frac{\begin{bmatrix} s_e & m^+ & j_{2,e} \\ i_{e+1} & j_{2,e} & m^- \end{bmatrix}}{\theta(s_e, i_e, i_e)} \frac{\begin{bmatrix} s_e & i_e & m^+ \\ j_{2,e-1} & m^- & i_e \end{bmatrix}}{\theta(s_e, j_{2,e}, j_{2,e})} \frac{\begin{bmatrix} s_e & j_{2,e} & i_e \\ j_{1,e} & i_e & j_{2,e} \end{bmatrix}}{\theta(s_e, m^-, m^+)}. \quad (5.37)$$

Hence, we can factor M_e as follows:

$$(M_e)^{j_{2,e} i_{e+1}}_{j_{2,e-1} i_e} = \frac{(i_e+1)\,\psi_{2,e-1}(j_{2,e-1})}{\theta(j_{2,e}, i_{e+1}, m^-)\,\theta(j_{2,e}, i_{e+1}, m^+)} \sum_{s_e, j_{1,e}} \frac{\psi_{1,e}(j_{1,e})\Delta_{s_e}}{\theta(j_{2,e}, i_e, j_{1,e})}$$
$$\frac{\begin{bmatrix} s_e & m^+ & j_{2,e} \\ i_{e+1} & j_{2,e} & m^- \end{bmatrix}}{\theta(s_e, i_e, i_e)} \frac{\begin{bmatrix} s_e & i_e & m^+ \\ j_{2,e-1} & m^- & i_e \end{bmatrix}}{\theta(s_e, j_{2,e}, j_{2,e})} \frac{\begin{bmatrix} s_e & j_{2,e} & i_e \\ j_{1,e} & i_e & j_{2,e} \end{bmatrix}}{\theta(s_e, m^-, m^+)}. \quad (5.38)$$

Graphically, this rewriting can be show to be a factorization:

$M_e =$ 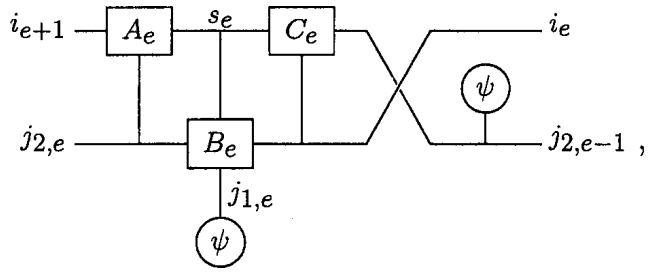

, (5.39)

where the factors are given explicitly by

$$(A_e^{j_{2,e}})^{i_{e+1}}_{s_e} = \frac{\begin{bmatrix} s_e & m^+ & j_{2,e} \\ i_{e+1} & j_{2,e} & m^- \end{bmatrix}}{\theta(j_{2,e}, i_{e+1}, m^-)\,\theta(j_{2,e}, i_{e+1}, m^+)}, \quad (5.40)$$

$$(\psi\text{-}B_e^{s_e})^{j_{2,e}}_{i_e} = \sum_{j_{1,e}} \frac{\psi_{1,e}(j_{1,e})\Delta_{s_e}}{\theta(j_{2,e}, i_e, j_{1,e})} \frac{\begin{bmatrix} s_e & j_{2,e} & i_e \\ j_{1,e} & i_e & j_{2,e} \end{bmatrix}}{\theta(s_e, j_{2,e}, j_{2,e})}, \quad (5.41)$$

$$(C_e^{i_e})^{s_e}_{j_{2,e-1}} = (i_e+1) \frac{\begin{bmatrix} s_e & i_e & m^+ \\ j_{2,e-1} & m^- & i_e \end{bmatrix}}{\theta(s_e, i_e, i_e)\,\theta(s_e, m^-, m^+)}. \quad (5.42)$$

The decomposition is not completely unique; some of the terms may be distributed differently among the factors. However, in this factorization, the dependence of $\psi_{1,e}$ can only be generalized to $(j_{1,e}, j_{2,e})$.

Thus M_e is clearly decomposed into sparse factors, as each of A_e, B_e and C_e is dense in some indices, but diagonal in others. Computing the run time complexity, we get $O(j^7)$, as $d = 2$, $D = 2 + 1$, and $2 + d + D = 7$, while $f = 0$, $F = 3$ and $F + f = 3$ for filling either A or C. Note that the matrices B_e contracted with the $\psi_{1,e}$ factors do not depend on $m^{\pm}$. Hence, their computation can be done outside the $m^{\pm}$ summation loops and becomes completely subdominant.

Curiously, the most practically efficient implementation of the algorithm described in this section, as carried out by Christensen [11], turns out to be a hybrid of $O(j^8)$ and $O(j^7)$ versions. The factorization (5.39) greatly speeds up the matrix filling step, while the simplicity of the dense version of the product-trace operation is still advantageous for all inputs tried to date (up to $j_0 = 10$).

5.3.4 New vertices with boundary states

For the EPR and FK models, consider respectively

$$\Psi(\{j_{c,e}, i_e\}) = \prod_{c,e} \psi_{c,e}(j_{c,e}) \prod_{i_e} \psi_e(i_e) \tag{5.43}$$

and

$$\Psi(\{j_{c,e}, i_e, k^x_{c,e}\}) = \prod_{c,e} \psi_{c,e}(j_{c,e}) \prod_{i_e} \psi_e(i_e) \prod_{c,e} \psi_{x,c,e}(k^x_{c,e}). \tag{5.44}$$

Again, we shall only discuss the FK model explicitly, as the EPR model can be directly obtained by dropping k-dependent ψs and substituting $k = j$ everywhere else.

Essentially, we want to compute the quantity Z_Ψ from equation (5.31) with a suitably factorable boundary state Ψ and the vertex amplitude specified by equation (5.25). This expression for Z_Ψ can be cast into the form (5.32) with the following

redefinition of M_e, given directly in graphical form:

$M_e =$ 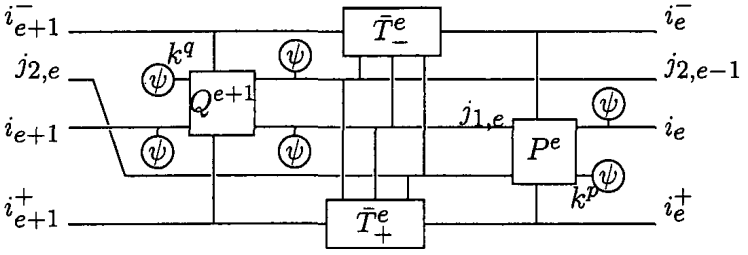

, (5.45)

where $\bar{T}$ denotes a product of T and N from equations (5.26) and (5.27). Writing out this factorization of M_e with all indices shown explicitly, while straight forward, is cumbersome and not particularly enlightening. It should now be clear that, for this factorization of the M_e, individual factors of the boundary state may depend on clusters of spins of the form $(i_e, j_{1,e}, j_{2,e}, k^p_{1,e}, k^p_{2,e})$ as well as $(i_{e+1}, j_{1,e}, j_{2,e-1}, k^q_{1,e}, k^q_{2,e-1})$, which are compatible with possible factorizations of the boundary states proposed in sections 5.2.1 and 5.2.2.

Each M_e is of size $O(j^4) \times O(j^4)$, hence $d = 4$. However, because of the sparseness of the $\bar{T}$, P, and Q factors, each matrix-vector multiply takes $O(j^6)$ operations, since $D = 4 + 2$ for P and Q multiplies and, equivalently in terms of complexity, $D = 5 + 1$ for each $\bar{T}$ multiply. These numbers are identical for both EPR and FK models. On the other hand, filling the P and Q matrices for the EPR model does not involve summations over k-spins. Thus, the EPR filling complexity is parametrized by $f = 1$, $F = 5$, and $F + f = 6$, while the FK filling complexity is parametrized by $f = 3$, $F = 5$, and $F + f = 8$. The overall runtime complexity of the algorithm is $O(j^{12})$, $2+d+D = 12$, both for the EPR and FK models. By conventional standards, this algorithm has a very high polynomial complexity exponent. However, it is still a substantial improvement over the naive $O(j^{22})$ or $O(j^{42})$ estimates found earlier.

5.4 Applications of the algorithms

The algorithms described in the preceding sections have already been implemented and applied in several contexts. Alesci, Bianchi, Magliaro and Perini [1] have used one variation to extend the original wave packet propagation calculations of [22], both to larger input spins and to different kinds of observables (although still keeping the j-spins frozen). Also, a highly optimized version of the algorithm presented in section 5.3.3 has been implemented by Christensen [11] and used to extract next-to-leading-order asymptotics information from the BC graviton propagator (cf. sec-

tion 5.2.2), as a followup to [13]. While the method used in [13] is capable of handling higher input spins, the advantage of the new algorithm is much greater precision, which is better suited for subdominant asymptotics analysis.

Here, we apply the new algorithms to the problem of wave packet propagation described in section 5.2.1. We have already established that the boundary states proposed in that section are factored states compatible with the new algorithms. However, being gaussian, they do not have finite support. Fortunately, strong gaussian decay allows us to impose a finite cutoff while maintaining acceptable precision. The cutoff chosen for all computations presented below was 2.8 standard deviations about the mean. As a consequence, the range of each spin sum involved in the computation is still of order $O(j)$, as assumed by our run time complexity estimates.

First, we can show the effect of introducing a non-zero τ in (5.11) and comparing with the calculations of [22], which kept $\tau = 0$, freezing all j-spins at the background value j_0. According to equation (5.13), the size of τ is inversely proportional to the parameter α. Figure 5.2 compares the reference wave packet ψ [cf. (5.12)] with several propagated wave packets ϕ (each with a different value of α) depending on the single fixed i-spin. The wave packets have been normalized such that their absolute values squared sum to 1. The wave packet with the largest value of α is essentially identical to the one obtained with all j-spins frozen at j_0. In that case, as shown previously in [22], the reference state ψ resembles the propagated wave packet in shape and mean. Unfortunately, as the width of the gaussian factors associated to j-spins increases (α decreases), the propagated wave packet quickly departs from ψ in both shape and mean. Notably, the mean shifts to a significantly higher value of i.

Second, we can compare the wave packets propagated by the three different models in the 1-9 geometry. Figure 5.3 shows the reference wave packets ψ [cf. (5.11)] and propagated wave packets ϕ, depending on the fixed j-spin and for two choices of α. These wave packets are also normalized. The BC wave packets appear to be pathological. They are completely dominated by zero spin. The EPR and FK wave packets do have a peak-like shape, however the mean and width of these peaks differ significantly from each other and the reference gaussian state.

Lastly, we compare the wave packets propagated by the three different models in the 4-6 geometry. In general, the propagated wave packet will depend on the four fixed j-spins. Unfortunately, it is impractical to either compute or display functions on a 4-dimensional domain. Thus, all calculations have been done with the four fixed j-spins set equal. Figure 5.4 shows the reference wave packet ψ [cf. (5.11)] and propagated wave packets ϕ, depending on the common value of the fixed j-spins for

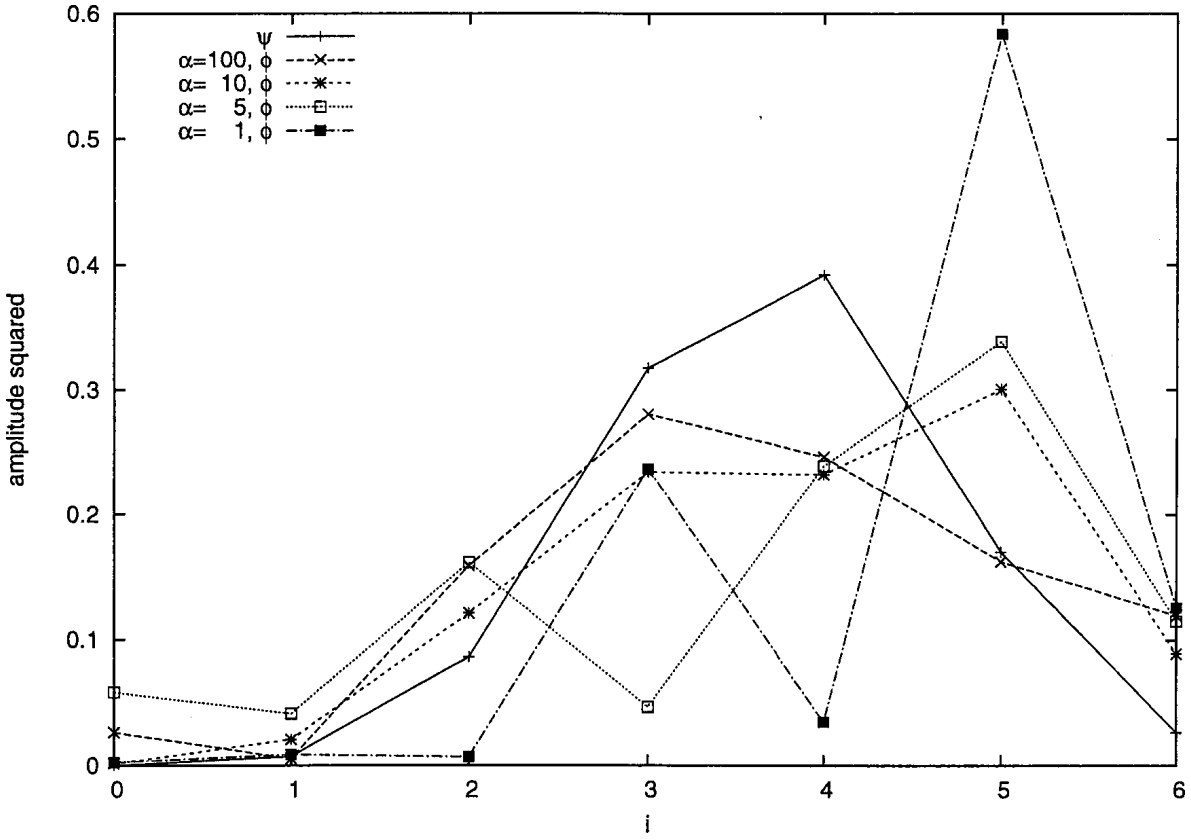

Figure 5.2: EPR 4-1 propagated (ϕ) and reference (ψ) wave packets, with $j_0 = 3$.

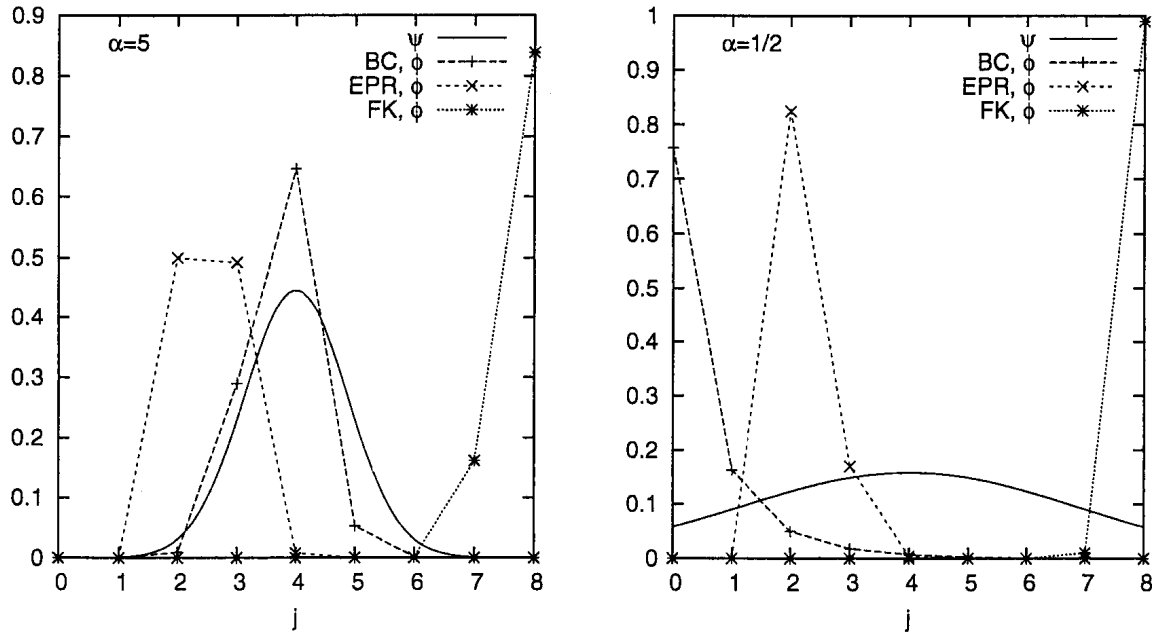

Figure 5.3: 1-9 propagated and reference wave packets for different models, with $j_0 = 4$.

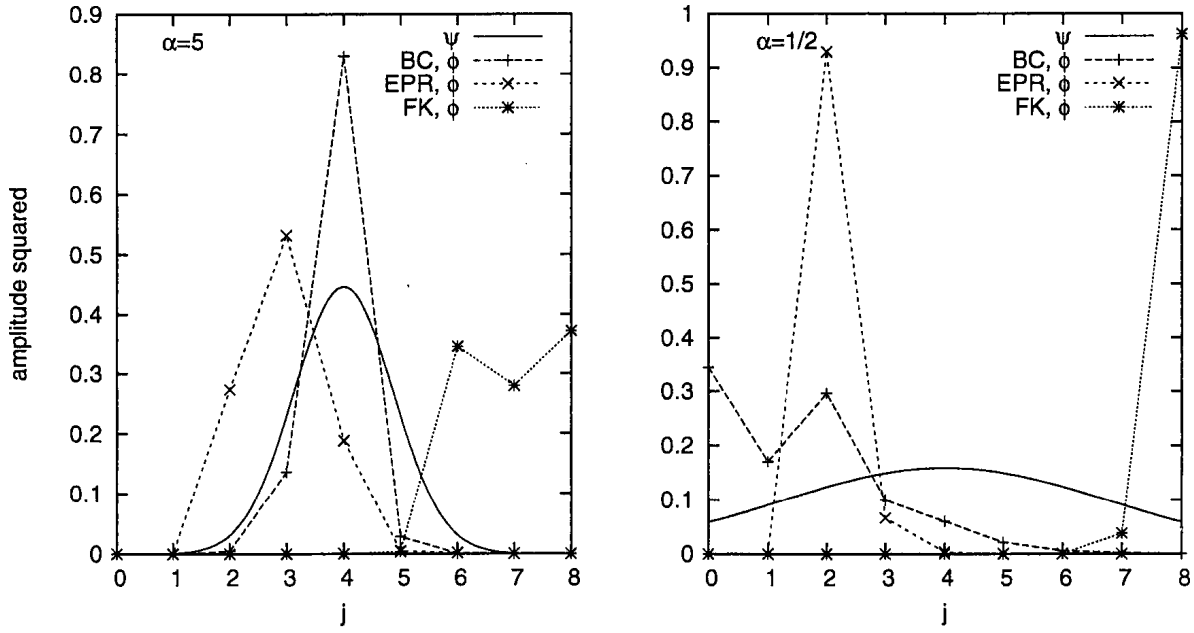

Figure 5.4: 4-6 propagated and reference wave packets for different models, with $j_0 = 4$.

two choices of α. These wave packets are again normalized. As is clearly seen from the figure, the propagated wave packets have in general very little similarity with the reference one. More pathological behavior is observed in the FK and BC models, the latter at $\alpha = 1/2$, since none of these curves resemble a well formed gaussian wave packet. In all cases, the propagated wave packet has little in common with the reference one.

5.5 Conclusion and Outlook

We have discussed open spin foam models with boundary states. Two prominent examples fitting into this framework that have appeared in the literature are the problems of semiclassical wave packet propagation (in the context of the EPR model) and computation of the graviton propagator matrix elements (in the context of the BC model). In section 5.2, we have extended both problems to each of the BC, EPR, and FK models. At the same time, we have proposed a uniform methodology for comparing results among the three models, despite their different spin argument structures.

A family of efficient numerical algorithms, capable of attacking these problems, has been constructed and implemented. The run time complexity of these algorithms

has been analyzed and shown to be orders of magnitude superior to more naive approaches. Reference [22] had put forward the hypothesis that semiclassical wave packets, propagated using the EPR dual vertex amplitude, approximate a certain reference gaussian shape, which was demonstrated under somewhat restrictive conditions. An application of the numerical algorithms described above allowed a broader investigation of this question. The results indicate that this hypothesis does not hold under more general conditions, neither for the EPR nor for the other models.

These algorithms have also already been implemented and applied by other authors, as discussed in section 5.4. While, several wave packet propagation geometries have been examined, there are many other ones. Is any one of them theoretically preferrable to the others? Another immediate possibility for further investigation is the computation of the graviton propagator matrix elements in the EPR and FK models.

Acknowledgments

The author would like to thank Dan Christensen for suggesting this project. Also, Wade Cherrington, Carlo Rovelli, and Elena Magliaro have contributed through helpful discussions. The author was supported by an Ontario Graduate Scholarship and a SHARCNET Fellowship. Computational resources for this project were provided by SHARCNET.

Bibliography

[1] Alesci E, Bianchi E, Magliaro E, and Perini C 2008 Intertwiners dynamics in the flipped vertex (*Preprint* arXiv:0808.1971)

[2] Alesci E and Rovelli C 2007 Complete LQG propagator: Difficulties with the Barrett-Crane vertex *Physical Review D* **76** 104012–104033 (*Preprint* arXiv:0708.0883)

[3] Alesci E and Rovelli C 2008 Complete LQG propagator. II. Asymptotic behavior of the vertex *Physical Review D* **77** 044024–044034 (*Preprint* arXiv:0711.1284)

[4] Baez J C 1998 Spin foam models *Classical and Quantum Gravity* **15** 1827–58 (*Preprint* arXiv:gr-qc/9709052)

[5] Baez J C 2000 An introduction to spin foam models of quantum gravity and BF theory *Lecture Notes in Physics* **543** 25–94 (*Preprint* arXiv:gr-qc/9904025)

[6] Baez J C, Christensen J D, and Egan G 2002 Asymptotics of $10j$ symbols *Classical and Quantum Gravity* **19** 6489–513 (*Preprint* arXiv:gr-qc/0208010)

[7] Baez J C, Christensen J D, Halford T R, and Tsang D C 2002 Spin foam models of Riemannian quantum gravity *Classical and Quantum Gravity* **19** 4627–48 (*Preprint* arXiv:gr-qc/0202017)

[8] Barrett J W and Crane L 1998 Relativistic spin networks and quantum gravity *Journal of Mathematical Physics* **39** 3296–302 (*Preprint* arXiv:gr-qc/9709028)

[9] Bianchi E, Modesto L, Rovelli C, and Speziale S 2006 Graviton propagator in loop quantum gravity *Classical and Quantum Gravity* **23** 6989–7028 (*Preprint* arXiv:gr-qc/0604044)

[10] Carter J S, Flath D E, and Saito M 1995 The classical and quantum $6j$-symbols (*Mathematical Notes* vol 43) (Princeton, NJ: Princeton University Press)

[11] Christensen J D *Private communication.*

[12] Christensen J D and Egan G 2002 An efficient algorithm for the Riemannian $10j$ symbols *Classical and Quantum Gravity* **19** 1184–93 (*Preprint* arXiv:gr-qc/0110045)

[13] Christensen J D, Livine E R, and Speziale S 2007 Numerical evidence of regularized correlations in spin foam gravity (*Preprint* arXiv:0710.0617)

[14] Conrady F and Freidel L 2008 Path integral representation of spin foam models of 4d gravity (*Preprint* arXiv:0806.4640)

[15] Engle J, Pereira R, and Rovelli C 2007 The loop-quantum-gravity vertex-amplitude *Physical Review Letters* **99** 161301–161304 (*Preprint* arXiv:0705.2388)

[16] Engle J, Pereira R, and Rovelli C 2008 Flipped spinfoam vertex and loop gravity *Nuclear Physics B* **798** 251–290 (*Preprint* arXiv:0705.1236)

[17] Freidel L and Krasnov K 2008 A new spin foam model for 4d gravity *Classical and Quantum Gravity* **25** 125018–125053 (*Preprint* arXiv:0708.1595)

[18] Kauffman L H and Lins S L 1994 Temperley-Lieb recoupling theory and invariants of 3-manifolds (*Annals of Mathematics Studies* vol 134) (Princeton, NJ: Princeton University Press)

[19] Khavkine I 2008 Evaluation of new spin foam vertex amplitudes To appear.

[20] Khavkine I and Christensen J D 2007 q-deformed spin foam models of quantum gravity *Classical and Quantum Gravity* **24** 3271–3290 (*Preprint* arXiv:0704.0278)

[21] Livine E R and Speziale S 2006 Group integral techniques for the spinfoam graviton propagator *Journal of High Energy Physics* **11** 092–114 (*Preprint* arXiv:gr-qc/0608131)

[22] Magliaro E, Perini C, and Rovelli C 2007 Numerical indications on the semiclassical limit of the flipped vertex (*Preprint* arXiv:0710.5034)

[23] Modesto L and Rovelli C 2005 Particle scattering in loop quantum gravity *Physical Review Letters* **95** 191301–191304

[24] Rovelli C 2006 Graviton propagator from background-independent quantum gravity *Physical Review Letters* **97** 151301–151304 (*Preprint* arXiv:gr-qc/0508124)

[25] Wald R M 1984 General Relativity (Chicago, IL: University of Chicago Press)

Chapter 6
Conclusion and Outlook

All computations described in this thesis were done using the `spinnet` software library designed and implemented by the author, in collaboration with Dan Christensen. This library includes routines for evaluating simple spin networks, which are the building blocks of more complicated algorithms. These spin networks can be computed in either classical or q-deformed form. They can also be computed in real or complex floating point form, in rational form, or even in symbolic form. The library also implements the spin foam vertex amplitude algorithms described above, some highly optimized. And it includes code to manage 4-dimensional triangulations and to statistically evaluate corresponding spin foam partition functions. The library is written in `C` with `Python` bindings. The code is freely available upon request.

Section 1.1 provided a focused historical overview of the quantum gravity literature leading up to spin foam models. As a useful reference for the rest of the thesis, section 1.2, section 1.3, and chapter 2 summarized some mathematical background and notation used in the definition of spin foam models and in the evaluation of spin networks.

In chapter 3, we have computed physical observables of variations of the BC spin foam model defined on non-trivial triangulations and incorporating a positive cosmological constant via q-deformation. The calculations indicate that observables exhibit discontinuous behavior in the limit of zero cosmological constant (with the limit passing through primitive roots of unity q-deformations). These results provide the first data concerning the long standing problem of incorporating and investigating the effects of a cosmological constant in spin foams. The observed behavior is seemingly at odds with the expected one, based on classical considerations, and deserves further examination. Also, the computed single spin distribution suggests that the spin foam partition function, for the Perez-Rovelli and Baez-Christensen variations of the BC model, is dominated by so-called isolated bubble spin foams.

In chapter 4, we have described spin foam vertex evaluation algorithms for so-called new models. The efficiency of these algorithms, for the first time, allows an exploration of these amplitudes' large spin asymptotics. These asymptotics were

compared to that of the standard BC model. All models show polynomial decay in their effective single vertex amplitudes. The presence of an oscillating exponentiated Regge action in the leading asymptotic term, as inspired by the Ponzano-Regge model, is not found. However, such a term may still be found in subdominant contributions, as in the BC model.

Chapter 5 extended these algorithms to include the evaluation of spin foam vertex amplitudes contracted with factored boundary states. These algorithms are significantly more efficient than methods previously used to investigate the wave packet propagation problem for the EPR model. The formulation of this problem as well as of the graviton propagator calculation were extended to also encompass the BC and FK models. The wave packet propagation calculations were, for the first time, compared across the three models. The results do not strictly confirm hypotheses previously put forward regarding the semiclassical limit of the new vertices and call for their further investigation.

The graviton propagator calculations are another important test of the expected semiclassical behavior and should be addressed in future work. Other interesting physical observables should also be identified and studied. Another avenue of investigation is the application of the tools developed for q-deformed spin networks in chapter 3 to incorporate a cosmological constant into the formulation of the new models.

Finally, it is entirely possible that yet other and more sophisticated spin foam models will be proposed in the future. It is important to increase the flexibility and power of the computational tools available to lower the barrier to their thorough investigation. One possible direction is to develop an algorithm to automatically evaluate any trivalent spin network, which would simplify the task of section 4.3.1. Another is to develop an automatic optimizer to find the optimal order and number of summation loops necessary to evaluate complicated spin networks like vertex amplitudes. Such an optimizer would automate the construction of algorithms like the ones described in sections 4.3.2 and 5.3.

Appendix A
Copyright Permissions

APS Copyright Policies and Frequently Asked Questions

For Chapter 2

What is copyright? http://www.copyright.gov
Copyright is a form of legal protection for original works of authorship. Copyright covers both published and unpublished works.

What does copyright protect?
Copyright, a form of intellectual property law, protects original works of authorship including literary, dramatic, musical, and artistic works, such as poetry, novels, movies, songs, computer software, and architecture. Copyright does not protect facts, ideas, systems, or methods of operation, although it may protect the way these things are expressed. See Circular 1, Copyright Basics, section "What Works Are Protected", see http://www.copyright.gov/circs/circ1.html#wwp

How is a copyright different from a patent or a trademark?
Copyright protects original works of authorship, while a patent protects inventions or discoveries. Ideas and discoveries are not protected by the copyright law, although the way in which they are expressed may be. A trademark protects words, phrases, symbols, or designs identifying the source of the goods or services of one party and distinguishing them from those of others.

What is the difference between copyright infringement and plagiarism? Top
Copyright infringement occurs when an author's work is reused or republished without the permission of the copyright owner, whether or not author attribution accompanied the reuse.

Plagiarism occurs when an author's work has been reused or republished in such a manner as to make it appear as someone else's work, e.g., without quotation marks and citation of the original work.

Why should I transfer copyright to APS? Top
Like many other scientific publishers, the American Physical Society (APS) requires authors or their employers to provide transfer of copyright prior to publication. This permits APS to publish the article and to defend against improper use (or even theft) of the article. It also permits APS to mount the article online and to use the article in other forms or media, such as PROLA. By the APS transfer agreement, authors and their employers retain substantial rights in the work, as specified in the agreement (http://forms.aps.org/author/copytrnsfr.pdf) and discussed in this document.

Why should I transfer copyright to APS before the article is accepted for publication by an APS journal?
Transferring copyright early in the process avoids the possibility of delaying publication if the transfer has to be obtained later in the process. By the terms of the copyright transfer agreement itself, it has no effect until the paper is accepted by an APS journal. The author retains the copyright until acceptance, and has the full freedom, for example, to withdraw the paper from consideration by an APS journal and submit it elsewhere.

Does transferring copyright affect my patent rights?
No. Copyright is separate from any patent rights, and the APS transfer agreement specifically states that patent rights are not affected. However, you should be aware that submitting a manuscript to a journal without first taking steps to protect your patent rights (e.g., filing for a patent) could endanger those rights. Consult your patent attorney.

As the author of an APS-published article, can I post my article or a portion of my article on my own website? Top
Yes, the author or the author's employer can use all or part of the APS published article, including the APS-prepared version (e.g., the PDF from the online journal) without revision or modification, on the author's or employer's website as long as a fee is not charged. If a fee is charged, then APS permission must be sought. In all cases, the appropriate bibliographic citation and notice of the APS copyright must be included.

What happens if the author has posted an APS-published article on a free access e-print server or on the authors' or institutions' web page and subsequently a fee is imposed for access to those sites?
When a fee is imposed, the author must either obtain permission from APS or withdraw the article from the e-print server or Institutional Repository.

As the author, can I post my article or a portion of my article on an e-print server?
The author has the right to post and update the article on a free-access e-print server using

files prepared and formatted by the author. Any such posting made or updated after acceptance of the article for publication by APS shall include a link to the online abstract in the APS journal or to the entry page of the journal. In all cases, the appropriate bibliographic citation and notice of the APS copyright must be included. If the author wishes to use the APS-prepared version (e.g., the PDF from the online journal) on an e-print server other than authors' or employer's website, then APS permission must be sought. Similarly, if the author wishes to post the article (any version) on an e-print server that charges a fee for use, APS permission must be sought.

As the author of an APS-published article, can I use figures, tables, graphs, etc. in future publications?
Yes, as the author you have the right to use figures, tables, graphs, etc. in subsequent publications using files prepared and formatted by the author. However, if the APS-prepared version is used then APS permission is required. The appropriate bibliographic citation and notice of the APS copyright must be included.

As the author, can I include my article or a portion of my article in my thesis or dissertation?
Yes, the author has the right to use the article or a portion of the article in a thesis or dissertation without requesting permission from APS, provided the bibliographic citation and the APS copyright credit line are given on the appropriate pages.

As the author of an APS published article, may I give permission to a colleague or third party to republish all or part of the article in a print publication? Top
Yes, as the author you can grant permission to third parties to republish print versions of the article provided the APS-prepared version (e.g., the PDF from the online journal, or a copy of the article from the print journal) is not used for this purpose, the article is not published in another journal, and the third party does not charge a fee. The appropriate bibliographic citation and notice of the APS copyright must be included.

As the author of an APS published article, may I give permission to a colleague or third party to republish all or part of the article in an online journal, book, database compilation, etc.?
Authors should direct the third party request to APS.

As the author of an APS published article, may I provide a PDF of my paper to a colleague or third party?
The author is permitted to provide, for research purposes as long as a fee is not charged, a PDF copy of his/her article using either the APS-prepared version or the author prepared version.

As a third party (not an author), can I request permission to republish an article or portion of an article published by APS? Top
Yes, APS will grant permission to republish articles or portions of articles (e.g., tables, graphs, excerpts) published by APS. Depending on the reuse and medium APS has the right to grant permission subject to APS terms and conditions and a fee may be assessed. APS will generally require the third party to obtain the author's permission also.

As a third party, can I use articles published by APS for lecture and classroom purposes?
Yes, you may use photocopied articles published by APS for lecture and classroom purposes for a single semester without asking permission from APS. However, if the article becomes part of your course material beyond one semester, you must obtain permission from APS. Also, there is no limitation on the use of APS articles using links to the material accessible through institutional subscriptions.

How do I request permission to republish APS-copyrighted material? Top
To request permission to republish APS-copyrighted material, please provide the following information:

1. Title of journal
2. Title of article
3. Name of author
4. Volume number, page number (or article identifier), year
5. Indicate if you are requesting to republish in print, online, CD-ROM, and/or other format
6. Indicate if you wish to republish all or portion of article; if a portion describe the specific material, e.g., figure numbers, excerpt
7. Indicate how the material will be used, e.g., in a book, journal, proceeding, thesis, etc.
8. Indicate the title of publication
9. Indicate the name of the publisher
10. Indicate whether or not a fee will be charged for the publication

All permission requests must be in writing (email is acceptable). Blanket permissions are not granted. Please note all requests are subject to APS terms and conditions and a fee may be assessed.

Please allow 3-5 business days for us to respond to a permission request provided all the above information is provided at the time of the request.

Send all permission requests to:

Associate Publisher
American Physical Society
One Physics Ellipse
College Park, MD 20740
Email: assocpub@aps.org

If your questions have not been addressed and you need further assistance, please call: 301-209-3283.

How do I provide a proper bibliographic citation and notice of the APS copyright? Top
Provide the following information in this order:

Authors names, journal title, volume number, page number (or article identifier), year of publication. "Copyright (year) by the American Physical Society."

For further information about copyright in general, please refer to the Library of Congress FAQ at: http://www.copyright.gov/help/faq/

Journals published by the American Physical Society can be found at http://publish.aps.org/

APS COPYRIGHT TRANSFER FORM can be found at
http://forms.aps.org/author/copytrnsfr.pdf Top

FAQ Version: January 1, 2006

IOP | electronic journals

For Chapter 3

▶ Feedback

Ref: : CQG/247664/PAP/166688

ASSIGNMENT OF COPYRIGHT and DECLARATION OF RESPONSIBILITY

1. IOP Publishing Ltd ("the Publisher") agrees to publish

Manuscript title: q-deformed spin foam models of quantum gravity (**"The Article"**) written by

Names of all Authors: Igor Khavkine, J D Christensen (**"the Named Authors"**)

In the following journal: Classical and Quantum Gravity (**"the Journal"**)

2. Transfer of Copyright Agreement

2.1 On acceptance for publication the undersigned author(s) ("Author") of the Article assigns exclusively to IOP worldwide copyright in the Article for the full term and for all media and formats in all material published as part of the Article, which expression includes but is not limited to the text, abstract, tables, figures and graphs, but excludes any supplementary material.

2.2 If any of the Named Authors are Government employees, on acceptance for publication the Author shall grant IOP a royalty free exclusive licence for the full term of copyright for all media and formats to do in relation to the Article all acts restricted by copyright worldwide.

2.3 On acceptance for publication the Author shall grant IOP a royalty free non-exclusive licence for the full term of copyright for all media and formats to do in relation to any supplementary material deemed to be part of the Article all acts restricted by copyright worldwide.

3. Author Rights

3.1 IOP grants the Named Authors the rights specified in 3.2 and 3.3. All such rights must be exercised for non-commercial purposes, if possible should display citation information and IOP's copyright notice, and for electronic use best efforts must be made to include a link to the on-line abstract in the Journal. Exercise of the rights in 3.3 additionally must not use the final published IOP format but the Named Author's own format (which may include amendments made following peer review).

3.2 The rights are:

3.2.1 To make copies of the Article (all or part) for teaching purposes;

[3.2.2 To include the Article (all or part) in a research thesis or dissertation;]

3.2.3 To make oral presentation of the Article (all or part) and to include a summary and/or highlights of it in papers distributed at such presentations or in conference proceedings; and

3.2.4 All proprietary rights other than copyright.

3.3 The additional rights are to:

3.3.1 Use the Article (all or part) without modification in personal compilations or publications of a Named Author's own works (provided not created by third party publisher);

3.3.2 Include the Article (all or part) on a Named Author's own personal web site;

3.3.3 Include the Article (all or part) on web sites of the Institution (including its repository) where a Named Author worked when research for the Article was carried out; and

3.3.4 Include the Article (all or part) on third party web sites including e-print servers, but not on other publisher's web sites.

Signature

In signing this Agreement the Author represents and warrants that the Article is the original work of the Named Authors, it has not been published previously in any form (other than as permitted under clause 3.2.2 which fact has been notified to IOP in writing), all Named Authors have participated sufficiently in the conception and writing of the Article, have received the final version of the Article, agree to its submission and take responsibility for it, and

For Chapter 3

Frequently Asked Questions (FAQ)

Use of figures

1. **I am writing a (review) article for an IOP journal. Do I need to obtain permission for reproducing figures taken from prior publications?**
   Yes, the use of all material that has been published previously must be approved by the Publisher in each case and, depending on the Publisher's policy, the author as well, before it can be used in any IOP article (whether a normal paper or a review article). This assumes that the Publisher owns the rights but you should check to see if there is a citation next to the figure indicating that copyright is in fact owned by a third party. If that is the case then that third party's permission should be sought. The permission request form can be customised for use when making such requests and all responses should be submitted to the IOP journal, along with the article.
   Note that IOP is a signatory to the STM 2003 Permissions Guidelines. This is an agreement between Publishers which allows signatory Publishers to use small numbers of figures and small amounts of text in journal articles free of charge. If the Publisher who owns the copyright in the figure you wish to use is also a signatory, permission should be given free of charge provided the conditions in the Guidelines are complied with. IOP is also a signatory to the STM Scholarly Publisher Guidelines for Quotation & Other Academic Uses of Excerpts from Journal Articles 2006 which covers the re-use of small amounts of material, without the need to seek permission. It is possible that the Publisher of the material you wish to re-use is also a signatory to these Guidelines. Both sets of Guidelines can be linked from STM's home page.
2. **Who do I need to contact about obtaining permission to make use of some figures from articles published in IOP journals if I am not the author of those articles?**
   Please send your enquiry to permissions@iop.org and we will respond to your request as quickly as we can.
3. **As the author of an IOP published article, can I re-use figures, tables, graphs, etc. in future publications?**
   Yes, IOP authors may use their own figures, tables, graphs, artwork, illustrations and data from their articles without seeking permission from IOP provided that
   - credit is accurately given to the original article,
   - modifications to the presentation of previously published data are noted and distinguished from the introduction of any new data, and
   - re-use is not made for direct commercial purposes.

   Where there are co-authors, the other authors should be informed. In all other cases please contact the Managing Editor, Copyright and Permissions at permissions@iop.org for advice. In this context the re-use of figures, tables, graphs etc in after dinner speeches or in conference presentations is not considered by IOPto be use for a direct commercial purpose even where the author is paid to speak.
   See also Questions 14 and 15 regarding use of the full article for teaching and at conferences.
4. **I have downloaded a figure/photo from the Internet. Do I need any permission to use it?**
   Permission should always be requested from the source of any figure or photograph taken from the Internet, before this is used elsewhere. You will need to supply full details of the planned re-use when sending your request, mentioning whether it will be for print and/or electronic formats. Even if permission appears not to be required it is good practice to notify the copyright owner of the re-use.

Signing the Copyright form

5. **What sections of the Assignment of Copyright must I sign?**
   If you hold the copyright in your work then you only need to sign as the author. However, if your terms of employment state that the copyright in any articles written in the course of your employment belongs to your employer then you will need to obtain a second signature, on behalf of your employer, in support of your submission.
   See also Questions 23–26.
6. **What if I am not sole author?**
   Only one author should sign the form, as authorised agent on behalf of all the named authors. Before signing on behalf of all named authors the signatory must get consent from all the others.
7. **I am a UK government employee.**
   Your article will be governed by Crown Copyright and is therefore not eligible for copyright transfer. A licence should be issued by your employer to enable IOP to publish your work. Please contact permissions@iop.org with any queries.
8. **All authors of the article are US Government employees, so where do I sign?**
   One signature is required at the end of the Copyright form, confirming that all authors are employees of the US Government and the article is not eligible for copyright.
9. **Some but not all of the authors are US Government employees, so where do I sign?**
   One author signature who is not a US Government employee only is required in the first signature section, on behalf of all the authors.
10. **Can I send a scanned or faxed copy of the form?**
    Yes, forms can be returned by fax, e-mail or post. But see also the next question regarding signatures.
11. **Can I include a digital signature on the form?**
    Currently a digital signature superimposed on the document is unacceptable, for UK legal reasons. Instead we require a handwritten signature on the printed form, which can then be scanned for return to IOP.

e-print servers

12. **I have submitted my article to an IOP journal. Can I also submit it to arXiv.org or any other repository as well?**
    Yes, articles may be posted on non-commercial third party websites, including arXiv and other repositories. The author's own original format should be used (which may include amendments made by the author following peer review). This is the version commonly known as the accepted manuscript. If possible, citation information should be included with IOP's copyright notice. Once the final version has been published, best efforts must also be made to include a link to the online abstract of the paper in the journal. Authors MUST NOT deposit the published IOP formatted version. IOP also requests that you include the following statement of provenance: 'This is an author-created, un-copyedited version of an article accepted for publication in [insert name of journal]. IOP Publishing Ltd is not responsible for any errors or omissions in this version of the manuscript or any version derived from it. The definitive publisher authenticated version is available online at [insert DOI].'
    When submitting an article to arXiv you have to select a licence or declaration which gives the arXiv the rights necessary to distribute your article. IOP is happy for you to select the first option offered, namely 'arXiv.org perpetual, non-exclusive licence to distribute your article'. Please do not accept any of the other options without consulting with IOP in advance at permissions@iop.org.
    See also Question 17 below.
13. **What is IOP's policy with regard to UK PubMed Central and NIH?**
    On or after acceptance for publication IOP authors may deposit their articles in PubMed/NIH provided the articles are embargoed for public release for 12 months from the official date of publication and further provided the deposited version is in the author's own original format (which may include amendments made by the author following peer review). This is the version commonly known as the accepted manuscript. Authors MUST NOT deposit the published IOP formatted version. IOP also requests that you include the following statement of provenance: 'This is an author-created, un-copyedited version of an article accepted for publication in [insert name of journal]. IOP Publishing Ltd is not responsible for any errors or omissions in this version of the manuscript or any version derived from it. The definitive publisher authenticated version is available online at [insert DOI].'
    IOP is currently considering introducing a service to deposit articles at UK PubMed Central and NIH for authors in the future.

Author's rights after publication by IOP

14. **After the copyright in my article has transferred to IOP, may I still use the article for teaching or in a thesis or dissertation?**
    Yes, the Assignment of Copyright document sets out the rights that IOP authors retain in clause 3. These include copying the article (all or part) for teaching purposes, and including the article (all or part) in research theses or dissertations. These rights must be exercised for non-commercial purposes. If possible citation information and IOP's copyright notice should be displayed and for electronic use best efforts must be made to include a link to the online abstract in the journal.
15. **After the copyright in my article has transferred to IOP, may I still use it for lecturing and at conferences?**
    Yes, you may make oral presentations of the article (all or part) and include a summary and/or highlights of it in papers distributed at presentations or conference proceedings. Papers distributed should display citation information and IOP's copyright notice. If a proceedings is intended for publication in a peer-reviewed journal you may not include a work which is substantially similar to one published in an IOP journal.
16. **After the copyright in my article has transferred to IOP, may I include it in a compilation work?**
    The article (all or part) may be included without modification in personal compilations or publications of a named author's own work provided this is not created by a different Publisher. This right must be exercised for non-commercial purposes, the publications should if possible display citation information and IOP's copyright notice and for electronic use best efforts must be made to include a link to the online abstract in the journal. You should not use the final published IOP format, but your own format which may include amendments made following peer review.
    If the compilation is being prepared for commercial sale by another Publisher please contact permissions@iop.org.
17. **May I post my paper on my personal website or my institutional website?**
    Yes, IOP authors can place their papers (all or part) on their own personal website or on the website of the institution (including its repository) where a named author worked when research for the article was carried out, but they must not use the IOP formatted version of record (PDF or HTML). Instead they can make use of the article in their own format, which can include amendments made following peer review. This is the version commonly known as the accepted manuscript. The purpose of the posting must be non-commercial, if possible should display citation information and IOP's copyright notice. Once the final version has been published, best efforts must be made to include a link back to the online abstract in the journal. Authors MUST NOT post the published IOP formatted version. IOP also requests that you include the following statement of provenance: 'This is an author-created, un-copyedited version of an article accepted for publication in [insert name of journal]. IOP Publishing Ltd is not responsible for any errors or omissions in this version of the manuscript or any version derived from it. The definitive publisher authenticated version is available online at [insert DOI].'
    For posting on e-print servers see Question 12 above.
18. **As the author of an IOP published article, may I provide a pdf of my paper to a colleague or third party or would this violate your copyright?**
    Yes, authors can provide colleagues with the link to the online abstract of their article, so that they can access it if their institution has the necessary rights.
    Under IOP's Free for Thirty days Policy, which applies to most IOP journals, colleagues will be able to access the article for thirty days whether or not their institution has a subscription. Authors may also send or transmit the final published article in any format to colleagues on specific request provided no fee is charged and it is not done systematically through, for example, mass-mailings, posting on list-servs or other open websites.
19. **May I reuse the abstract of my article?**
    Yes, IOP authors may re-use or post their article abstracts on any website for non-commercial purposes. No changes may be made to the abstract. Any links, brands, trademarks, or copyright notices embedded in the abstract must remain intact. Wherever possible the abstract should provide a link back to the online version on the IOP website.
20. **May I reuse supplementary material forming part of my article?**
    Yes, you may re-use supplementary material. The author retains copyright in supplementary material which forms part of the article as IOP only takes a non-exclusive licence to publish supplementary material. Examples of supplementary material are online multimedia, video and data sets (meaning sets/ collections of raw data captured in the course of research). IOP adheres to STM's 2006 Statement Databases, Datasets, and Data Accessibility – Views and Practices of Scholarly Publishers.

Non-ownership of copyright

21. **What if I do not own copyright of the article I have written?**
Please contact the Managing Editor, Copyright and Permissions via permissions@iop.org for advice on how to proceed.

What is the position if my article is rejected?

22. **My article has been rejected by an IOP journal, so what happens to the copyright now?**
The Assignment of Copyright document only becomes valid once an article has been accepted for publication. If an article is rejected by IOP then the copyright remains with the author and the form has no significance.

General queries

23. **What is copyright?**
As soon as an original idea is expressed in a physical medium, such as writing on paper, it qualifies for copyright protection. This right is automatically vested in the author or their employer depending on the contract of employment and the relevant jurisdiction.
As a matter of statute law the copyright holder of a work has the right to prevent others from reproducing, distributing and communicating the work electronically to others. Copyright infringement occurs whenever someone other than the copyright holder reproduces, distributes or communicates the work electronically to others without permission from the copyright holder.
As far as academic journals published by IOP are concerned IOP believes that academic authors have the rights they need to use the articles for education and research purposes notwithstanding the copyright issue.
See Questions 14–21 above.
24. **Why does IOP request transfer of copyright?**
When the copyright in a work is transferred to IOP it enables IOP to ensure that the work can be given maximum exposure via our international systems and through our publishing expertise. There are several reasons why this is so and a summary of the most important of these follows:
    - Owning copyright comes with certain obligations which Publishers are well placed to carry out. For example, the owner of copyright needs to respond to requests for permissions from other authors and Publishers and from institutions perhaps for course packs. There is also the obligation to negotiate licences with institutions and sub-licences such as with document suppliers. Then there is the duty to register copyright in certain jurisdictions. We believe that Publishers are better placed to do these things than authors. For example, do authors really want to familiarize themselves with the procedures for registering their copyright in certain jurisdictions?
    - Then there is the issue of multiple authors who would automatically own copyright jointly. If they retained copyright they would have to deal with all the above on a joint basis. Having a single copyright holder eases the management of copyright. One party can deal with these things much more easily than a multitude.
    - From IOP's point of view, as the holder of the copyright IOP's rights are not limited in time. This is in contrast to if IOP were a licensee as licences are sometimes limited in time either by contract or as a matter of the local law of the licensors (authors). Having rights which are unlimited by time enables IOP to licence perpetual rights which many libraries want. Further, by having rights unlimited by time IOP can move safely into new formats and publication platforms which may arise years after the original document is signed by the authors. IOP has the right to make use of the articles in the future, without having to seek the authors' permission again. This is beneficial to the whole community. The grant of rights unlimited in time provides the legal incentives necessary for Publishers to undertake the investment needed to disseminate the scientific record worldwide and to maintain the integrity of that record.
    - In addition, it makes enforcement of rights much easier, enabling IOP to protect the work against infringers. Authors rarely defend themselves against infringers, pirates and plagiarists as they do not have the expertise, time or money to do so. IOP is much better placed to do this.
    - Some query whether Publishers need to hold copyright and say that by doing so authors are prevented from using their articles for academic research or educational reasons. But as can be seen from the answers to questions 14–20 the fact that the copyright has been transferred to IOP does not prevent the authors from using the article in most of the ways they would want for ongoing research, education and outreach. In addition, it does not deny the authors' other rights such as the moral right to be identified as the author or patent rights.
    - For further discussion of this issue please see also the STM position paper **Publishers Seek Copyright Transfers (Or Transfers Or Licences Of Exclusive Rights) To Ensure Proper Administration & Enforcement of Author Rights.**
    - Finally, note that IOP does not take a copyright assignment for supplementary material (see Question 20 above.)
25. **Why does IOP believe it needs exclusive rights?**
If IOP only had a non-exclusive licence the owner could publish the work in another publication in addition to the IOP journal. This is regarded as unethical. See Question 30 below.
26. **Does the assignment of copyright deny the author other intellectual property rights?**
No, authors retain other rights including their moral rights to, for example, be named as the author, to object to derogatory treatment of the work (such as changes being made to the work which the author objects to) as well as the right to patent any inventions described in the article.
27. **Do all articles require a signed Assignment of Copyright form?**
Authors should complete an Assignment form and have returned this to IOP by the time their paper is accepted for publication. This ensures that IOP is mandated to publish the article on the author's behalf and that the author confirms all the conditions relating to the article. If you think that you require an exclusive licence rather than an assignment of copyright please contact permissions@iop.org.
28. **As a third party, can I use articles published by IOP for lecture and classroom purposes?**
This is normally possible for requests relating to small numbers of copies or parts of articles, but requests for multiple copies are better handled by the Copyright Licensing Agency (CLA), which deals with the licensing and collection of fees from copying and scanning of published material in the UK. The CLA acts on IOP's behalf in this area. In the USA such requests should be sent to the Copyright Clearance Center (CCC).
29. **As a third party (not an author), can I request permission to re-publish an article or portion of an article published by IOP?**
This may be possible. Please let us know the full details of your intentions, such as where the material will appear and in what format, if it will be produced by another Publisher etc. Please send as much background to the request as you can to permissions@iop.org and we will respond to your enquiry.
30. **What is the situation regarding dual publication? (see IOP Ethical Policy)**
Dual publication of identical articles is regarded as unethical in the STM publishing field and Publishers work together wherever possible to ensure that instances of this are minimized. The overlap between research papers, conference papers and review articles can be subtle and conventions vary in different scientific fields. Please consult IOP's Ethical Policy and the Editorial Office of the journal concerned for advice on specific questions.
31. **Does IOP publish any open-access journals?**
IOP publishes some open-access journals and for these journals IOP requests an Assignment of Copyright (for the same reasons as in Question 24). Authors still have the right to use the article in any way they might wish provided there is no commercial use. There should be a citation and for electronic use best efforts should be made to include a link back to the abstract in the IOP published journal.
32. **Other queries**
If you have a query which has not been answered in these FAQs please e-mail permissions@iop.org.

Close this window